Distribution Agreement

In presenting this thesis or dissertation as a partial fulfillment of the requirements for an advanced degree from Emory University, I hereby grant to Emory University and its agents the non-exclusive license to archive, make accessible, and display my thesis or dissertation in whole or in part in all forms of media, now or hereafter known, including display on the world wide web. I understand that I may select some access restrictions as part of the online submission of this thesis or dissertation. I retain all ownership rights to the copyright of the thesis or dissertation. I also retain the right to use in future works (such as articles or books) all or part of this thesis or dissertation.

Signature:

_____ _____

Chen Zhu Date

Enzyme on Ice: Kinetic and EPR Spectroscopic Characterization of the Co^{II}-Substrate Radical Decay Reaction in Coenzyme B_{12}-Dependent Ethanolamine Ammonia-Lyase

By

Chen Zhu
Doctor of Philosophy

Physics

_____

Dr. Kurt Warncke
Advisor

_____

Dr. Boi Hanh (Vincent) Huynh
Committee Member

_____

Dr. Dale E. Edmondson
Committee Member

_____

Dr. Keith Berland
Committee Member

_____

Dr. Laura Finzi
Committee Member

Accepted:

_____

Lisa A. Tedesco, Ph.D.
Dean of the James T. Laney School of Graduate Studies

_____

Date

Enzyme on Ice: Kinetic and EPR Spectroscopic Characterization of the Co^{II}-Substrate Radical Decay Reaction in Coenzyme B_{12}-Dependent Ethanolamine Ammonia-Lyase

By

Chen Zhu
B.S., Nankai University, China, 2003

Advisor: Kurt Warncke, Ph.D.

An abstract of
A dissertation submitted to the Faculty of the
James T. Laney School of Graduate Studies of Emory University
in partial fulfillment of the requirements for the degree of
Doctor of Philosophy
in Physics
2010

Abstract

Enzyme on Ice: Kinetic and EPR Spectroscopic Characterization of the Co^{II}-Substrate Radical Decay Reaction in Coenzyme B_{12}-Dependent Ethanolamine Ammonia-Lyase

By Chen Zhu

The transient decay reaction kinetics of 1,1,2,2-$^1H_4$- and 1,1,2,2-$^2H_4$-aminoethanol-generated Co^{II}-substrate radical pair catalytic intermediate in ethanolamine ammonia-lyase (EAL) have been measured by using time-resolved, X-band continuous-wave electron paramagnetic resonance (EPR) spectroscopy in frozen aqueous solution from 190 to 223 K. The decay is biexponential at temperature T<214 K (^{1}H) or <210 K (^{2}H), with fast and slow phase first-order rate constants $k_{obs,f}$ and $k_{obs,s}$, respectively. The decay becomes monoexponential at temperature $T\geq$214 K, with rate constant $k_{obs,m}$. The $k_{obs,f}$ and $k_{obs,m}$ values adhere to the same linear relation on a ln$k$ versus T^{-1} (Arrhenius) plot, and therefore represent the same mechanism, which is proposed to be the native forward reaction of the substrate radical through the radical rearrangement step. The ^{1}H/^{2}H isotope effect (IE) on $k_{obs,f}$ of 1.4±0.1 at 190 $\leq T\leq$207 K is assigned to an α-secondary hydrogen kinetic IE on the rearrangement step. The $k_{obs,s}$ values obey a different Arrhenius relation, and display an inverse kinetic IE (0.8±0.1). The slow decay phase is proposed to be associated with the forward reaction, but with a different rate determining step. The ^{1}H/^{2}H IE on $k_{obs,m}$ increases continuously at T>210 K, to 2.1±0.1 at 223 K. A three-state (substrate radical, product radical, diamagnetic products), two-step [rearrangement, and subsequent hydrogen atom transfer, (HT)] model is used to generate a consistent fit to the temperature dependence of the $k_{obs,f}$, $k_{obs,m}$ values and IEs at low

temperature with k_{cat} values and IEs at 277 K (IE=5.5) and 293 K (IE=7.8). The model shows that the four decade-old paradox of $^{1}H/^{2}H$ and $^{1}H/^{3}H$ IEs in EAL, and the temperature dependent IE, are caused by a significant negative activation entropy for the HT step, relative to rearrangement. The bifurcation of the decay kinetics at $207<T<214$ K is addressed by measuring the detailed (1 K intervals) temperature dependence of samples prepared with only slow phase population. The steep ln$k$ versus T^{-1} dependence is discontinuous with the fast and slow phase relations. The origin of the kinetic bifurcation is proposed to arise from a protein dynamical transition, which is coupled to the core adiabatic reaction in EAL.

Enzyme on Ice: Kinetic and EPR Spectroscopic Characterization of the Co^{II}-Substrate Radical Decay Reaction in Coenzyme B_{12}-Dependent Ethanolamine Ammonia-Lyase

By

Chen Zhu
B.S., Nankai University, China, 2003

Advisor: Kurt Warncke, Ph.D.

A dissertation submitted to the Faculty of the
James T. Laney School of Graduate Studies of Emory University
in partial fulfillment of the requirements for the degree of
Doctor of Philosophy
in Physics
2010

Acknowledgments

I gratefully acknowledge my Ph.D. advisor Dr. Kurt Warncke, who continuously supports, inspires and guides me during my Ph.D. study. Without his supervision and persistent help, this dissertation would not have been possible. I also acknowledge Dr. Boi Hanh (Vincent) Huynh for his critical advice and help in my research. I sincerely thank Dr. Laura Finzi, Dr. Keith Berland, and Dr. Dale E. Edmondson for their insightful comments on my committee meetings and dissertation.

I wish to express appreciation to the faculty, staff, and fellow students in the Physics Department. They made my life at Emory an invaluable memory. Special thanks go to Dr. Jeffrey Canfield, who taught me a lot on EPR experimentation as I joined Dr. Warncke's lab.

I would also like to thank my parents, Dad Xiuqi Zhu, Mom Yingping Zheng. They were always supporting me with their best wishes.

Finally, I would like to thank my wife, Tian Tang. She was always there encouraging me, and stood by me through the good times and bad.

Table of Contents

List of Figures

Page

List of Schemes

List of Tables

Page

Chapter I

Introduction

1.1 Coenzyme B_{12}-dependent Enzymes

1.1.1 The Coenzyme B_{12}-dependent Enzyme Superfamily

The coenzyme B_{12} (adenosylcobalamin or AdoCbl)-dependent enzymes perform atom migration or elimination reactions,[1-3] and can be divided into three classes. Class I and III are mutases, and class II are eliminases. Class I coenzyme B_{12}-dependent enzymes include glutamate mutase[7,8], 2-methylene-glutarate mutase[9,10], isobutyryl-CoA mutase[11] and methyl-malonyl-CoA mutase[12], which catalyze carbon skeleton rearrangement reactions. Class III enzymes include 2,3-aminomutase[13] and ornithine 4,5-aminomutase[14], which catalyze amino migration reactions. Class II coenzyme B_{12}-dependent enzymes include ethanolamine ammonia lyase (EAL)[4,15], propane-1,2-diol dehydratase[16], glycerol dehydratase[17] and ribonucleotide reductase[18]. Eliminases perform migration of hydroxyl or amino group during their catalysis on substrates. However, they eliminate water or ammonia in the final product, instead of promoting the re-attachment of the group at the adjacent carbon atom, as in the Class III mutases.

Members of the coenzyme B_{12}-dependent enzyme superfamily utilize AdoCbl for the formation of highly reactive free radical. Their main unique ability is to enhance the cleavage of cobalt-carbon (Co-C) bond in AdoCbl by 10^{11} fold.[19-21] The homolytic dissociation energy of Co-C bond in AdoCbl is reduced to < 15 kcal/mol from 30 kcal/mole by the coenzyme B_{12}-dependent enzymes.[3] The existence and accumulation of free radical intermediates during enzyme catalysis makes the electron paramagnetic resonance (EPR) spectroscopy technique a powerful tool for characterizing enzyme mechanism. In this dissertation, we investigate the catalytic mechanism and kinetics of EAL.

1.1.2 Coenzyme B_{12} (Adenosylcobalamin)

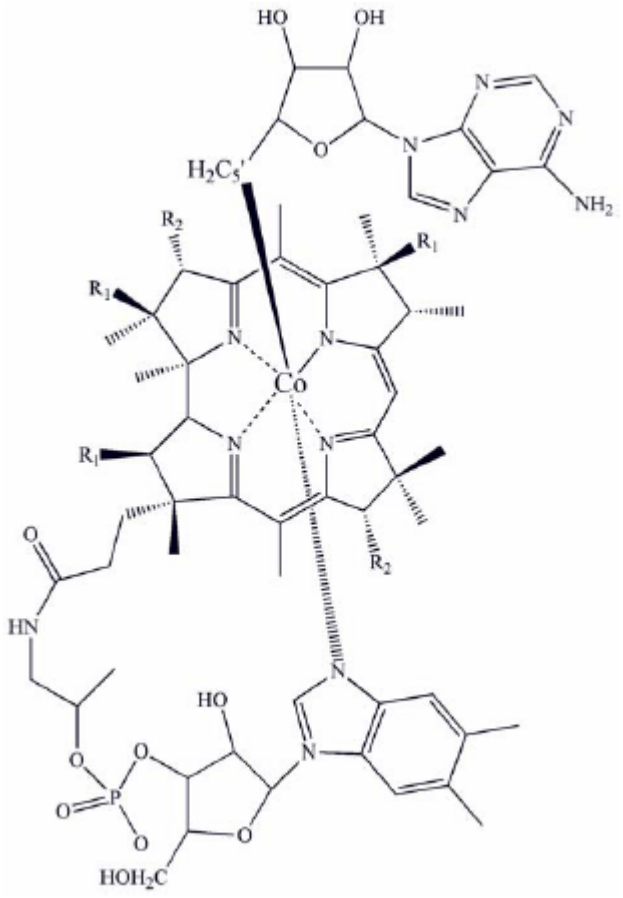

Figure 1.1: Structure of coenzyme B_{12}.

Vitamin B_{12} (cyanocobalamin), coenzyme B_{12} (adenosylcobalamin or AdoCbl) (Figure 1.1) and their analogues are the only biomolecules discovered that contain a stable carbon-metal bond.[22,23] The first X-ray crystal structure of Vitamin B_{12} was resolved in the lab of Dorothy Hodgkin in 1955.[22] Here, we focus on the coenzyme B_{12}, a water soluble molecule. The most noticeable feature of the molecule is the roughly planar corrin ring system, which consists of four linked pyrrole subunits. The cobalt ion is

equatorially coordinated to the nitrogen of each pyrrole ring. The ligands, 5,6-dimethyl-benzimidazole and 5'-deoxyadenosyl, are axially coordinated to the cobalt ion from the α-face and β-face of the corrin ring, respectively.[24]

1.1.3 Survey of Coenzyme B_{12}-dependent Enzyme, Ethanolamine Ammonia-lyase (EAL)

Scheme 1.1: Simplest scheme of EAL enzyme catalysis.[6] X represents the amino group that is eliminated in the final product.

EAL, originally discovered in a *Clostridium* species,[25,26] catalyzes coenzyme B_{12} dependent conversion of ethanolamine or (*S*)- or (*R*)-2-aminopropanols to ammonia and the corresponding aldehyde.[5] The catalysis is an isomerization process, as shown in Scheme 1.1, where the amino group (X) from C2 position exchanges for the hydrogen atom from C1 position.[6] The amino group is then eliminated from the product. The turnover rates of EAL on ethanolamine, (*S*)-2-aminopropanol, and (*R*)-2-aminopropanol have been reported as 30-50 s^{-1}, 0.12-0.27 s^{-1}, and 0.067 s^{-1} at room temperature,

respectively.[27-29] EAL also shows stable activity between pH 6.6 and pH 8.2,[4] as shown in Figure 1.2.

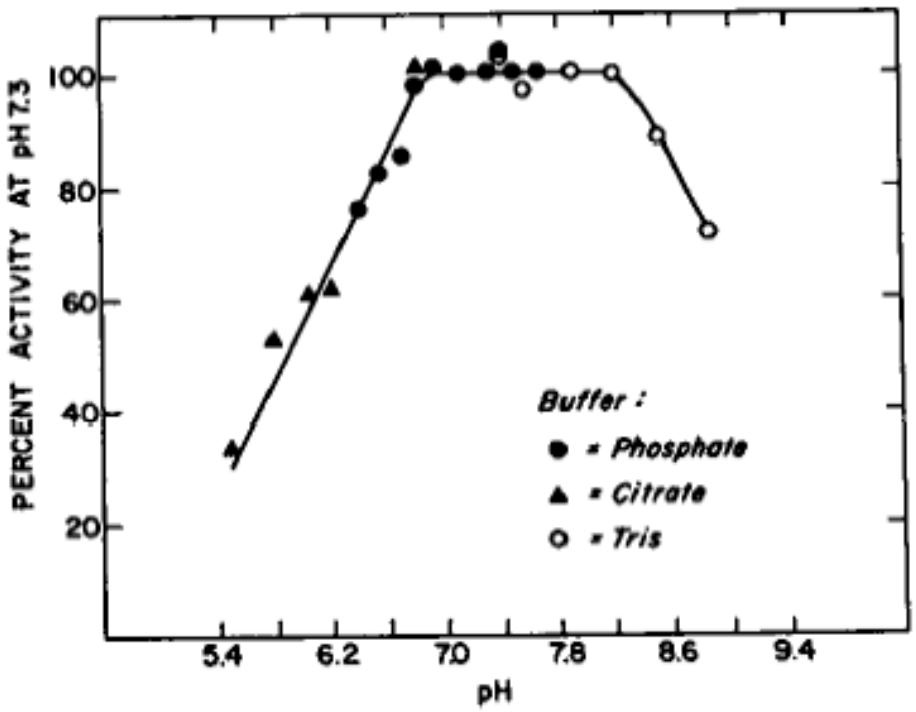

Figure 1.2: The activity of EAL versus pH.[4]

The native EAL molecule is an $\alpha_6\beta_6$ oligomer, with a molecular mass of approximately 500 kDa. The α and β subunits are the 453-residue, 49.4 kDa EutB protein subunit and the 286-residue, 32.1 kDa EutC protein subunit, respectively.[30-32] Kinetic simulations indicate that there are six active sites per oligomer,[33] which is supported by stoichiometric single turnover inactivation of EAL by hydroxyethylhydrazine (HEH).[34-36] Substrate binds to the EutB protein subunit, whose 3D structure has been proposed by comparative modeling method.[37] The X-ray crystallographic structure of EutB from *Listeria monocytogenes* was reported recently.[38] These results provide better

understanding about the structure of EAL, and the interactions among substrate, AdoCbl and EAL.

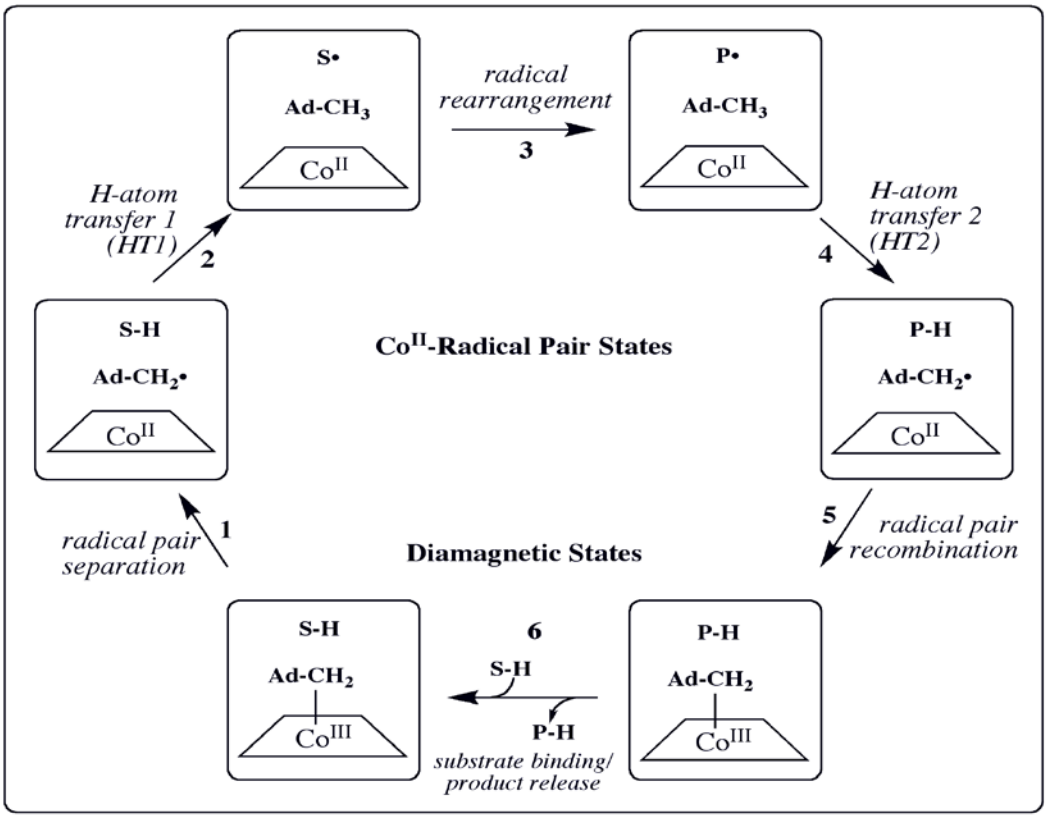

Figure 1.3: Minimal mechanism of catalysis for coenzyme B_{12}-dependent ethanolamine ammonia-lyase (EAL).[5] The forward direction of reaction is indicated by arrows. The steps are: (1) radical pair separation, (2) first hydrogen atom transfer (HT1), (3) radical rearrangement, (4) second hydrogen atom transfer (HT2), (5) radical pair recombination and (6) product release/substrate binding. Substrate-derived species are designated S-H (bound substrate), S$^{\bullet}$ (substrate radical), P$^{\bullet}$ (product radical), and P-H (diamagnetic products). The 5'-deoxyadenosyl axial ligand is represented as Ad-CH_2 in the intact coenzyme, and as Ad-$CH_2^{\bullet}$ (5'-deoxyadenosyl radical) or Ad-CH_3 (5'-deoxyadenosine) following cobalt-carbon bond cleavage. The cobalt ion and its formal oxidation states are depicted. The corrin ring is represented by a square and the dimethylbenzimidazole α-axial ligand of the coenzyme are not shown for clarity.

The minimum catalytic mechanism for EAL is shown in Figure 1.3.[5,39] The binding of aminoethanol to the holoenzyme triggers the homolytic cleavage of the cobalt-carbon bond in coenzyme B_{12}, generating S = ½ Co^{II} and proposed S = ½ 5'-deoxyadenosyl radical. The 5'-deoxyadenosyl radical migrates to the substrate binding site, and abstracts a hydrogen from the C1 carbon of the substrate (HT1), forming 5'-deoxyadenosine and the substrate radical (S˙).[40-42] The substrate radical rearranges to the product radical (P˙) by the migration of the amino group.[43,44] A hydrogen atom is then transferred from 5'-deoxyadenosine to the product radical (HT2), yielding a diamagnetic product and the 5'-deoxyadenosyl radical. Finally, the 5'-deoxyadenosyl radical recombines with Co^{II} to regenerate coenzyme B_{12}, and products acetaldehyde and ammonia are released, to complete catalytic cycle.[26,45] The molecular structure for the aminoethanol substrate, substrate radical, product radical and product are shown in Scheme 1.2.

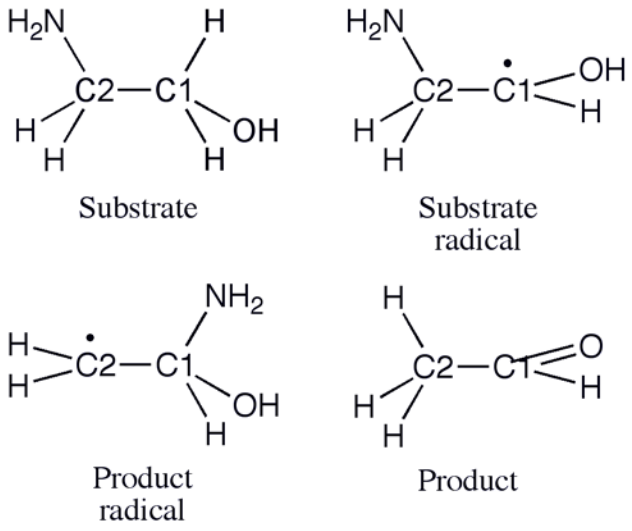

Scheme 1.2: Molecular structures of substrate, substrate radical, product radical and product.

The mechanism of EAL catalysis has been extensively studied.[4,5,46,47] However, there are still unresolved issues in EAL catalysis. There is controversy regarding whether the rearrangement step or the HT2 step is the rate limiting step.[48,49] The accumulation of the Co^{II}-substrate radical pair during the steady-state turnover of EAL on aminoethanol implies that the radical rearrangement step is at least partially rate-limiting for the catalytic cycle at room temperature. This observation is consistent with the expression of an aminoethanol $^{14}N/^{15}N$ steady-state kinetic IE of 1.0017 on V/K_M (V, maximum velocity; K_M, Michaelis constant), which is proposed to arise from C2-N bond cleavage in the rearrangement step.[48,50] However, the following hydrogen isotope effects suggest that the hydrogen transfer, especially the HT2 step, is the rate limiting step for steady-state turnover: (a) a steady-state $^1H/^2H$ isotope effect on k_{cat} of 7.4[4] or 7.5,[29] and (b) a $^1H/^3H$ of 100 on hydrogen transfer from C5'-methyl group to the product radical.[4,5] The anomalously large $^1H/^3H$ IE relative to the $^1H/^2H$ IE has remained unexplained for nearly 40 years.[5,43] Further, the proposed Co^{II}-product radical pair and Co^{II}-5'-deoxyadenosyl radical pair have never been trapped and detected. The cryotrapping of the Co^{II}-substrate radical pair, and the subsequent observation of its decay, at annealing temperatures of 190 to 223 K, have provided a unique opportunity to isolate the radical rearrangement step and the HT2 step for detailed kinetic study, allowing the outstanding mechanistic issues to be addressed, and resolved. In addition, the studies on Co^{II}-substrate radical pair decay at low temperatures (190 to 223 K) provide new insight into the protein dynamical features of radical rearrangement catalysis in EAL.

1.2 EPR Spectroscopic Studies of EAL

The Co^{II}-substrate radical pair catalytic intermediate accumulates during the steady state turnover of EAL on the substrate ethanolamine or 2-aminopropanol.[40,51] The Co^{II}-substrate radical pair can be cryotrapped and investigated by EPR spectroscopy. Following is a brief summary of EPR spectroscopy, and EPR studies of EAL.

1.2.1 Continuous-wave (CW) EPR Spectroscopy

Electron paramagnetic resonance (EPR) or electron spin resonance (ESR) spectroscopy is a technique that detects unpaired electrons in chemical species, such as free radicals or transition metal ion.[52,53] It was first discovered by Yevgeny Zavoisky, in 1946 and later, independently by Brebis Bleaney. The basic physical concepts of EPR and nuclear magnetic resonance (NMR) are similar. Electron spin transitions are measured in EPR spectroscopy, while nuclear spin transitions are measured in NMR spectroscopy. EPR spectroscopy is much more sensitive compared to NMR, because electron magnetic moment is three orders of magnitude larger than nuclear magnetic moment, and is widely used in chemistry, physics, biology and medicine in systems that have unpaired electrons.[54,55] Stable molecules have all electrons paired, and do not yield EPR signals,[56] which allows EPR to specifically detect the paramagnetic species without interference from other molecules in the system.

To explain the origin of the EPR signal, a simple free electron case is considered first. An electron possesses a magnetic moment, which is proportional to its spin angular momentum $\boldsymbol{S}$ = ½. In the presence of an external magnetic field B_0, the electron magnetic moments aligns either parallel (m_s = -½) or antiparallel (m_s = +½) to the magnetic field. The energy of the electron is expressed as:

$$H = g\mu_B \vec{B} \cdot \vec{S} = g\mu_B B_0 m_s \quad (1.1)$$

where g is the electron g-factor, and μ_B is the Bohr magneton.

In an external field, the energy degeneracy of the two electron states (m_s = ±½) is lifted. This phenomenon is called the Zeeman effect. The energy splitting, ΔE, between the two states is:

$$\Delta E = g\mu_B B_0 \quad (1.2)$$

At thermodynamic equilibrium, the ratio of the populations of the two states can be described by the Maxwell-Boltzmann equation as:

$$N_{+\frac{1}{2}} / N_{-\frac{1}{2}} = \exp(-\frac{\Delta E}{RT}) \quad (1.3)$$

Transition between the two m_s states is induced by absorbing or emitting electromagnetic radiation when the frequency v satisfies the following relation:

$$hv = g\mu_B B_0 \quad (1.4)$$

where h is the Plank constant, and v is the electromagnetic frequency.

The ratio of the populations of the two states approaches to unity under saturating electromagnetic radiation with appropriate frequency given by equation 1.4. However, the ratio given by equation 1.3 is less than unity at thermal equilibrium. Electron spin-lattice relaxation causes spins to return to m_s = -½ states from m_s = +½ states, and overall absorption of electromagnetic radiation is observed. In standard EPR spectroscopy measurements, the electromagnetic frequency in equation 1.4 is fixed, and the magnetic field is swept from low magnetic field to high magnetic field. A method of magnetic

modulation with phase sensitive detection is utilized to minimize the background noise. The EPR signal is measured as the first-derivative of absorption of electromagnetic radiation as a function of magnetic field.

The section above only discusses EPR absorption of free electrons. However, the energies of the eigen-states of unpaired electrons in molecules are usually affected by its environment, such as magnetic nuclei, or other unpaired electrons, nearby. The Hamiltonian then has the following form:

$$\boldsymbol{H} = \mathbf{EZ} + \mathbf{NZ} + \mathbf{HF} + \mathbf{EX} + \mathbf{EDIP} \quad (1.5)$$

Where EZ, NZ, HF, EX and EDIP represent electron Zeeman term, nuclear Zeeman term, electron-nuclear hyperfine coupling term, electron spin-spin isotropic exchange term and electron spin-spin dipolar interaction term, respectively.

1.2.2 Continuous-wave EPR Studies of EAL

In the coenzyme B_{12}-dependent EAL, there are three possible paramagnetic states in the minimal mechanism, which are Co^{II}-5'-deoxyadenosyl radical pair, Co^{II}-substrate radical pair and Co^{II}-product radical pair. Studies show that only the Co^{II}-substrate radical pair accumulates above the EPR detectable level during turnover of EAL.[40,41,57] The previous continuous-wave EPR simulation shows that Co^{II}-C1 separation for (*S*)-2-aminopropanol-generated Co^{II}-substrate radical pair is 11 ± 1 Å,[41,42] whereas the Co^{II}-C1 separation is 9.3 ± 1 Å for aminoethanol-generated Co^{II}-substrate radical pair.[50,58,59] The separation for (*S*)-2-aminopropanol-generated substrate radical is approximately 2 Å further away from the Co^{II} radical, compared to that of aminoethanol-generated substrate

radical. This is proposed to arise from steric interaction of the protein with the extra methyl group in aminopropanol.

1.2.3 Electron Spin Echo Envelope Modulation (ESEEM) Spectroscopy

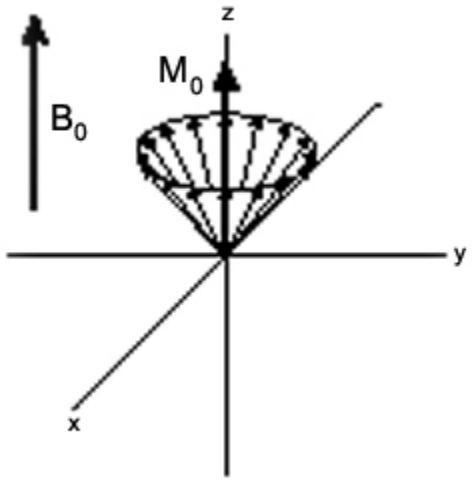

Figure 1.4: The Larmor precession and the resultant stationary magnetic moment M_0.

Electron spin echo envelope modulation (ESEEM) is a magnetic resonance effect that is observed in pulsed-EPR experiments.[60,61] It was discovered by Bloch that nuclear induction can be observed by applying a radio frequency magnetic field at resonance perpendicular to the constant magnetic field.[62,63] Hahn in 1950 showed that pulses of intense radio frequency, separated by time, τ, instead of continuously applying radio frequency, can induce spin echoes after a time τ, following the second pulse.[64] A simple interpretation of pulsed-EPR is shown as follows.

As an electron spin with magnetic moment μ_e is placed in an external magnetic field B_0 (along the *Z*-axis), it performs Larmor precession along the *Z*-axis with a frequency of ω_L:

$$\omega_L = \frac{2\mu_e}{\hbar} B_0 \tag{1.6}$$

In an ensemble of electrons, the transverse components of the magnetic moment cancel, which results in a stationary magnetic moment M_0 that is aligned along the Z-axis, as shown in Figure 1.4.

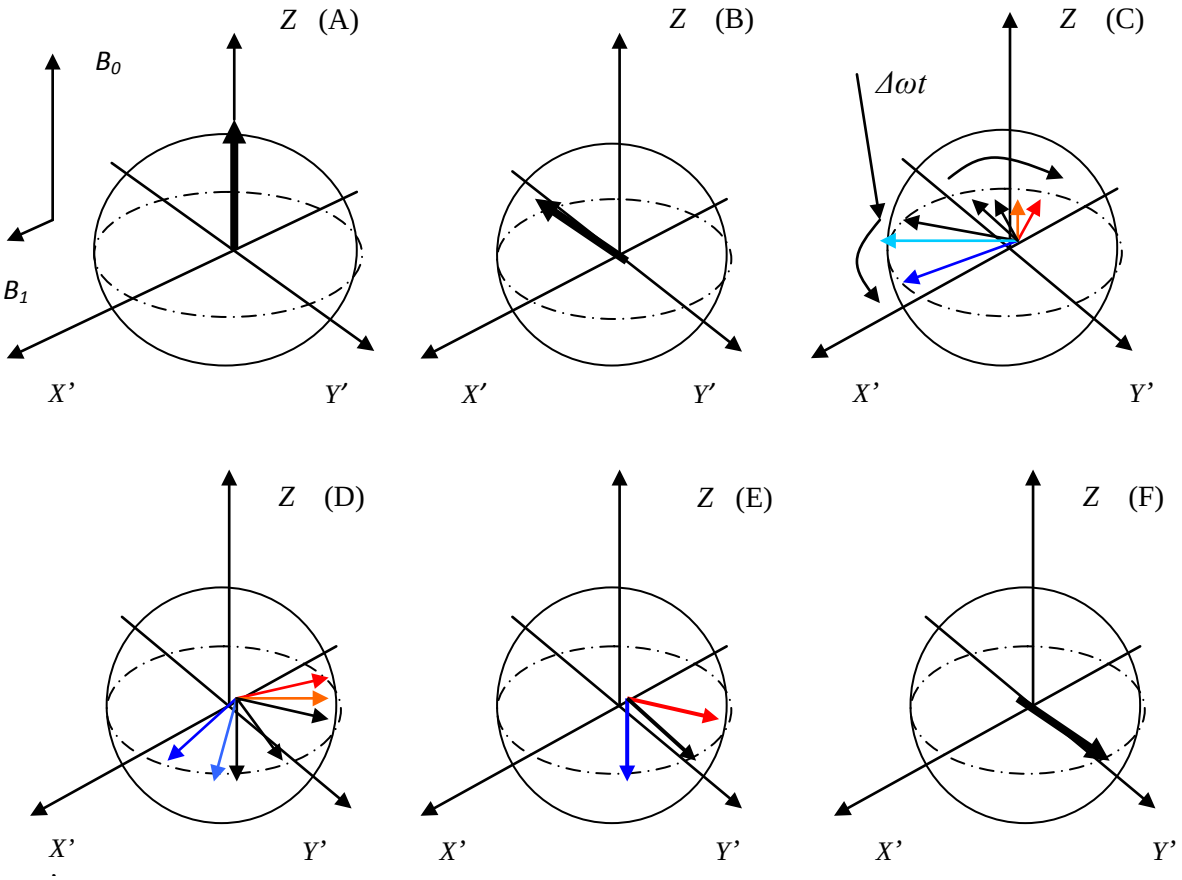

Figure 1.5: Magnetization vector manipulation by two-pulse EPR.

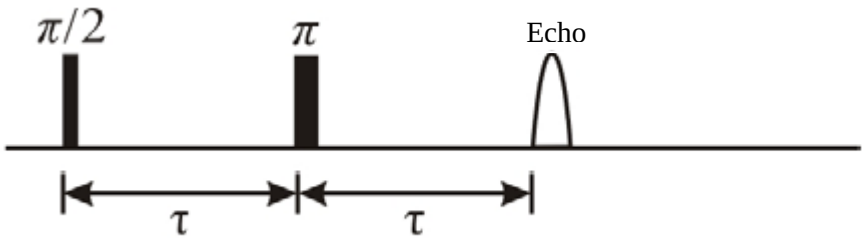

Figure 1.6: Pulse timing diagram for the two-pulse ESEEM.

A rotating magnetic field, B_1 of frequency ω_L is applied, perpendicular to B_0, where $B_1 << B_0$. Figure 1.5 shows the process of simplified schematic 2-pulse electronic spin echo. The lab *X*-, *Y*-axes are transformed into *X'*- and *Y'*-axes, with rotating frequency ω_L about the *Z*-axis. From (A) to (B) in Figure 1.5, a microwave field pulse is applied, and M_0 rotates about the *X'*-axis to *Y'*-axis. From (B) to (C), the net magnetic moment M_0 fans out for a time interval, τ, which arises from the slightly different magnetic field that sub-populations of electrons experience, from interactions with nearby magnetic nuclei, and other electrons. From (C) to (D), another intense microwave pulse is applied, which is twice as long as the first pulse, and the de-phased electron magnetic moments are flipped by the angle, π, around the *X'*-axis. After the second pulse, the magnetic moments begin to re-focus. At a time interval, τ, after the second pulse, the macroscopic magnetic moment reaches a maximum, and the electron spin echo can be observed. Figure 1.6 shows the schematic timing diagram for two-pulse EPR experiments. Basically, ESEEM measures the echo amplitudes as a function of τ, which contains the information of local magnetic field shift of electrons that arise from the hyperfine and super-hyperfine couplings with nearby magnetic nuclei. Thus, pulsed-EPR is sensitive to the local environment of the electron spin. Besides two-pulse ESE experiment discussed above,

the three-pulse-ESE experiment is also widely used, which we do not explore in detail here.

1.2.4 ESEEM Studies of EAL

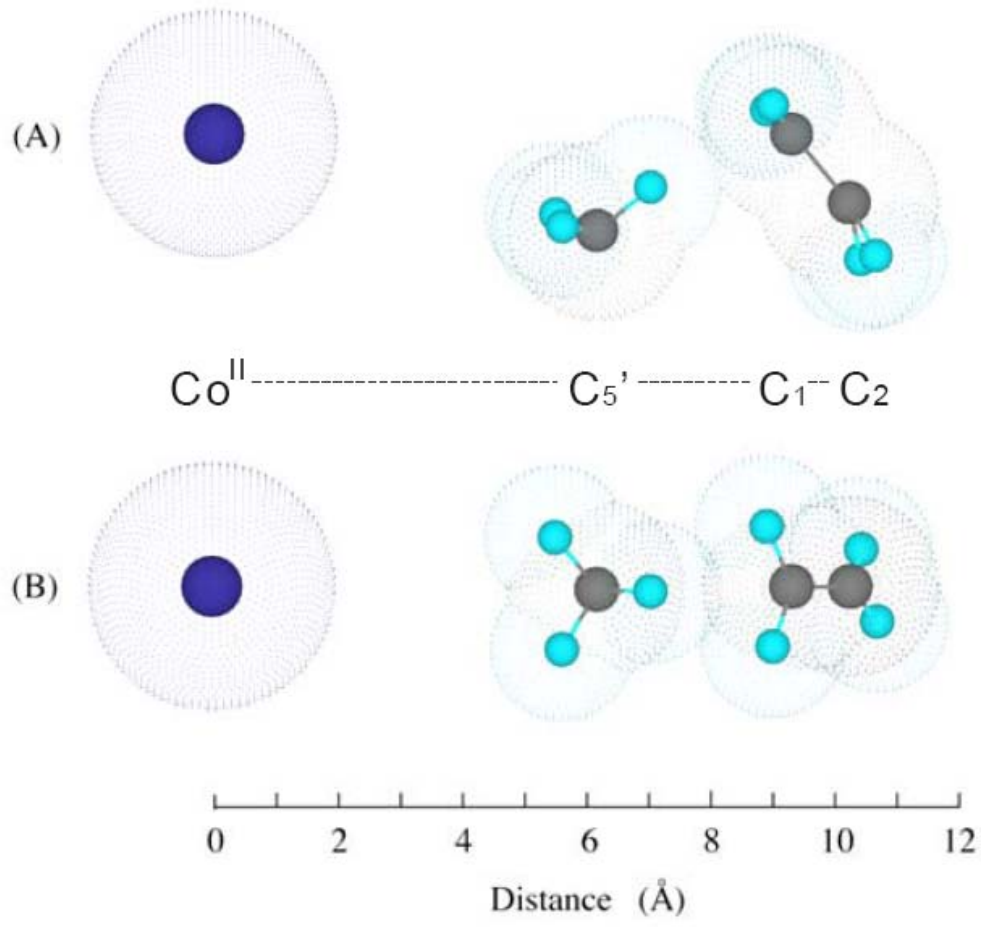

Figure 1.7: Model for the structure of the reactant center in the active site of the Co^{II}-substrate radical pair state in ethanolamine ammonia-lyase. (A) View along the line perpendicular to the Co^{II}-C1-C2 plane. (B) View after $\pi/2$ rotation about the Co^{II}-C1 axis, relative to view in (A).

Aminoethanol-generated and (*S*)-2-aminopropanol-generated substrate radical catalytic intermediates have been studied by ESEEM spectroscopy.[42,59,65-68] The unpaired

electron in (*S*)-2-aminopropanol-generated substrate radical has been found to be delocalized onto a nitrogen from protein backbone, but not the substrate nitrogen, by performing substrate $^{14}N/^{15}N$ ESEEM.[65,69] Taking together the distance information for Co^{II}-C1, obtained by CW-EPR simulations, and orientation-selection and multi-frequency powder ESEEM studies on the Co^{II}-substrate radical pair intermediates, a three dimensional model of the active site reaction center, including substrate, C5'-methyl group and Co^{II} has been developed.[68,70] Figure 1.7 shows the structure of the active site reaction center. In this model, C5' is between Co^{II} and C1, and the distance between Co^{II} and 5' radical reaction center is approximately 6.3 Å. The model also suggests that formation of Co^{II}-substrate radical is mediated by the migration of the C5' radical reaction center of the 5'-deoxyadenosyl group over 4 ± 1 Å, from the position that is 2 Å from the cobalt atom to the position near substrate radical.[68] Figure 1.8 shows a diagram of active site reaction center of aminoethanol-generated Co^{II}-substrate radical pair with full cofactor included.

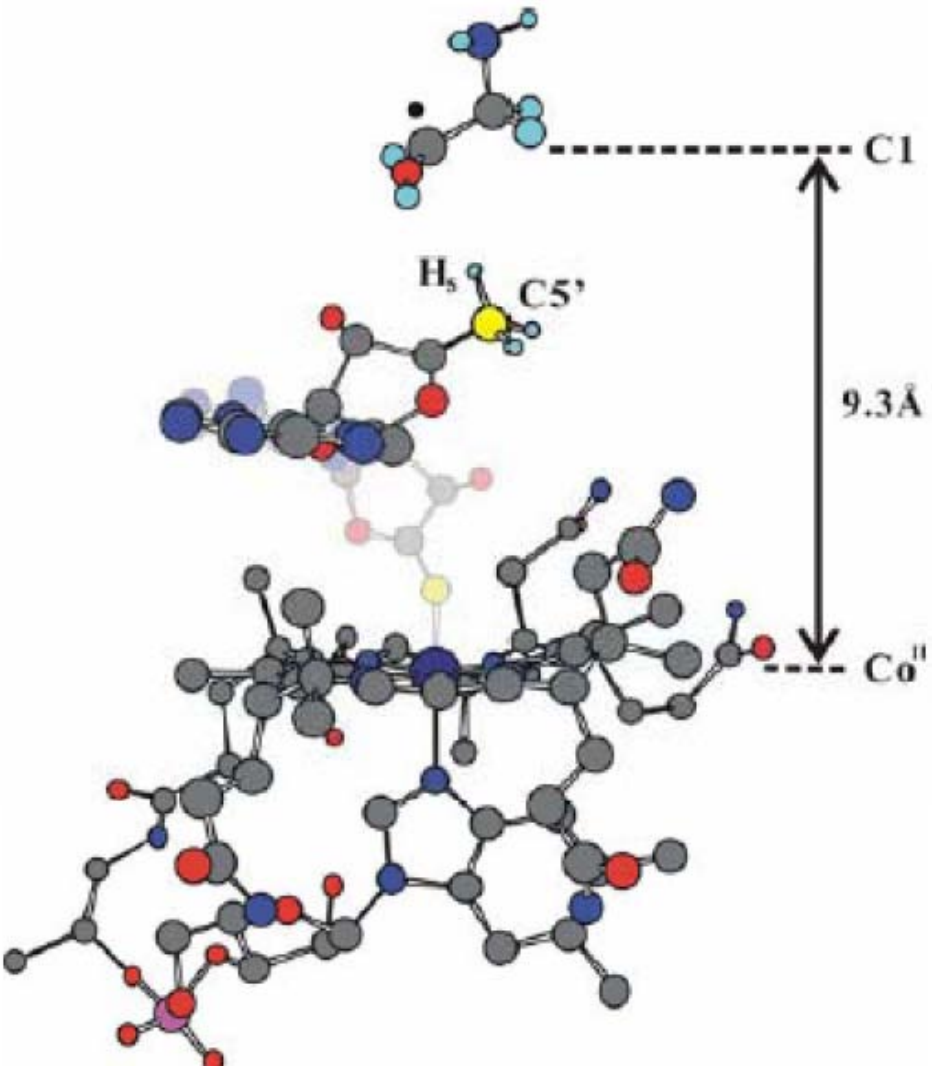

Figure 1.8: Diagram of C1-Co^{II} radical pair separation in Co^{II}-substrate radical pair intermediate state of EAL.

1.3 The "Glass Transition" in Protein Dynamics

The dynamical properties of proteins experience dramatic changes within the temperature range of 180 to 220 K.[71,72] This range overlaps the range of annealing temperatures (190 to 223 K), used for Co^{II}-substrate radical decay kinetics measurements in EAL. The atomic motion of the iron atom in sperm whale metmyoglobin as a function of temperature, which was measured by Mössbauer spectroscopy, implied unusual

temperature-dependent protein dynamics at approximately 200 to 220 K.[73] Atomic motion of atoms in proteins has been investigated by the inelastic neutron scattering technique on the 0.1 to 100 ps time scale.[74] The motions of myoglobin below approximately 200 K can be modeled essentially by only vibrational motion. Above 200 K, there is a dramatic dynamic transition, which is proposed to arise from transitions between at least two conformational states.[74] The mean-square displacement measurement on the back-bone of myoglobin as a function of temperature showed a discontinuity of slope at around 200 K by X-ray crystallography, which is consistent with the mean-square displacement of the heme iron measurement by Mössbauer spectroscopy as a function of temperature.[75] Simulation of molecular dynamics of hydrated myoglobin also shows that atomic fluctuations of carboxy-myoglobin protein exhibit a glass-like transition at approximately 210 K, which is in agreement with the neutron scattering experiments.[76]

An aqueous environment is necessary for normal protein function, and the surfaces of a protein are covered with a layer of solvent molecules, which is called the hydration layer, or shell. Whether the protein dynamical transition is caused by the transition in protein, the bulk solvent, the bound solvent or a combination of them, has been addressed by many investigators.[77-80] Infrared spectroscopy and calorimetry have been employed to study the water of hydration in myoglobin crystals and solutions.[77] A broad transition in mobility and specific heat of hydration water between 180 and 207 K has been found, and the correlation between the solvent mobility transition and protein transition is proposed to arise from protein-water hydrogen-bond network.[77] Further studies on protein bound solvent shows that bound water molecules on protein surfaces can be categorized into

several classes, from completely disordered water molecules, to well-ordered water molecules that are always found in the same position in nearly all structures of proteins.[79] The well-ordered water molecules are found to have comparable Debye-Waller factors as those of well-ordered protein atoms, and are proposed to contribute to the stability of protein structures.[79] Using a Nose-Hoover thermostat to differentially regulate the temperature of the solvent and protein, simulation studies imply that solvent mobility is the dominant factor for the atomic fluctuations of protein above 180 K.[81] However, experiments by Lee and Wand, which used NMR relaxation methods to study the temperature dependent dynamics of side chains in a calmodulin-peptide complex, suggest that internal motion of the protein alone can explain the temperature dependence of atomic fluctuation observed by neutron scattering.[82] The underlying mechanism of the glass transition in protein dynamics remains unsolved.

In contrast to the conclusion of the above studies, analysis by Sokolov argues that the sharp rise of the atomic mean-square displacement of hydrated protein at $T \sim$ 200-230 K, as measured by neutron scattering, does not arise from the protein dynamical transition, but comes from the protein's relaxation time reaching the accessible frequency window of neutron scattering spectra.[83,84] Experiments combining dielectric and neutron scattering data over an extremely broad frequency range, performed by Sokolov and co-workers, demonstrates that protein's structural relaxation shows smooth temperature dependence over the temperature range from 180 to 295 K.[84,85]

The investigation of the low temperature dynamical turnover of protein by using both reaction-kinetic and spectroscopic assessments, provides an opportunity to resolve the discrepant views about the nature, functional significance, or even existence, of a

dynamical transition in proteins. The Co^{II}-substrate radical pair decay reaction in the temperature range of 190-223 K offers a unique system in which we address these issues.

1.4 Outline of Dissertation

In this dissertation, we have investigated the kinetic mechanism of the decay of the cryotrapped Co^{II}-substrate radical pair, and contributions of protein dynamics in frozen aqueous solution, by using real-time EPR spectroscopy.

Chapter II introduces the low temperature, solid state system, and develops the model for the kinetic decay of natural abundance, ^{1}H-substrate-derived Co^{II}-substrate radical pair from 190 to 223 K. The search for paramagnetic intermediates other than Co^{II}-substrate radical pair is also described. The role of protein dynamics in the Co^{II}-substrate radical pair decay is discussed.

Chapter III further characterizes the radical rearrangement reaction from 190 to 223 K, and identifies the rate limiting step of the turnover of EAL on ethanolamine, by performing decay experiments for 1,1,2,2-$^{2}H_4$-ethanolamine-derived Co^{II}-substrate radical pair from 190 to 207 K, and comparing the results to the ^{1}H-substrate radical results.

In Chapter IV, kinetic isotope effects (IE) on the decay of $^{1}H/^{2}H$ substrate radical have been studied from 190 to 223 K, and we propose a three-state, two-step model to resolve the $^{2}H/^{3}H$ steady-state kinetic isotope effect paradox, which has been existed for nearly four decades.

In Chapter V, studies of substrate radical decay over the transition temperature range (207-214 K) with 1 K increment have been performed. We discuss the mechanism of the

dynamical transition, and partitioning of the monoexponential population into the fast and slow decay populations.

In Chapter VI, we propose and discuss a reverse-reaction experiment to trap and detect the proposed Co^{II}-product radical pair.

Chapter II

Characterization of the Co^{II}-[^{1}H]-substrate Radical Pair Decay Kinetics in Frozen Aqueous Solution from 190 to 223 K

2.1 Background and Introduction

2.1.1 Survey of Synchronization of Biomolecular Reactions

The molecular mechanism of the core reactions in enzyme catalysis are often complicated by the kinetic complexity and asynchrony of steady-state turnover. There are generally three methods that have been developed to investigate single, or short sequences of, reaction steps in metalloproteins by synchronizing reaction initiation. These three methods usually involve formation and spectroscopic monitoring of reaction intermediates in solid state samples at cryogenic temperatures. The first method is cryoreduction, in which reduction of a previously redox-poised metal center in protein is induced by γ-irradiation of a frozen sample at 77 K.[86,87] The perturbed non-equilibrium, reduced center metal center is thermally activated by graded-annealing, which relaxes through protein conformational changes, electron transfer, or reaction sequence. This technique has been applied to heme[86-95] and non-heme[96-99] iron proteins. The second method is the low temperature photodissociation of metal ligand complexes. The prototype is optically monitored migration and rebinding of carbon monoxide (CO) or dioxygen (O_2) to the heme iron in myoglobin (Mb) after photolysis of the carboxy- or oxy-heme state in frozen solutions at temperatures from 10 to 270 K.[100,101] This technique has been developed further with Mb[102-105], and has been applied to other heme[106-108] proteins and metalloproteins.[109,110] The third method is to prepare and cryotrap a kinetically unstable enzyme state, which can be promoted to relax by raising the temperature to allow annealing.[111] This chapter of the dissertation reports an experiment of the third type. Continuous-wave, full-spectrum EPR is used to monitor the relaxation of the Co^{II}-substrate radical pair intermediate at the annealing temperature in EAL from

Salmonella typhimurium. The experiment aims at characterizing the mechanistic features of the core reactions of EAL catalysis, and lays down the foundations for future work.

2.1.2 Temperature Step Initiation of the Relaxation of Cryotrapped Co^{II}-substrate Radical Pair

During the steady-state turnover of EAL on aminoethanol at room temperature, the Co^{II}-substrate radical accumulates as the only detectable paramagnetic intermediate,[112] and this state can be cryotrapped.[57,113] The minimal mechanism for the catalytic cycle of EAL is described in Chapter I and shown in Figure 1.3. The ^{3}H-labeled coenzyme B_{12} experiments suggests that the HT1 step is an irreversible step,[6] which is supported by $^{1}H/^{2}H$ isotope effect (IE) of substrate radical decay shown in the Chapter III.

In this chapter, the cryotrapped aminoethanol-generated Co^{II}-substrate radical is shown to relax to an EPR-silent state following temperature step to $T \geq 190$ K from a sample holding temperature of 160 or 180 K. The decay of the Co^{II}-substrate radical has been measured by full-spectrum CW-EPR. The time scale of the substrate radical decay in the temperature range 190 to 223 K is approximately 4×10^{5} to 1×10^{2} s. The instrument deadtime is $3.0\text{-}6.0 \times 10^{1}$ s, and the spectrum acquisition period is $1.0\text{-}2.0 \times 10^{1}$ s, which makes the measurement of substrate radical decay above 223 K implausible. Substrate binding and product release is restricted in the frozen, solid state of the aqueous solvent in the sample. Therefore, the decay of the Co^{II}-substrate radical pair is synchronized by cryotrapping the Co^{II}-substrate radical pair and initial temperature step.

2.1.3 Sample Preparations, Instrument Setup and Data Analysis

Enzyme was purified from the *Escherichia coli* overexpression strain incorporating the cloned *S. typhimurium* EAL coding sequence[30] essentially as described[114], with the exception that the enzyme was dialyzed against buffer containing 100 mM HEPES (pH 7.5), 10 mM potassium chloride, 5 mM dithiothreitol, and 10% glycerol[115]. Enzyme activity[116] was determined as described by using the coupled assay with alcohol dehydrogenase/NADH. The specific activity of the purified enzyme with aminoethanol as substrate was 20-30 µmol/min/mg.

Sample Preparation

Adenosylcobalamin (Sigma Chemical Co.), 1-^{13}C-aminoethanol and 1,1,2,2-$^{2}H_4$ aminoethanol (Cambridge Isotope Laboratories, Inc.), and natural abundance aminoethanol (Aldrich Chemical Co.) were purchased from commercial sources. The reactions were performed in air-saturated or anaerobic buffer containing 10 mM potassium phosphate (pH 7.5). The anaerobic samples were prepared by using the freeze-pump-thaw procedure, with argon gas backfill. All manipulations were carried out on ice under dim red safe-lighting. The final concentration of enzyme was 10-15 mg/ml, which is equivalent to 20 to 30 µM for a holoenzyme molecular mass of 500,000 g/mol [114], and an active site concentration of 120 to 180 µM, based on an active site/holoenzyme stoichiometry of 6:1 [33,35] (K. Warncke, unpublished). Adenosylcobalamin was added to 240 to 360 µM (2-fold excess over active sites).

The Co^{II}-substrate radical pair samples were prepared by using a procedure for fast cryotrapping of steady-state intermediate states in EAL.[117] Briefly, following manual mixing of the enzyme-adenosylcobalamin solution with substrate, the sample was loaded

into a 4 mm o.d. EPR tube, and the tube was plunged into liquid nitrogen-chilled isopentane (T = 150 K) to trap the Co^{II}-substrate radical pair state. The total elapsed time from mixing to isopentane immersion was 15 s.

Continuous-wave EPR Spectroscopy

EPR spectra were obtained by using a Bruker E500 ElexSys EPR spectrometer equipped with a Bruker ER4123 SHQE cavity. Temperature was controlled with a Bruker ER4131VT liquid nitrogen/gas flow cryostat system, with ER4121VT-1011 evaporator/transfer line, ER4121VT-1013 heater/thermocouple, and 26 liter liquid nitrogen reservoir. For the decay experiments, this temperature control system allowed rapid temperature step changes, relative to the more slowly responding Oxford ESR900 cryostat, and run times of up to 2 to 3×10^4 s, depending upon flow rate. Measurements were performed under dim light and with the EPR tubes inserted into the EPR resonator, which shielded the samples from direct exposure to light. Under these conditions with frozen samples, sample degradation owing to coenzyme photolysis is negligible.

Time-resolved EPR Measurements

EPR samples were held at a staging temperature of 160 K or 180 K in the ER4131VT cryostat system in the Bruker E560 spectrometer, and the microwave bridge was tuned. *T*-steps from 160 K or 180 K to the decay measurement temperatures of 190, 193, 197, 200, 203, 207, 210, 214, 217, 220 or 223 K were initiated by changing the E4131VT temperature set-point. Once the sample temperature stabilized at the set-point, the pre-set auto-tune/auto-scan mode of the spectrometer was triggered, and the sample was auto-

tuned at the high temperature set point, followed immediately by continuous spectrum acquisition. The time from initiation of the temperature step to the start of acquisition of the first spectrum was 3.0 to 6.0 × 10^1 s. The zero time of the decay was marked at the first collected EPR spectrum. The EPR spectra were acquired with a 6 to 24 s sweep time (2.56 ms time constant) depending on the points collected per spectrum. The reported temperatures represent the temperature at the sample, which was determined prior to each decay run by using an Oxford Instruments ITC503 temperature controller with a calibrated model 19180 4-wire RTD probe, which has ±0.3 K accuracy over the decay measurement temperature range. For measurements over the temperature range, 190 to 207 K, the ER4131VT cryostat/controller system provided a temperature stability of ±0.5 K over the length of the EPR sample cavity, as measured by using a thermocouple probe that was translated along the EPR tube axis to achieve different heights within a solution sample. The temperature was therefore stable to ± 0.5 K during each run. For measurements at 210, 214, 217, 220, and 223 K, the ER4121VT-1011 evaporator/transfer line and ER4121VT-1013 heater/thermocouple were replaced with the standard ER4131VT components, which increased the flow rate of the gas. This led to a more rapid change in temperature during the temperature step, and a desired diminished instrument deadtime. Under the faster gas flow in the ER4131VT system, the temperature stability was approximately ±0.7 K over the length of the EPR sample cavity.

Kinetic Analysis

EPR spectra acquired continuously during the decay were used directly in the kinetic analysis, or were averaged in blocks of from 2 to 20 spectra to increase the signal-to-

noise ratio (*SNR*), and the acquisition time was calculated as the average time for the block. For each EPR spectrum, the amplitude of Co^{II} was obtained from the difference between the baseline and the peak feature at $g \approx 2.3$, and the substrate radical amplitude was obtained from the difference between peak and trough amplitudes of the derivative feature around $g \approx 2.0$. All data processing programs were written in Matlab (Mathworks, Natick, MA). The observed decays were fitted to monoexponential (Eq. 2.1, $N = 1$) and biexponential (Eq. 2.1, $N = 2$) functions by using the following expression:

$$\frac{A(t)}{A(0)} = \sum_{i=1}^{N} A_i e^{-k_i t} \tag{2.1}$$

where $\frac{A(t)}{A(0)}$ is the normalized total amplitude, A_i is the normalized component amplitude ($\sum_{i=1}^{N} A_i = 1$ at $t = 0$), and k_i is the first-order rate constant. The data were also fitted to the power law function, where t_0 and n are adjustable parameters, as given by the following expression:

$$\frac{A(t)}{A(0)} = (1 + \frac{t}{t_0})^n \tag{2.2}$$

The power law function represents a distribution of monoexponential decay rates.[101] The fitting of the kinetics was performed by using Origin (OriginLab, Natick, MA).

Temperature-dependence of the First-order Rate Constant

The temperature dependence of the first-order rate constant, *k*, is given by the Arrhenius expression:[118]

$$k(T) = Ae^{\frac{-E_a}{RT}} \tag{2.3}$$

where E_a is the activation energy, R is the gas constant, and A is a prefactor that represents the value of k as $E_a \rightarrow 0$. In a plot of ln$k$ versus T^{-1} (Arrhenius plot), the intercept of the linear relation is given by ln$A$ and the slope is given by $-E_a/R$.

2.2 Results

2.2.1 EPR Spectrum of the Co^{II}-substrate Radical Pair

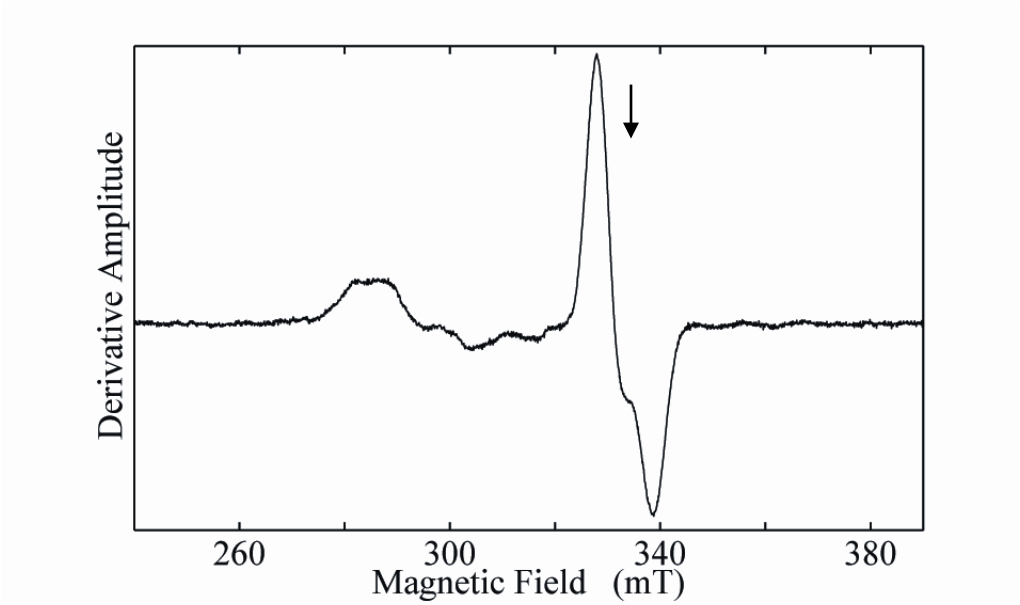

Figure 2.1: X-band continuous-wave EPR spectrum of the Co^{II}-substrate radical pair intermediate generated with aminoethanol and cryotrapped in EAL. The free electron resonance position at g = 2.0 is shown by the arrow. *Experimental Conditions:* microwave frequency, 9.3449 GHz; temperature, 180 K; microwave power, 20.25 mW; magnetic field modulation, 1.0 mT; modulation frequency, 100 kHz; scan rate: 6.52 mT/s; time constant, 2.56 ms.

Figure 2.1 shows the EPR spectrum of the aminoethanol-derived Co^{II}-substrate radical pair following cryotrapping and prior to annealing at 180 K. The $g_\perp$ value of isolated cob(II)alamin is approximately 2.26, which is consistent with prominent Co^{II} intensity found in the region around 285 mT.[119] However, compared to the isolated

cob(II)alamin signals, the Co^{II} features in the radical pair EPR spectrum are broadened by the interaction with the unpaired electron on the C1 of the substrate radical.[120] The line shape of substrate radical ranges from approximately 325 to 345 mT. The unresolved doublet splitting and inhomogeneous line broadening are caused by the interaction with the unpaired electron on Co^{II}.[117,120] All the features of the Co^{II}-substrate radical pair spectrum can be accounted by EPR simulations.[58,70]

2.2.2 Decay of the Co^{II}-substrate Radical Pair

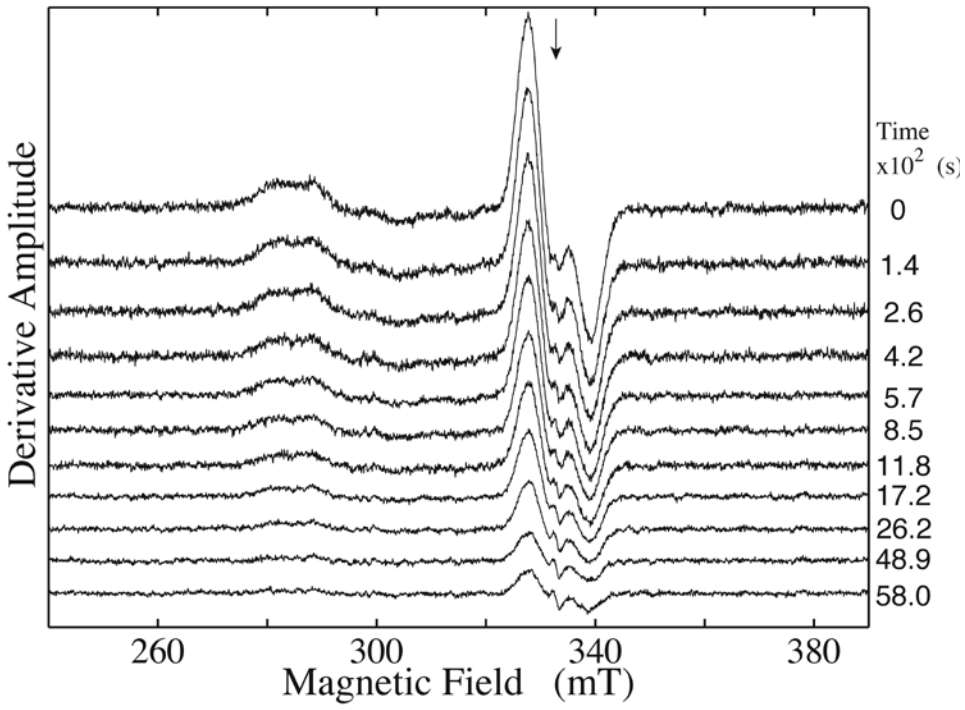

Figure 2.2: Dependence of the EPR spectrum of the Co^{II}-substrate radical pair state in EAL on time after temperature-step to T = 207 K. The free electron resonance position at g = 2.0 is shown by the arrow. *Experimental Conditions:* microwave frequency, 9.3434 GHz; temperature, 207 K; microwave power, 20.25 mW; magnetic field modulation, 1.0 mT; modulation frequency, 100 kHz; scan rate: 6.52 mT/s; time constant, 2.56 ms.

Figure 2.2 shows a stack plot of a selection of 11 of the 300 total EPR spectra collected during the course of a representative decay at 207 K, which does not show any sign of EPR lineshape change during decay. Figure 2.3 also shows the decay of EPR signals of Co^{II} and substrate radical as a function of time at 203 K after temperature step, respectively. The Co^{II} signal displays poorer signal to noise ratio (SNR) than the radical signal, because the maximum amplitude of Co^{II} is 14-fold lower than the peak-to-trough amplitude of the substrate radical signal. The Co^{II} and substrate radical display the same decay kinetics, to within the experimental error. The result suggests that the Co^{II}-substrate radical pair is the only EPR signal during decay, with the exception of a narrow free radical at g = 2.0. This signal, arising from an organic radical that is formed during the initial sample mixing and cryotrapping procedure, corresponds to < 1% of the initial Co^{II}-substrate radical pair amplitude, as previously reported.[117] The amplitude of this minor signal is independent of decay, and will not be discussed further.

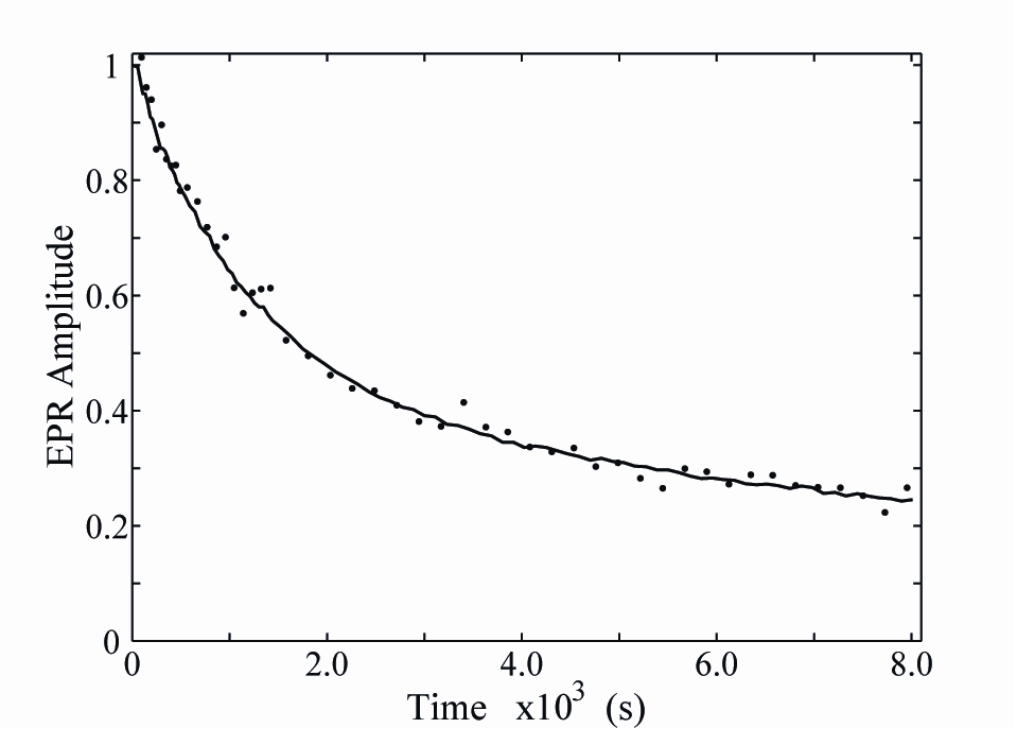

Figure 2.3: Comparison of the time-dependence of the decay of the Co^{II} and substrate radical EPR signals for *T* = 203 K. The substrate radical amplitude (line) was obtained from the peak minus trough amplitude. The Co^{II} signal amplitude (dots) was obtained from the maximum of the Co^{II} signal at the peak of the $g_{\perp}$ feature. *Experimental Conditions:* microwave frequency, 9.3413 GHz; temperature, 203 K; microwave power, 20.25 mW; magnetic field modulation, 1.0 mT; modulation frequency, 100 kHz; scan rate: 6.52 mT/s; time constant, 2.56 ms; average of 1-20 individual spectra minus average of 20 baseline spectra.

The substrate radical EPR signal at temperatures above 210 K is observed to decay to zero (within the noise level). At temperatures below 207 K, the long time scale of the decay, and measuring time limit of 6 to 8 h, imposed by the cryostat system, preclude the decay to the zero level. The complete decay of the substrate radical EPR amplitude indicates that at least one step in the recombination process can be considered as irreversible. This is consistent with the experiment showing that addition of excess acetaldehyde and ammonium to holoenzyme does not yield a detectable substrate radical

signal. Thus, one irreversible step is included in the following kinetic models of substrate radical decay.

The decays of the substrate radical as a function of time are shown at representative temperatures of 197, 200, 203 and 207 K, which are fitted by monoexponential function, biexponential function and power law function, in Figure 2.4, Figure 2.5, and Figure 2.6, respectively.

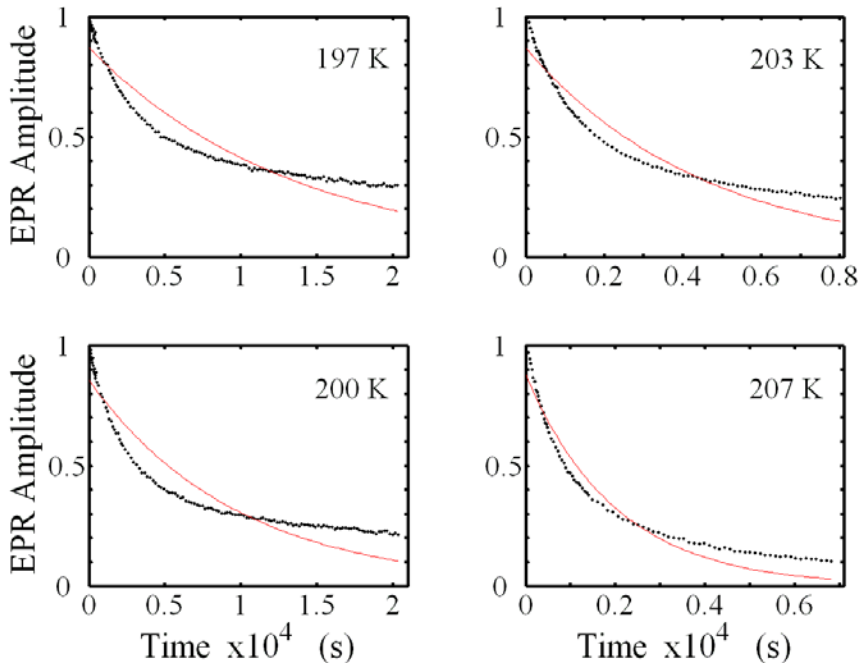

Figure 2.4: Decay of the Co^{II}-substrate radical pair as a function of time at different temperatures, and overlaid best-fit monoexponential functions. The experimental amplitude is normalized to the value at $t = 0$. The EPR experimental conditions are as described in the legend to Figure 2.2. *Simulation parameters*: 197 K: $A_0 = 0.871$, $k = 7.45 \times 10^{-5}$ s^{-1}, R^2=0.9812; 200 K: $A_0 = 0.855$, $k = 1.03 \times 10^{-4}$ s^{-1}, $R^2 = 0.9664$; 203 K: $A_0 = 0.870$, $k = 2.20 \times 10^{-4}$ s^{-1}, $R^2 = 0.9499$; 207 K: $A_0 = 0.878$, $k = 4.98 \times 10^{-4} s^{-1}$, $R^2 = 0.9542$.

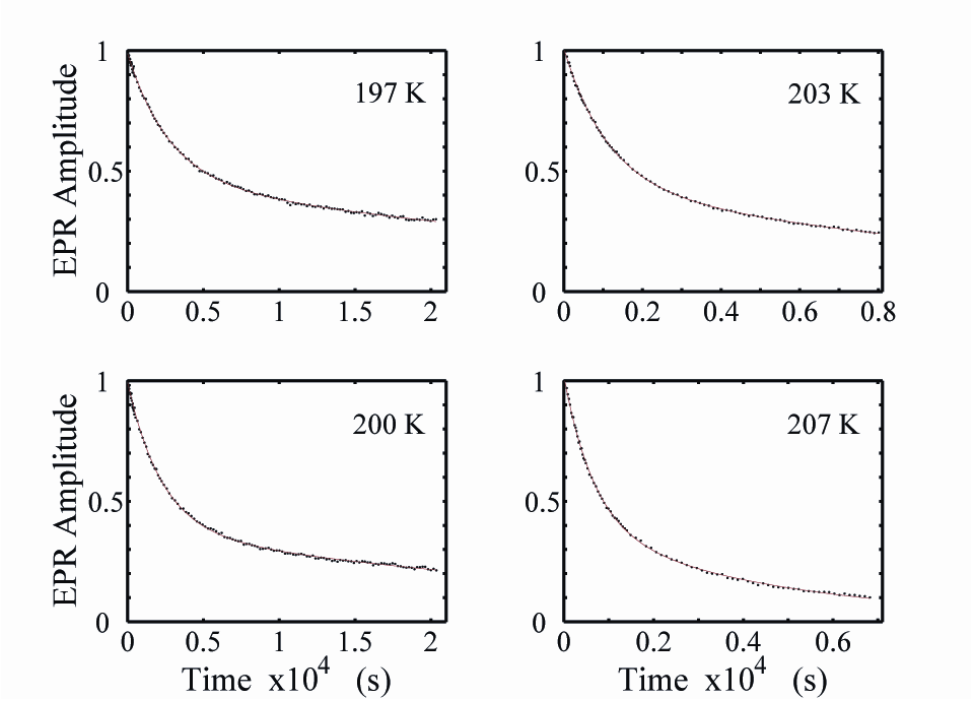

Figure 2.5: Decay of the Co^{II}-substrate radical pair as a function of time at different temperatures, and overlaid best-fit biexponential functions. The experimental amplitude is normalized to the value at $t = 0$. The EPR experimental conditions are as described in the legend to Figure 2.2. *Simulation parameters*: 197 K: $A_1 = 0.58$, $k = 3.70 \times 10^{-4}$ s^{-1}, $A_2 = 0.42$, $k = 2.20 \times 10^{-5}$ s^{-1}, $R^2 = 0.9995$; 200 K: $A_1 = 0.55$, $k = 5.69 \times 10^{-4}$ s^{-1}, $A_2 = 0.45$, $k = 4.65 \times 10^{-5}$ s^{-1}, $R^2 = 0.9989$; 203 K: $A_1 = 0.56$, $k = 8.88 \times 10^{-4}$ s^{-1}, $A_2 = 0.44$, $k = 7.65 \times 10^{-5}$ s^{-1}, $R^2 = 0.9997$; 207 K: $A_1 = 0.56$, $k = 1.72 \times 10^{-3}$ s^{-1}, $A_2 = 0.44$, $k = 3.25 \times 10^{-4}$ s^{-1}, $R^2 = 0.9999$.

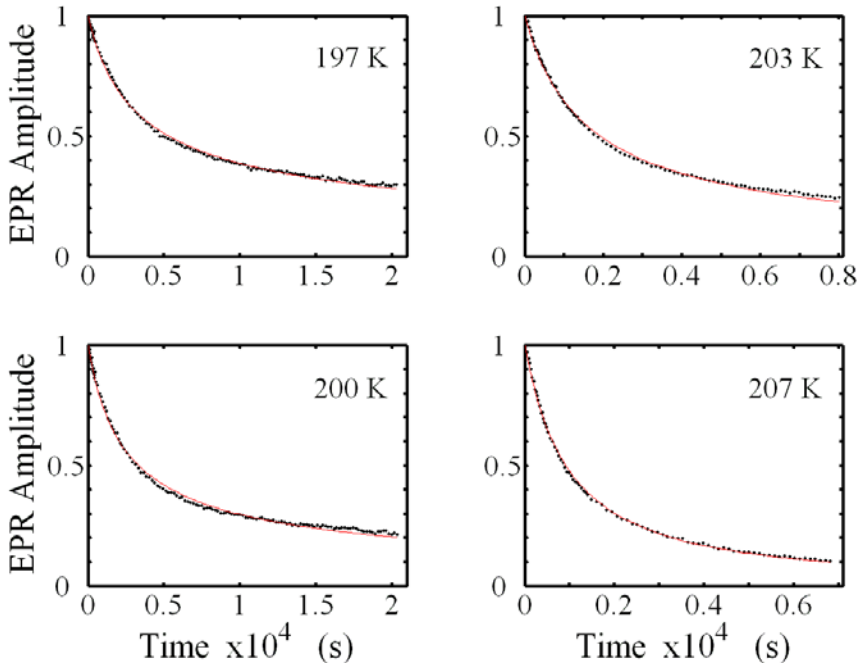

Figure 2.6: Decay of the Co^{II}-substrate radical pair as a function of time at different temperatures, and overlaid best-fit power law functions. The experimental amplitude is normalized to the value at t = 0. The EPR experimental conditions are as described in the legend to Figure 2.2. *Simulation parameters*: 197 K: t_0 = 1818 s, n = -0.506, R^2 = 0.9994; 200 K: t_0 = 1539 s, n = -0.601, R^2 = 0.9991; 203 K: t_0 = 1205 s, n = -0.727, R^2 = 0.9986; 207 K: t_0 = 1177 s, n = -1.202, R^2 = 0.9990.

The monoexponential function does not fit the substrate radical decay data from 190 to 207 K. Therefore, a two-state, single-step model is not tenable. Both the biexponential function and power law function give an excellent fit for the substrate radical decay from 190 to 207 K. Based on the above fitting functions, three possible kinetic models are proposed: a three-state/two-step model (single decay population; biexponential function), two-population/single-step model (biexponential function), and multi-population/single-step model (power law function). Single-step in the following discussion means that the decay of the substrate radical can be expressed by a single first-order rate constant, which

does not necessarily imply that there is no transient intermediate during the substrate radical decay. The three models will be tested and evaluated in the following discussion.

2.2.3 Evaluation of Three-state, Two-step Model for the Substrate Radical Decay Reaction

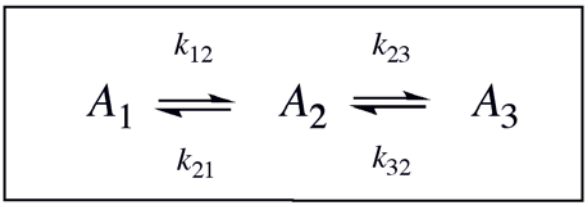

Scheme 2.1: The three-state, two-step kinetic mechanism for a homogeneous biexponential decay.

The equilibration among three linearly linked states shown in Scheme 2.1 is considered as a candidate mechanism for biexponential decay of the substrate radical for $T \leq 207$ K. The time evolution of normalized amplitudes of the states A_i and the relaxation time parameters λ_2 and λ_3 ($\lambda_1 = 0$) of the three-state, two-step model can be solved analytically, given the initial conditions, $\frac{[A_1]_{t=0}}{[A_1]_0} = 1, \frac{[A_2]_{t=0}}{[A_1]_0} = \frac{[A_3]_{t=0}}{[A_1]_0} = 0$, which hold for the system examined here.[118] The following expressions give the time-dependence of the normalized amplitudes of the states A_i:[118]

$$\frac{[A_1]_t}{[A_1]_0} = \frac{k_{21}k_{32}}{\lambda_2\lambda_3} + \frac{k_{12}(\lambda_2 - k_{23} - k_{32})}{\lambda_2(\lambda_2 - \lambda_3)} e^{-\lambda_2 t} + \frac{k_{12}(k_{23} + k_{32} - \lambda_3)}{\lambda_3(\lambda_2 - \lambda_3)} e^{-\lambda_3 t} \tag{2.4}$$

$$\frac{[A_2]_t}{[A_1]_0} = \frac{k_{12}k_{32}}{\lambda_2\lambda_3} + \frac{k_{12}(k_{32} - \lambda_2)}{\lambda_2(\lambda_2 - \lambda_3)} e^{-\lambda_2 t} + \frac{k_{12}(\lambda_3 - k_{32})}{\lambda_3(\lambda_2 - \lambda_3)} e^{-\lambda_3 t} \tag{2.5}$$

$$\frac{[A_3]_t}{[A_1]_0} = \frac{k_{12}k_{23}}{\lambda_2\lambda_3} + \frac{k_{12}k_{23}}{\lambda_2(\lambda_2 - \lambda_3)} e^{-\lambda_2 t} - \frac{k_{12}k_{23}}{\lambda_3(\lambda_2 - \lambda_3)} e^{-\lambda_3 t} \tag{2.6}$$

The k_{ij} are defined in Scheme 2.1. The relaxation rate parameters, λ_i, are related to the microscopic rate constants by the following expressions:

$$\lambda_2 = \frac{1}{2}\{k_{12} + k_{21} + k_{23} + k_{32} + [(k_{12} + k_{21} + k_{23} + k_{32})^2 - 4(k_{12}k_{23} + k_{21}k_{32} + k_{12}k_{32}]^{\frac{1}{2}}\} \quad (2.7)$$

$$\lambda_3 = \frac{1}{2}\{k_{12} + k_{21} + k_{23} + k_{32} - [(k_{12} + k_{21} + k_{23} + k_{32})^2 - 4(k_{12}k_{23} + k_{21}k_{32} + k_{12}k_{32}]^{\frac{1}{2}}\} \quad (2.8)$$

and $\lambda_1 = 0$.[118]

The Equations 2.4 to 2.7 are used to simulate the experimental biexponential decays, under the assumption that only one decay population was present, and that $k_{32} = 0$. A representative simulation is shown in Figure 2.7.

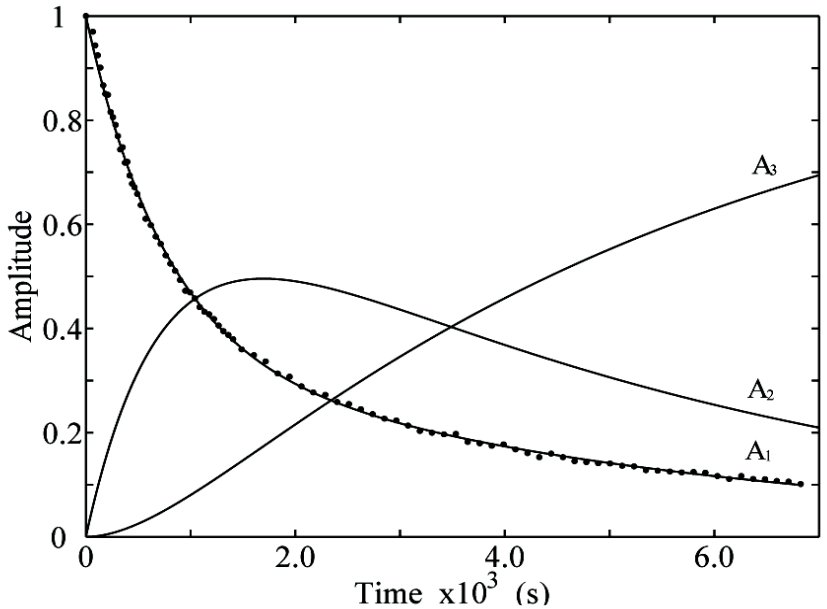

Figure 2.7: Simulation of the Co^{II}-substrate radical decay at 207 K by using the homogeneous linear two-step model (Scheme 2.1). The experimental decay data are shown as dots. The simulated normalized population of the A_1 ($\frac{[A_1]_t}{[A_1]_0}$, dotted line) state, and the calculated time dependence of the A_2 ($\frac{[A_2]_t}{[A_1]_0}$, solid line) and A_3 ($\frac{[A_3]_t}{[A_1]_0}$, dashed line) states, are shown. *Simulation parameters*: Initial normalized populations: $A_{1,0} = 1.0$, $A_{2,0} = A_{3,0} = 0$; $k_{12} = 9.73 \times 10^{-4}$ s^{-1}, $k_{21} = 3.87 \times 10^{-4}$ s^{-1}, $k_{23} = 3.09 \times 10^{-4}$ s^{-1}, $k_{32} = 0$ s^{-1} (fixed); $R^2 = 0.9994$.

Figure 2.7 shows a representative simulation of substrate radical decay using the three-state, two-step model at 207 K. The simulation predicts a maximum value of approximately 0.5 for $\frac{[A_2]_t}{[A_1]_0}$ during substrate radical deay, and simulations at other temperatures give similar results. The relative large value of $\frac{[A_2]_t}{[A_1]_0}$ implies the accumulation of the intermediate state A_2.

From the minimal mechanism of EAL shown in Figure 1.3, there are two candidate intermediates, Co^{II}-product radical pair or Co^{II}-5'-deoxyadenosyl radical pair, that could accumulate during the decay of substrate radical if three-state, two-step model is plausible. Isotope labeled substrates, 1,1,2,2-$^2H_4$-aminoethanol and 1-^{13}C-aminoethanol, are employed to detect whether Co^{II}-product radical pair accumulates during the decay of substrate radical. Low temperature EPR (6 K) experiment, which improves the SNR of EPR spectrum, is utilized to detect possible intermediate of Co^{II}-5'-deoxyadenosyl radical pair.

Figure 2.8 displays normalized EPR spectra acquired to detect Co^{II}-radical pair states, other than the Co^{II}-substrate radical pair. Figure 2.8A shows the normalized EPR spectra of 1,1,2,2-$^2H_4$-aminoethanol generated-substrate radical at different stages of the Co^{II}-substrate radical pair decay at 197 K. Using 1,1,2,2-$^2H_4$-aminoethanol as substrate can improve SNR of EPR spectra by approximately 3-fold compared to using natural abundance aminoethanol.[57] The averaged decay spectra, corresponding to normalized amplitude ranges of 99-90%, 79%-70% and 59-50%, are shown, together with the EPR spectrum of the pre-annealed sample measured at 160 K. The EPR lineshapes of the Co^{II}-substrate radical pair at different decay stages are identical to within the noise level. The SNR relative to the peak-to-trough amplitude of the substrate radical is 2.0 to 3.0 × 10^2.

Therefore, no Co^{II}-radical pair species, other than the Co^{II}-substrate radical pair, are found during the substrate radical decay at SNR of ~10^2, relative to the peak-to-trough amplitude of the substrate radical.

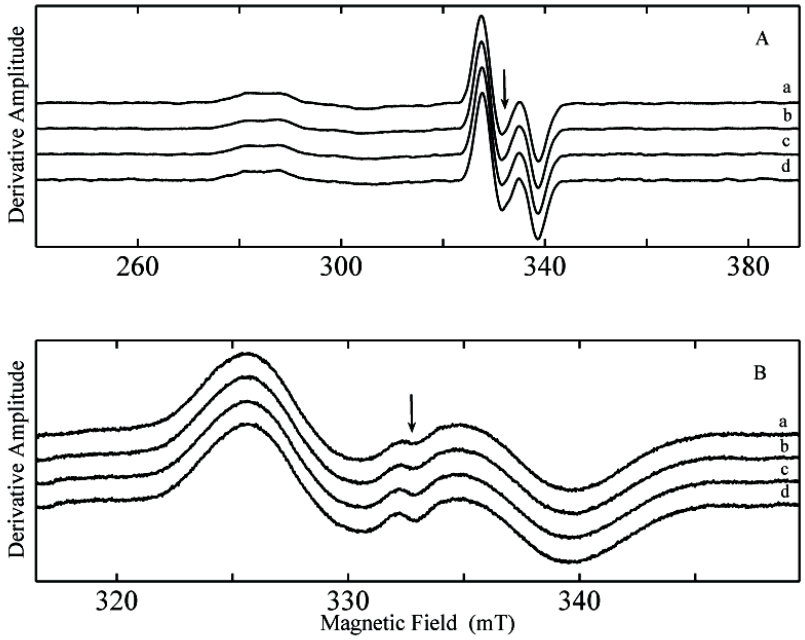

Figure 2.8: Comparison of the EPR spectra of the Co^{II}-substrate radical pair state prior to annealing and at different levels of decay, for decay performed at T = 197 K. (*A*) Co^{II}-substrate radical pair state generated by using 1,1,2,2-$^2H_4$-aminoethanol as substrate. (a) Pre-annealling spectrum, obtained at 160 K. (*b*) Average of spectra corresponding to amplitudes of 99-90% of initial amplitude. (*c*) Average of spectra corresponding to amplitudes of 79-70% of initial amplitude. (*d*) Average of spectra corresponding to amplitudes of 59-50% of initial amplitude. (*B*) Co^{II}-substrate radical pair state generated by using 1-^{13}C-aminoethanol as substrate. (a) Pre-annealling spectrum, obtained at 160 K. (*b*) Average of spectra corresponding to amplitudes of 99-90% of initial amplitude. (*c*) Average of spectra corresponding to amplitudes of 79-70% of initial amplitude. (*d*) Average of spectra corresponding to amplitudes of 59-50% of initial amplitude. *Experimental Conditions: Panel (A)*: microwave frequency, 9.3390 GHz; microwave power, 20.25 mW; magnetic field modulation, 1.0 mT; modulation frequency, 100 kHz; scan rate: 6.52 mT/s; time constant, 2.56 ms. *Panel (B)*: microwave frequency, 9.3390 GHz; microwave power, 20.25 mW; magnetic field modulation, 1.0 mT; modulation frequency, 100 kHz; scan rate: 6.52 mT/s; time constant, 2.56 ms.

Figure 2.8B shows results that use the same methods as that in Figure 2.8A, with the exception that 1-^{13}C-aminoethanol was used as the substrate. The average decay spectra are again the same within the noise level. The 1-^{13}C-label at the C1 radical center increases the substrate radical width by 2.4 mT relative to the natural isotopic abundance radical, which arises from the hyperfine interaction of the electron spin with the I = 1/2 ^{13}C nucleus. If the C2-centered product radical (Scheme 1.2) accumulates during the substrate radical decay, a narrow EPR line shape is expected to superimpose on the substrate radical spectrum, which is not observed.

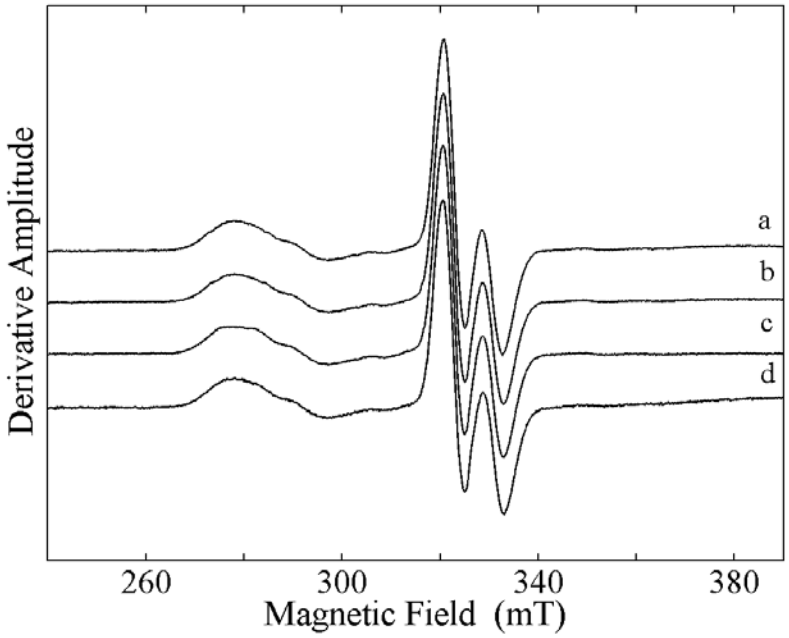

Figure 2.9: Comparison of the 6 K EPR spectra of the 1,1,2,2-$^{2}H_4$-aminoethanol-generated Co^{II}-substrate radical pair state prior to annealing and at different levels of decay, for decay performed at T = 203 K. Co^{II}-substrate radical pair state generated by using as substrate. (a) Pre-annealling spectrum. (*b*) EPR spectrum corresponding to amplitude of 90% of initial amplitude. (*c*) EPR spectrum corresponding to amplitude of 75% of initial amplitude. (*d*) EPR spectrum corresponding to amplitude of 50% of initial amplitude. *Experimental Conditions: Panel (A)*: microwave frequency, 9.4434 GHz; microwave power, 0.2024 mW; magnetic field modulation, 1.0 mT; modulation frequency, 100 kHz; scan rate: 0.22 mT/s; time constant, 163.84 ms.

Previous studies show that a triplet spin state (S = 1) is found in the sample of functional adenosylcobalamin analogue 5'-deoxy-3',4'-anhydroadenosylcobalamin (anAdoCbl) and diol dehydrase.[121] Isotope labeling (^{13}C and ^{2}H) experiments further identify that the triplet spin state is contributed by 5'-deoxy-3',4'-anhydroadenosyl radical and the low-spin Co^{II}.[121] Since the Co^{II}-5'-deoxyadenosyl radical pair is a candidate intermediate during the substrate radical pair decay, low temperature (6 K) EPR experiment, which improves the SNR, was performed to detect possible formation of the Co^{II}-5'-adenosyl radical pair. Figure 2.9 displays normalized EPR spectra of 1,1,2,2-$^{2}H_4$-aminoethanol-generated Co^{II}-substrate radical pair at 6 K. The Co^{II}-substrate radical pair was annealed at 203 K with EPR amplitude decreased to 90%, 75% and 50% relative to the initial EPR amplitude, and then was measured at 6 K. The EPR line shapes of the Co^{II}-substrate radical pair at different decay stages are identical to within the noise level. EPR evidence for a putative half-field transition, which is found in the Co^{II}-5'-deoxy-3',4'-anhydroadenosyl radical pair intermediate at approximately 150 mT,[121] is not observed here (unpublished data). Therefore, Co^{II}-radical pairs, except the Co^{II}-substrate radical pair, are not observed during the decay of the Co^{II}-substrate radical pair. The experiments above are consistent with the 5-9 kcal/mol higher free energy of the product radical relative to the substrate radical, which were calculated by using *ab initio* methods,[122-124] and with the experimentally determined limit on the free energy of the Co^{II}-5'-deoxyadenosyl radical pair of > 3.0 kcal/mol, relative to the Co^{II}-substrate radical pair state.[125]

In summary, it has been shown that Co^{II}-substrate radical pair is the only EPR detectable intermediate during the Co^{II}-substrate radical decay. This is inconsistent with

the prediction from simulation of the decay of a single population by using the three-state, two-step model. Therefore, the three-state, two-step decay of a single population of Co^{II}-substrate radical pair, is not a plausible model for the decay kinetics of the Co^{II}-substrate radical pair from 190 to 207 K.

2.2.4 Evaluation of the Multi-population, Single-step Model

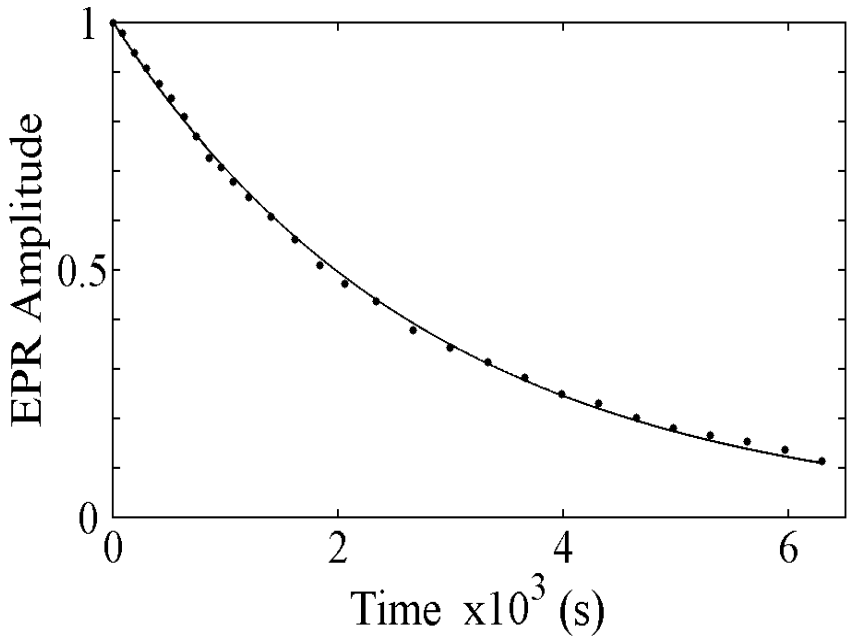

Figure 2.10: Decay of the substrate radical EPR amplitude at 207 K, following partial decay at *T* = 193 K. The sample was held at 193 K for 6 h, and the substrate radical amplitude decayed to 38% of the initial amplitude. The subsequent decay at T = 207 K is shown, with overlaid monoexponential fit to the data (solid line). *Experimental Conditions:* microwave frequency, 9.3439 GHz; temperature, 207 K; microwave power, 20.25 mW; magnetic field modulation, 1.0 mT; modulation frequency, 100 kHz; scan rate: 6.52 mT/s; time constant, 2.56 ms. *Simulation parameters*: first-order rate constant, 3.3×10^{-4} s^{-1}; $R^2 = 0.9987$.

A multi-population, single-step decay model of the Co^{II}-substrate radical decay is fitted by power law function, where the populations of the Co^{II}-substrate radical are characterized by a distribution of activation energies. A two-temperature annealing experiment was designed to address the distinction between biexponential and power law functional forms for the Co^{II}-substrate radical pair decay.

The Co^{II}-substrate radical pair was annealed at low temperature to reduce the amplitude to 35-40% of the initial amplitude. The low temperature was selected because the ratio of fast relaxation time to slow relaxation time increases with decreasing temperature. The process prepares a sample with a nearly "pure" proportion of the putative slow phase decay component. The sample is then raised to a higher temperature point where the decay of the substrate radical is measured. The decay for a representative two-step annealing experiment, performed at 193 and 207 K, is shown in Figure 2.10. The decay of the pre-annealed sample is well fit by a monoexponential function with a rate constant of 3.3×10^{-4} s^{-1}, which is comparable to the average rate constant of 2.9×10^{-4} s^{-1} obtained for the slow phase of the decay in the biexponential fits at 207 K. These results support a biexponential decay, rather than a power law decay, from 190 to 207 K. This implies that a multi-population, single-step model is not a tenable model for substrate radical decay.

2.2.5 Two-population, Single-step Model of Substrate Radical Decay

The two-population, single-step model for the substrate radical decay is depicted in Scheme 2.2. It is proposed that this model characterizes the Co^{II}-substrate radical pair decay at 190-207 K. The substrate radical decay can be characterized by $A_{obs,f}$, $A_{obs,s}$,

$k_{obs,f}$ and $k_{obs,s}$, which stand for normalized amplitude of the fast phase decay component, normalized amplitude of the slow phase decay component, first-order rate constant of fast decay component, and first-order rate constant of slow decay component, respectively. The normalized amplitudes of fast phase and slow phase decay remain constant from 190 to 207 K, with values of 0.55 ± 0.04 and 0.45 ± 0.04, respectively. The ratio of $k_{obs,f}/k_{obs,s}$ decreases from approximately 12 at 190 K to 6 at 207 K. On the other hand, measurement of the turnover rate (k_{cat}) of EAL on aminoethanol at room temperature only gives a single value. Further experiments discussed below on substrate radical decay at T > 207 K are performed to address the characteristics of the fast and slow decay components.

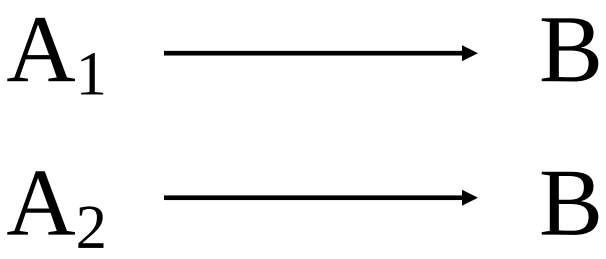

Scheme 2.2: Two-population, single-step kinetic mechanism for an inhomogeneous biexponential decay.

2.3 Kinetic Transition of Substrate Radical Decay at T > 207 K

The decay kinetics of Co^{II}-substrate radical pair are further examined at higher temperatures T > 207 K, up to 223 K. The 30 to 60 s deadtime of the EPR experiment restricts the measurement of the Co^{II}-substrate radical pair decay at T > 223 K. Figure 2.11 shows representative decays of the substrate radical EPR signals as a function of time at temperatures of 210 and 214 K. The biexponential fitting parameters of the

substrate radical decay for temperatures from 210 to 223 K are shown in Table 2.1. The decay of the Co^{II}-substrate radical pair is well-fit by a monoexponential decay function with rate constant ($k_{obs,m}$) at $T \geq 214$ K. These results show that there is a transition from a biexponential to monoexponential form of the substrate radical decay over the temperature range of $207 < T < 214$ K.

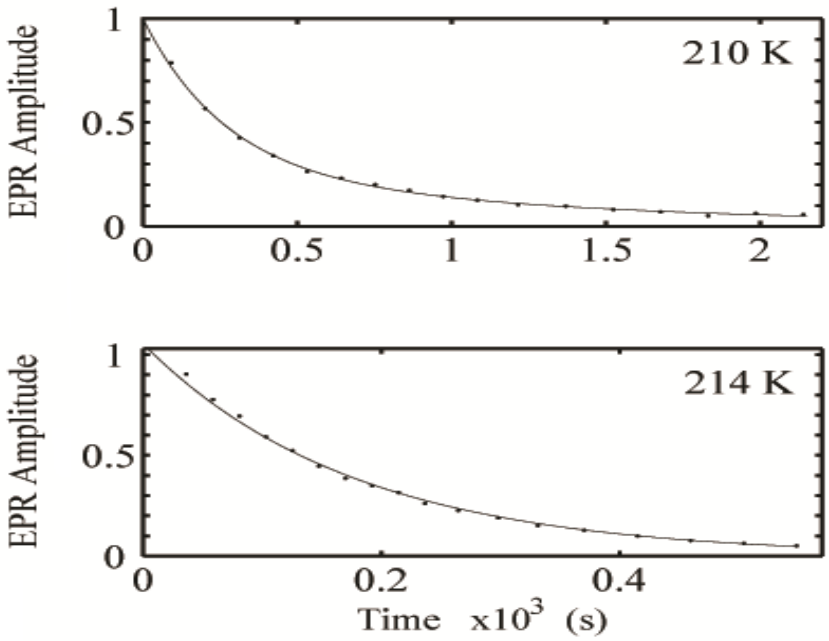

Figure 2.11: Decay of the substrate radical as a function of time at different temperatures from 210 to 214 K, and overlaid best-fit biexponential functions. The EPR experimental conditions are as described in the legend to Figure 2.5. The overlaid solid curves correspond to simulations of the decay with a biexponential function (210 K) or monoexponential function (214 K). The simulation parameters are presented in Table 2.1.

Table 2.1: First-order rate constant and amplitude parameters for the fit of the biexponential function to the Co^{II}-substrate radical pair decay kinetics at different temperatures for the natural abundance (^1H) states.

T (K)	$k_{obs,f}$ (s^{-1})	A_f [a]	$k_{obs,s}$ (s^{-1})	A_s [b]	R^2 [c]
190	$7.3(\pm0.6)\times10^{-5}$	0.53±0.07	$5.2(\pm0.1)\times10^{-6}$	0.47±0.07	0.9990
193	$1.4(\pm0.3)\times10^{-4}$	0.51±0.02	$1.3(\pm0.1)\times10^{-5}$	0.49±0.02	0.9994
197	$3.7(\pm0.1)\times10^{-4}$	0.56±0.03	$2.4(\pm0.2)\times10^{-5}$	0.44±0.03	0.9996
200	$5.8(\pm0.2)\times10^{-4}$	0.55±0.05	$4.7(\pm0.2)\times10^{-5}$	0.45±0.05	0.9994
203	$8.3(\pm0.6)\times10^{-4}$	0.58±0.02	$8.0(\pm0.5)\times10^{-5}$	0.42±0.02	0.9997
207	$1.5(\pm0.2)\times10^{-3}$	0.56±0.05	$2.9(\pm0.5)\times10^{-4}$	0.44±0.05	0.9993
210	$3.2(\pm0.7)\times10^{-3}$	0.58±0.17	$9.4(\pm3.0)\times10^{-4}$	0.42±0.17	0.9993
214	$4.0(\pm0.4)\times10^{-3}$	1.00±0.00	--	--	0.9981
217	$6.8(\pm0.4)\times10^{-3}$	1.00±0.00	--	--	0.9969
220	$1.1(\pm0.1)\times10^{-2}$	1.00±0.00	--	--	0.9993
223	$1.6(\pm0.1)\times10^{-2}$	1.00±0.00	--	--	0.9991

[a]The relative fitted amplitude for the fast phase, normalized to the sum, A_f+A_s.
[b]The relative fitted amplitude for the slow phase, normalized to the sum, A_f+A_s.
[c]R is Pearson's correlation coefficient.

Figure 2.12 shows a composite Arrhenius plot of the natural logarithms of the observed rate constants (from Table 2.1) for the monoexponential and fast and slow phases of the biexponential decay as functions of inverse absolute temperature (Equation 2.3). The natural logarithms of $k_{obs,m}$ and $k_{obs,f}$ are well-fit by the same linear relation. The adherence of the $k_{obs,m}$ and $k_{obs,f}$ values to the same Arrhenius relation suggests that they correspond to the same reaction pathway and rate limiting step, which is characterized by the same Arrhenius parameters, and therefore, $A_{app,m} = A_{app,f}$ and $E_{a,app,m} = E_{a,app,f}$. The natural logarithms of $k_{obs,s}$ values for $190 \leq T \leq 207$ K are also well-fit by a linear relation, which has different slope and intercept parameters from that of $k_{obs,m}$ and $k_{obs,f}$. The different linear relation for $k_{obs,s}$ for $190 \leq T \leq 207$ K implies that the slow phase of

substrate radical decay either follows a different pathway, or proceeds by the same pathway as for the fast phase, but with a different rate limiting step. The Arrhenius fitting parameters are shown in Table 2.2.

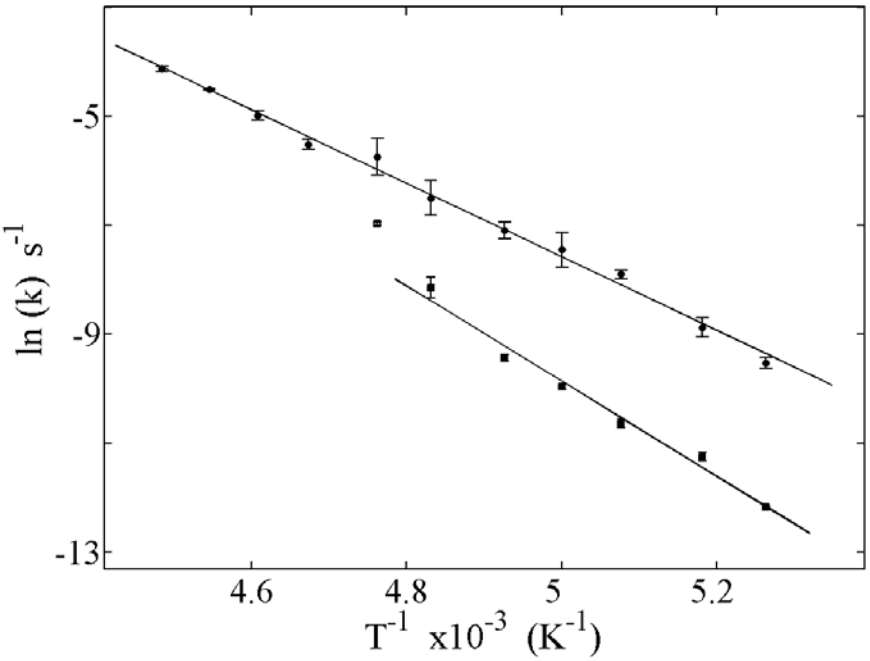

Figure 2.12: Arrhenius plots of the observed first-order rate constants for the decay of the Co^{II}-substrate radical pair, $k_{obs,m}$, $k_{obs,f}$ and $k_{obs,s}$. The combined $k_{obs,m}$ and $k_{obs,f}$ values (solid circles) are fitted by the upper line. The $k_{obs,s}$ values corresponding to $190 \leq T \leq 207$ K (solid squares) are fitted by the lower line. The $k_{obs,s}$ value for 210 K (open square) is not included in the fit. The data are from Table 2.1. The fitting parameters are presented in Table 2.2.

Figure 2.13 shows the dependence of the normalized amplitudes of the fast phase and slow phase of the biexponential decay on temperature. The decay of the substrate radical exhibits monoexponential kinetics at $T \geq 214$ K. Figure 2.13 shows that the temperature is decreased, the amplitude of the decay is partitioned into fast and slow components, $A_{obs,f}$ and $A_{obs,s}$, respectively, over the narrow temperature range $207 < T < 214$ K. Below 210 K ($190 \leq T \leq 207$ K), the normalized amplitudes of the fast and slow components remain constant, with values of 0.55 ± 0.04 and 0.45 ± 0.04, respectively. The constant

amplitudes of $A_{obs,f}$ and $A_{obs,s}$ at $T \leq 207$ K, and the linear Arrhenius relations for the corresponding rate constants, $k_{obs,f}$ and $k_{obs,s}$ in Figure 2.12, suggests that the two decay components are characterized by different rate limiting steps.

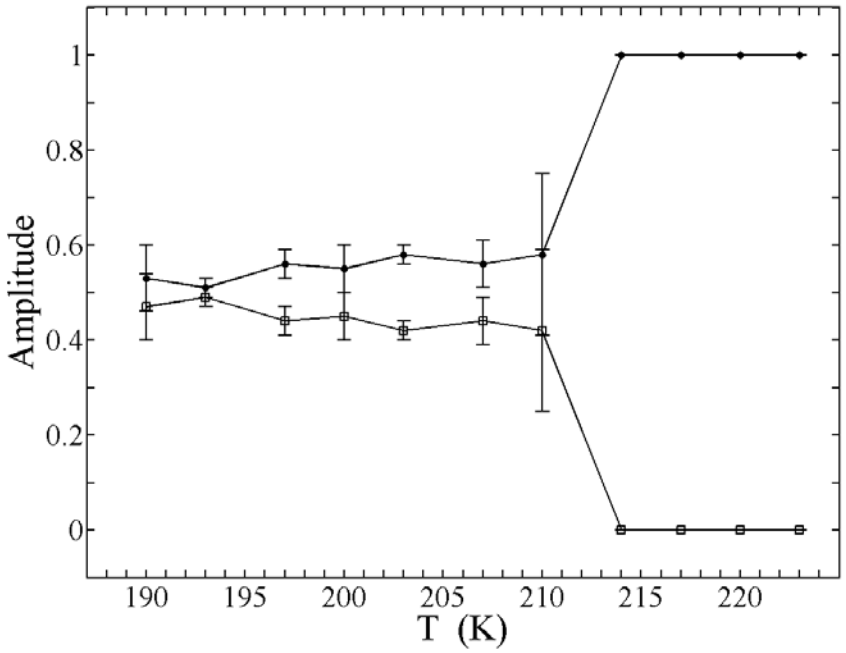

Figure 2.13: Amplitudes of the fast and slow decay phases of the biexponential decay of the Co^{II}-substrate radical pair, $A_{obs,f}$ and $A_{obs,s}$, respectively, as a function of temperature from 190 to 223 K. The amplitudes for 214, 217, 220 and 223 K correspond to the fit to the monoexponential decay function. The curves are drawn to guide the eye. The data are from Table 2.1.

Table 2.2: Fitting parameters for Arrhenius reaction rate expression for the fast and slow components of the Co^{II}-substrate radical pair decay kinetics.

Component	Log[A (s^{-1})]	E_a (kcal mol^{-1})	R^{2c}
Fast[a]	11.4(±0.4)	13.4(±0.2)	0.9973
Slow[b]	14.6(±1.2)	17.3(±0.6)	0.9817

[a]Fitting of the fast phase of the biexponential form and monoexponential form from 190 to 223 K
[b]Fitting of the slow phase of the biexponential form from 190 to 207 K
[c]R is Pearson's correlation coefficient.

2.4 Proposed Origins on Kinetic Decay Phases

Slow biexponential phase. The transition from biexponential to monoexponential behavior of the substrate radical decay with increasing temperature occurs in the temperature interval, $207 < T < 214$ K. Only the 210 K experiment data falls in the transition temperature range, at current sampling temperature interval of 3-4 K. Figure 2.12 and Table 2.1 shows that $k_{obs,f}$ at 210 K follows the same linear Arrhenius relation for $k_{obs,f}$ from 190-207 K. However, Figure 2.12 shows that the data point of $k_{obs,s}$ at 210 K lies significantly above the linear Arrhenius relation that fits $k_{obs,s}$ data for 190-207 K. The value of $k_{obs,s}$ at 210 K (9.4×10^{-3} s^{-1}) is approximately 2.2 fold higher than the value predicted by using the low temperature Arrhenius relation (4.2×10^{-3} s^{-1}). Therefore, the data at the temperature of 210 K suggests that the transition from biexponential to monoexponential decay with increasing temperature is associated with a super-Arrhenius temperature dependence of $k_{obs,s}$. We propose that $k_{obs,s}$ approaches $k_{obs,f}$ as the temperature is increased through the transition region.

The super-Arrhenius relation for the slow phase decay $k_{obs,s}$ of substrate radical in the temperature interval 207-214 suggests a change in the potential energy surface for the slow phase in the transition region. The chemical reaction is unlikely to display a mechanistic discontinuity over this temperature range, and it is proposed that the transition arises from a change in the properties of the protein. A liquid-glass transition also exhibits a change in the potential energy surface over relatively narrow temperature range < 7 K.[126] Different proteins display a solvent-dependent, glass-like transition, or "dynamical transition", within the temperature range of 180 to 220 K.[71] In order to characterize the temperature dependent of $k_{obs,s}$ and gain deeper insight into the nature of the transition, a finer temperature sampling interval, and two-temperature experiments

(T_{low} = 193 K, T_{high} = 208 to 213 K), such as those in Figure 2.10, are further performed and discussed in Chapter V.

Fast biexponential phase and monoexponential decay processes. Extrapolation of the linear Arrhenius relation for $k_{obs,f}$ and $k_{obs,m}$ to 293 K gives a value for the decay rate constant of 35 s^{-1}, which is consistent with k_{cat} values of 30 to 80 s^{-1} per active site that have been reported for EAL in room temperature steady-state kinetic experiments.[27,29,48] Previous studies of the hydrogen exchange of ^{3}H, between [^{3}H]-adenosylcobalamin labeled at C5' methylene carbon and aminoethanol in EAL, show no detectable ^{3}H equilibration with the free substrate.[43,44] Therefore, the reaction of the Co^{II}-substrate radical pair through the reverse of the first hydrogen atom transfer (HT1) is strongly disfavored, which is also supported by further isotope experiments of 1,1,2,2-$^{2}H_4$-aminoethanol discussed in Chapter III and IV. Therefore, we assign the observed rate constants for the fast phase of the biexponential decay (190 to 210 K) and the monoexponential decay (214 to 224 K) to the native forward reaction of the substrate radical, through the rearrangement step.

2.5 Conclusion

During the decay course of the Co^{II}-substrate radical pair at temperatures from 190 to 223 K, no paramagnetic species, other than the Co^{II}-substrate radical pair, is detected above the noise level.[113] The two-*T* experiments have been performed to characterize the decay of the Co^{II}-substrate radical pair. A two-population model is proposed to explain the decay of the Co^{II}-substrate radical pair from 190 to 207 K.[113] The decay kinetics of the Co^{II}-substrate radical pair in the observed temperature range of 190 to 223 K includes

three characteristic regions, which are defined as follows: (i) Low temperature range, 190 $\leq T \leq$ 207 K: Biexponential decay with constant fast phase ($A_{\mathrm{obs,f}}$) and slow phase ($A_{\mathrm{obs,s}}$), and the temperature independent apparent Arrhenius prefactor and activation energy parameters for the fast phase ($A_{\mathrm{app,f}}$, $E_{a,app,f}$) and slow phase ($A_{\mathrm{app,s}}$, $E_{a,app,s}$) of the decay. (ii) Transition range, 207 < T < 214 K: Biexponential decay, where the $A_{\mathrm{pp,f}}$ and $E_{a,app,f}$ obtained from the low temperature range are maintained, and $k_{obs,s}$ displays non-Arrhenius dependence on temperature (change in $A_{\mathrm{app,s}}$, $E_{a,app,s}$, or both). (iii) High temperature range, $T \geq$ 214 K: Monoexponential decay, with the same Arrhenius parameters for the decay rate constant as for the fast phase of the biexponential decay ($A_{\mathrm{app,m}} = A_{\mathrm{app,f}}$, $E_{a,app,m} = E_{a,app,f}$).[113] The kinetic rate constants $k_{obs,f}$ from fast phase decay component (190-210 K) and those $k_{obs,m}$ from the monoexponential decay form (≥ 214 K) are assigned to the native, forward reaction, through the rearrangement step. The sharp dependence of $k_{obs,s}$ in the temperature range 207 < T < 214 K is proposed to be associated with a protein dynamics transition, and discussion on this topic will be further explored in Chapter V.

Chapter III

Characterization of Substrate Hydrogen Isotope Effects on the Co^{II}-substrate Radical Pair Decay Kinetics

3.1 Background and Introduction

We have discussed in Chapter II that the cryotrapped Co^{II}-substrate radical pair intermediate in coenzyme B_{12}-dependent EAL [EC 4.3.1.7; cobalamin (vitamin B_{12})-dependent enzyme superfamily][127] from *Salmonella typhimurium*[3,5,128] relaxes to diamagnetic products during annealing over the temperature range of 190 to 223 K.[113] The reaction of the substrate radical is monitored by using time-resolved, full-spectrum electron paramagnetic resonance (EPR) spectroscopy.[113] In this chapter, we present results for the decay of the Co^{II}-substrate radical pair, generated with 1,1,2,2,-$^2H_4$-aminoethanol, from 190 to 207 K, in order to gain insight into the rate-limiting steps and mechanism.

The accumulation of the Co^{II}-substrate radical pair during the steady-state turnover of EAL on aminoethanol implies that the radical rearrangement step is at least partially rate-limiting for the catalytic cycle at room temperature. This observation is consistent with aminoethanol $^{14}N/^{15}N$ steady-state kinetic IE of 1.0017 on V/K_M (V, maximum velocity; K_M, Michaelis constant), which is proposed to arise from C2-N bond cleavage in the rearrangement step.[48,50] Reed and his coworkers also reported higher $^{14}N/^{15}N$ steady-state kinetic IE on V than that on V/K_M.[50] However, the following hydrogen isotope effects suggest that the hydrogen transfer, especially HT2, is the rate limiting step for steady-state turnover: (a) a steady-state $^1H/^2H$ isotope effect on k_{cat} of 7.4[4] or 7.5,[29] and (b) a $^1H/^3H$ of 100 on hydrogen transfer from C5'-methyl group to the product radical.[4,5] The anomalously large $^1H/^3H$ IE, relative to the $^1H/^2H$ IE, has remained unexplained for nearly 40 years.[5,43]

The 1,1,2,2-$^{2}H_4$-aminoethanol-generated Co^{II}-substrate radical has been cryotrapped, and the decay kinetics of the fast and slow populations after temperature step to 190 to 207 K has been measured. Turnover on $^{2}H_4$-aminoethanol incorporates ^{2}H into all catalytically exchangeable hydrogen sites, after two enzyme turnovers.[29] Prior to cryotrapping, the ^{2}H-aminoethanol substrate samples execute > 20 turnovers. Therefore, in the starting state of the low temperature decay of the $^{2}H_4$-substrate radical, the C1-methylene, C2-methylene, and C5'-methyl hydrogen sites are all ^{2}H-labeled, and HT2 proceeds by deuteron transfer. The first-order decay rate constants for the ^{2}H-substrate radical are compared with the previously measured first-order decay rate constants obtained for the natural abundance, ^{1}H-substrate radical at temperatures $190 \leq T \leq 207$ K. If the HT2 step participates in rate limitation, then a primary kinetic IE that is significantly larger than unity is expected. We observe modest IE for each kinetic phase, which are inconsistent with rate determination by HT2, and conclude that $k_{obs,f}$ represents the rate constant for radical rearrangement. Extrapolation of the low temperature Arrhenius relationship to room temperature suggests that the radical rearrangement is also the slow step in the steady-state turnover of EAL on ^{1}H-aminoethanol.

3.2 Kinetic Characterization of Substrate Radical Decay

3.2.1 Kinetics of 1,1,2,2-$^{2}H_4$-aminoethanol-generated Substrate Radical Decay

Figure 3.1 displays a stack plot of a selection of 11 of the 300 total EPR spectra that were collected during a representative decay time course of the $^{2}H_4$-aminoethanol-generated Co^{II}-substrate radical pair at 207 K. The decay data of $^{2}H_4$-aminoethanol-generated Co^{II}-substrate radical pair were collected at temperatures of 190, 193, 197 200,

203 and 207 K. As found for the decay of the $^{1}H_4$-aminoethanol generated Co^{II}-substrate radical pair,[113] the EPR signals of Co^{II} and substrate radical decay in synchrony. No paramagnetic species, other than Co^{II}-substrate radical pair, have been detected above noise level at a SNR of 10^2 for the peak-to-trough amplitude of the substrate radical, relative to the baseline root mean square spectral noise.

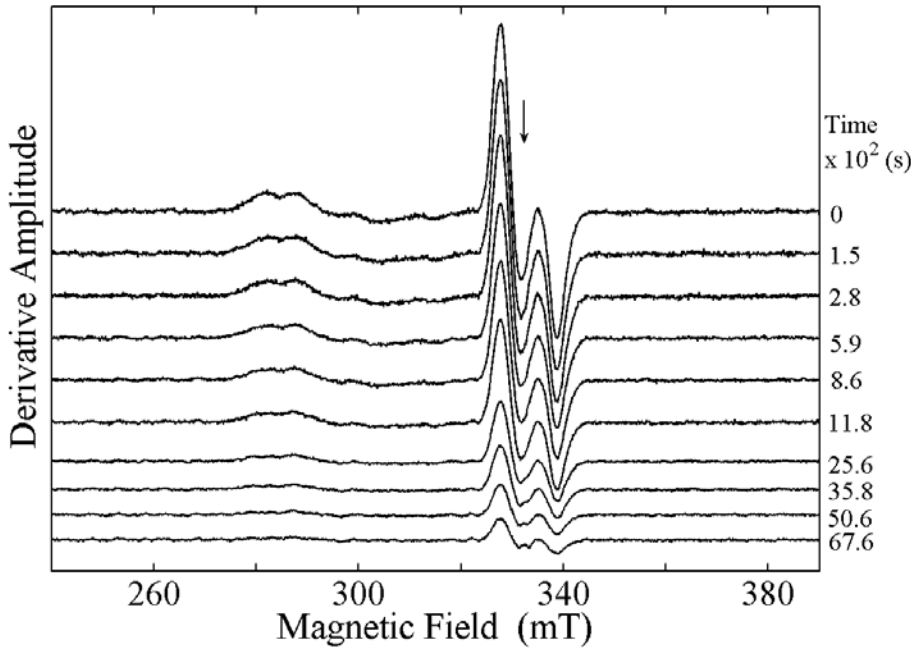

Figure 3.1: Dependence of the EPR spectrum of the $^{2}H_4$-aminoethanol-generated Co^{II}-substrate radical pair state in EAL on time after temperature-step to T = 207 K. The free electron resonance position at g = 2.0 is shown by the arrow. *Experimental Conditions:* microwave frequency, 9.3434 GHz; microwave power, 20.25 mW; magnetic field modulation, 1.0 mT; modulation frequency, 100 kHz; scan rate: 6.52 mT/s; time constant, 2.56 ms.

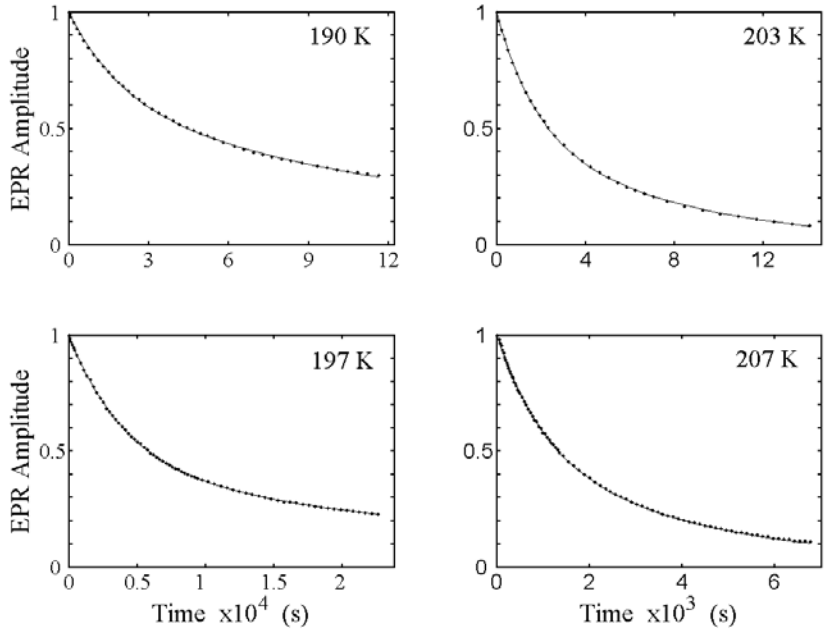

Figure 3.2: Decay of the amplitude of the $^2H_4$-aminoethanol-generated substrate radical as a function of time at selected temperatures from 190-207 K, and overlaid best-fit biexponential functions. The EPR experimental conditions are as described in the legend to Figure 3.1. The simulation parameters are presented in Table 3.1.

Figure 3.2 shows representative EPR signal decay of substrate radical as a function of time at temperatures of 190, 193, 197 and 207 K, which are overlaid by fits of a biexponential function (Equation 2.1, N = 2). The biexponential function provides an excellent fit to the decay at temperatures from 190 to 207 K. The rate constants, $k_{obs,f}$ and $k_{obs,s}$, and normalized amplitude coefficients, $A_{\mathrm{obs,f}}$ and $A_{\mathrm{obs,s}}$ for the fast phase and slow phase of the biexponential functions are shown in Table 3.1. Table 3.1 shows that $A_{\mathrm{obs,f}}$ and $A_{\mathrm{obs,s}}$ remain approximately constant from 190 to 207 K, with mean values and standard deviations as: $A_{\mathrm{obs,f}}$ = 0.46 ±0.10 and $A_{\mathrm{obs,s}}$ = 0.54 ±0.10. The kinetic results are consistent with complete decay at all temperatures. The complete decay of the ^{2}H-

substrate radical EPR amplitude suggests that at least one step in the recombination relaxation is detectably irreversible, as found for the ^{1}H-substrate radical decay.

Table 3.1: First-order rate constant and amplitude parameters for the fit of the biexponential function to the decay kinetics of the ^{2}H-labeled Co^{II}-substrate radical pair and $^{1}H/^{2}H$ hydrogen kinetic isotope effects at different temperatures, 190 to 207 K.

T (K)	$k_{obs,f}$ (s^{-1})	A_f [a]	$k_{obs,s}$ (s^{-1})	A_s [b]	R^2 [c]	KIE_f	KIE_s
207	$1.1(\pm0.3) \times 10^{-3}$	0.53±0.05	$2.9(\pm0.6) \times 10^{-4}$	0.47±0.05	0.9997	1.36±0.22	1.00±0.22
203	$5.7(\pm0.8) \times 10^{-4}$	0.52±0.06	$1.1(\pm0.1) \times 10^{-4}$	0.48±0.06	0.9999	1.46±0.12	0.73±0.05
200	$4.4(\pm1.2) \times 10^{-4}$	0.41±0.09	$7.7(\pm1.8) \times 10^{-5}$	0.59±0.09	0.9997	1.31±0.06	0.61±0.04
197	$2.6(\pm0.2) \times 10^{-4}$	0.44 ±0.11	$3.6(\pm0.8) \times 10^{-5}$	0.56±0.11	0.9998	1.42±0.05	0.67±0.07
193	$1.2(\pm0.2) \times 10^{-4}$	0.37±0.02	$1.5(\pm0.3) \times 10^{-5}$	0.63±0.02	0.9995	1.17±0.30	0.87±0.08
190	$5.3(\pm0.5) \times 10^{-5}$	0.38±0.02	$6.1(\pm0.1) \times 10^{-6}$	0.62±0.02	0.9995	1.38±0.13	0.87±0.02

[a]The relative fitted amplitude for the fast phase, normalized to the sum, $A_{obs,f}+A_{obs,s}$.
[b]The relative fitted amplitude for the slow phase, normalized to the sum, $A_{obs,f}+A_{obs,s}$.
[c]R is Pearson's correlation coefficient.

3.2.2 Characterization of the Fast Phase of Decay of Substrate Radical

The $^{1}H/^{2}H$ IE values for the rate constants, $k_{obs,f}$ and $k_{obs,s}$, at each temperature from 190 to 207 K are shown in Table 3.1. The IE values are calculated by using the ratio of the k_{obs} values for the ^{1}H-substrate radical ($k_{obs,s,H}$, and $k_{obs,f,H}$) reported previously[113] (Table 2.1), and the corresponding k_{obs} values for the ^{2}H-substrate radical ($k_{obs,s,D}$, and $k_{obs,f,D}$) presented in Table 3.1. Figure 3.3 displays the $^{1}H/^{2}H$ IE values for the fast phase of decay of the substrate radical as a function of temperature. The $^{1}H/^{2}H$ IE values remain approximately constant from 190 to 207 K, with mean value and standard deviation (which is the standard deviation of the six mean $^{1}H/^{2}H$ IE values from 190 to 207 K) of 1.35 ±0.08. The value of 1.35 is lower than the steady-state $^{1}H/^{2}H$ IE on k_{cat} (or equivalently, the maximum velocity, V) of 7.4[43] or 7.5,[29] and also lower than the $^{1}H/^{2}H$ IE

of 25 on hydrogen transfer from C5' to product radical, which is predicted from the $^{1}H/^{3}H$ IE, by using classical theory.[34] Therefore, a primary hydrogen kinetic IE from HT2 does not significantly rate-determine the fast phase of the substrate radical decay reaction in the frozen aqueous system at 190-207 K.

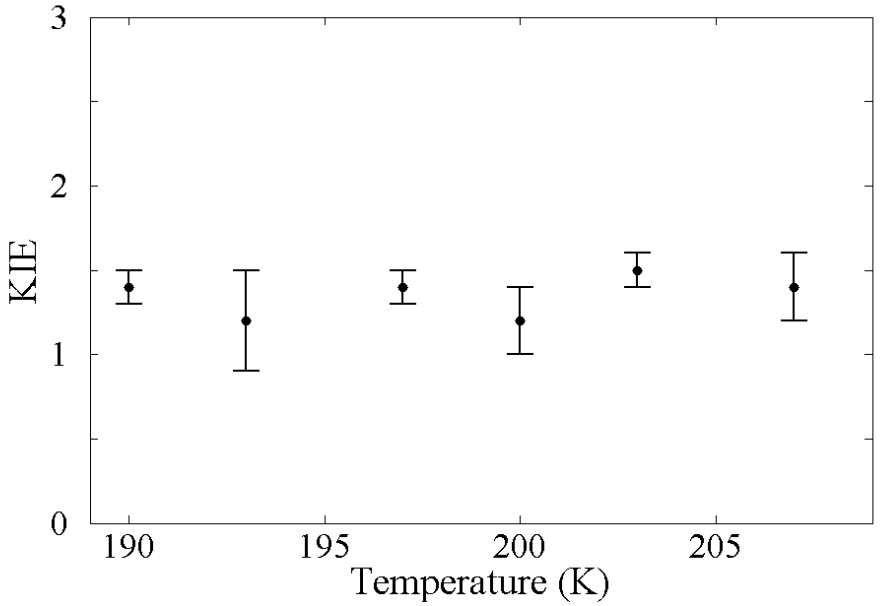

Figure 3.3: The $^{1}H/^{2}H$ IE values of the fast phase of the substrate radical decay as a function of temperature from 190 to 207 K. The data is presented in Table 3.1.

A minimal kinetic model for the irreversible substrate radical decay through the rearrangement and HT2 step is presented in Scheme 3.1. The following general expression for $k_{obs,f}$ is derived from this model:[118]

$$k_{obs,f} = \frac{k_{SP}\, k_{HT}}{k_{PS} + k_{HT}} \tag{3.1}$$

Here, k_{SP}, k_{PS}, and k_{HT}, represent the first-order rate constants for the forward and reverse rearrangement steps, and for HT2, respectively. The absence of a strong, primary hydrogen IE on $k_{obs,f}$ is consistent with Equation 3.1, if the condition, $k_{PS} << k_{HT}$, holds. In this case, $k_{obs,f} = k_{SP}$, and the hydrogen IE on $k_{obs,f}$ corresponds to $k_{SP,H}/k_{SP,D}$.

Therefore, we propose that the fast phase of decay of the substrate radical is rate-determined by the radical rearrangement step for both ^{1}H- and ^{2}H- substrate, and that $k_{obs,f}$ represents the observed first-order rate constant for the rearrangement step.

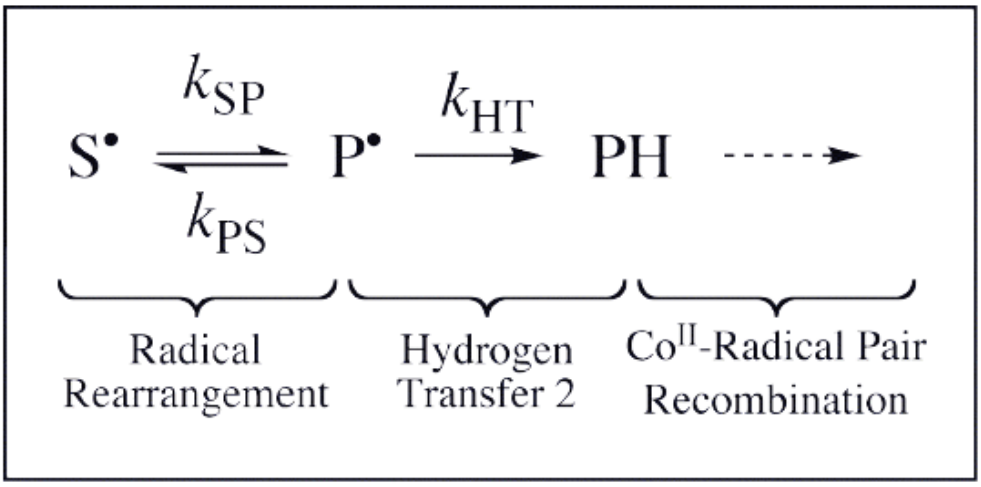

Scheme 3.1: Simple kinetic model for the decay reaction of the cryotrapped substrate radical following temperature-step to 190 to 207 K. The states are designated, as follows: S•, substrate radical; P•, product radical; PH, diamagnetic product state.

Rate limitation by the radical rearrangement is consistent with the observed accumulation of the substrate radical under steady-state turnover conditions.[50] It is also consistent with the substrate ^{14}N/^{15}N IE on the steady-state kinetic parameters, which has been proposed to arise from the C2-N bond cleavage in the substrate radical during the rearrangement step.[28,50] The observed IE of 1.35 on $k_{obs,f}$ suggests an α-secondary kinetic IE, arising from changes in the force constants of the C-H bonds in the substrate, that are associated with the migration of the amino group from C2 to C1.[129,130] The α-secondary kinetic IE for the change of hybridization of carbon from sp^3 to sp^2 is typically 1.1-1.2, and the theoretical maximum value has been calculated to be 1.4.[131] Thus, an α-secondary kinetic IE of 1.35 at C2, which arises from the zero-point energy difference for ^{1}H and ^{2}H

in the C2-H bonds,[118] is consistent with both the general conclusion that rearrangement step is the rate-limiting step in substrate radical decay, which is based on the observed steady-state accumulation of substrate radical, and with the contribution to the rate determination by the microscopic event of C2-N cleavage.[28,50]

Figure 3.4 shows plots of the natural logarithms of the observed rate constants $k_{obs,f}$ and $k_{obs,s}$ as a function of inverse absolute temperature, for the relaxation of ^{1}H-substrate and ^{2}H-substrate radicals, and overlaid linear fits to the four sets of data (Equation 2.3). Table 3.2 shows the logarithms of the Arrhenius prefactors, A_{app}, and activation energies E_a for the fast and slow phases of the ^{1}H- and ^{2}H-substrate radical decays.

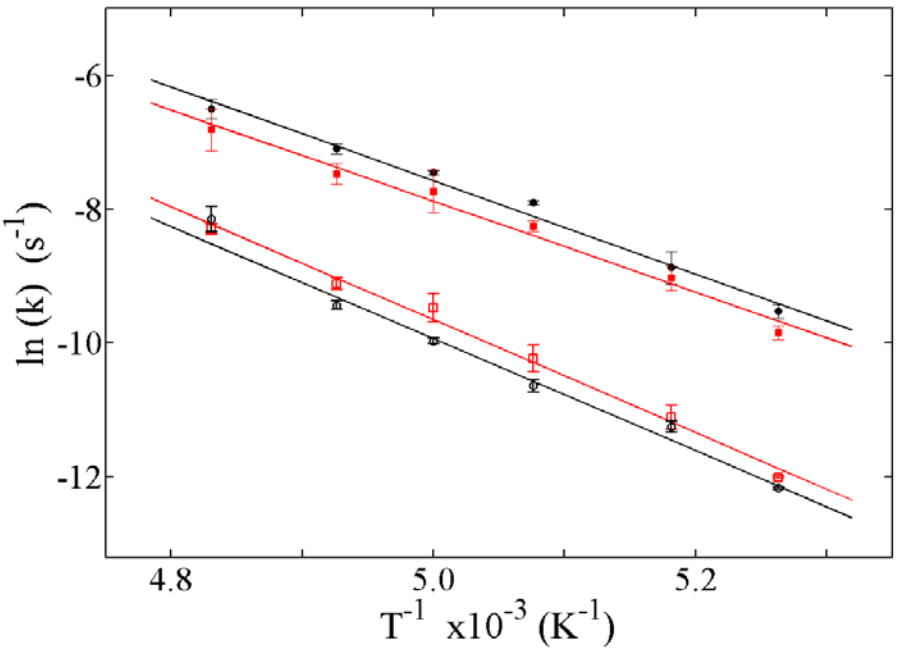

Figure 3.4: Arrhenius plots of the observed first-order rate constants for the decay of the natural abundance $^1H_4$-aminoethanol- and $^2H_4$-aminoethanol-generated substrate radicals from 190 to 207 K. Data from Table 2.1 for the ^{1}H-substrate radical $k_{obs,f}$ (black solid circles) and $k_{obs,s}$ (black open circles), and Table 3.1 for the ^{2}H-substrate radical $k_{obs,f}$ (red solid squares) and $k_{obs,s}$ (red open squares) are shown. The linear fits of the Arrhenius expression for the ^{1}H-substrate radical (black lines) and for the ^{2}H-substrate radical (red lines) are overlaid on the data. The A and E_a values derived from the fitting parameters are collected in Table 3.2.

The activation energies of the fast phase decay for the ^{1}H-substrate radical ($E_{a,H}$) and ^{2}H-substrate radical ($E_{a,D}$) from Arrhenius plots are 13.9±0.4 kcal/mol and 13.5 ±0.4 kcal/mol (Table 3.2), which correspond to E_a values for a radical rearrangement step in the coenzyme B_{12}-dependent EAL catalysis on ^{1}H-substrate and ^{2}H-substrate, respectively. The values of the Arrhenius prefactors of 2.5×10^{11} to 7.9×10^{11} s^{-1} differ by less than 17-fold from $k_B T/h = 4.2 \times 10^{12}$ s^{-1} at T = 200 K, which indicates that the rate determining events in rearrangement are accompanied by relative small entropy contributions (< 5.6 cal/mol/K). Therefore, comparisons of the experimental E_a values with values obtained by high-level quantum chemical calculations on restricted-atom models are appropriate. Values of 16 kcal/mol[132] and 12-15 kcal/mol were obtained from *ab initio* calculations for the rearrangement reaction in EAL.[124] The calculations were based on models that included the aminoethanol substrate, and different associated molecules, which represented putative active site amino acid side chains.[124,132,133] The auxiliary molecules assisted the nitrogen migration by the formation of hydrogen bonds with the ammonium group ("push" catalyst)[134] or the substrate hydroxyl oxygen ("pull" catalyst).[134] Active site arginine and glutamate side chains have been identified as substrate hydrogen bonding partners in the structural proteomics model for the EutB protein of EAL.[27,135] The protein structure and experimental E_a values are consistent with the proposed "synergistic retro-push-pull" hydrogen bonding model of radical rearrangement catalysis in EAL.[132,134]

Linear extrapolation of the low temperature Arrhenius plot for $k_{obs,f,H}$ in Figure 3.4 to 298 K gives a value of 6.2×10^{1} s^{-1}, which is comparable with our measured value k_{cat} = 5.2×10^{1} s^{-1} for EAL turnover on ^{1}H-aminoethanol. This implies that the relaxation

of $^{1}H_4$-aminoethanol-generated Co^{II}-substrate radical pair at low temperature and steady-state turnover of EAL on $^{1}H_4$-aminoethanol at room temperature have the same rate limiting step, which is, therefore, the radical rearrangement step. This is consistent with the substrate $^{14}N/^{15}N$ IE on V/K_M and V.[28,50] Therefore, HT2 is not rate-limiting for the steady-state turnover of EAL on ^{1}H-aminoethanol at room temperature. However, the HT2 step is at least partially rate-limiting for steady-state turnover of EAL on ^{2}H-aminoethanol. This suggests that the intrinsic $^{1}H/^{2}H$ IE on the HT2 step is not fully manifested in the steady-state $^{1}H/^{2}H$ IE on k_{cat} of 7.4[43] or 7.5,[29] which may lead to anomalously large observed $^{1}H/^{3}H$ IE (100)[5] for the transfer of hydrogen from the C5'-methyl group to the product radical, because a larger proportion of the intrinsic ^{3}H IE is manifested in the observed IE for k_{cat} and for hydrogen transfer from C5' to the product radical, relative to the ^{2}H IE. The observed room temperature $^{1}H/^{2}H$ IE on k_{cat} also suggests that $k_{obs,f,D}$ must deviate from the linear extrapolation at $T > 207$ K. Experiments and a proposed model to test this prediction, and further address the paradox of $^{1}H/^{2}H$ and $^{1}H/^{3}H$ IE, will be presented in Chapter IV.

Table 3.2: Fitting parameters for Arrhenius reaction rate expression for the fast and slow phases of the ^{2}H- and ^{1}H-substrate radical decay kinetics for the temperature range, 190 to 207 K.

Kinetic Phase	Log[A (s^{-1})]	E_a (kcal mol^{-1})	R^{2a}
^{2}H-Labeled			
Fast	11.4 (±0.9)	13.5 (±0.4)	0.9920
Slow	14.7 (±0.8)	17.3 (±0.3)	0.9969
^{1}H-Labeled			
Fast	11.9 (±0. 9)	13.9 (±0.4)	0.9935
Slow	13.8 (±1.0)	17.3 (±0.6)	0.9933

[a] R is Pearson's correlation coefficient.

3.2.3 Characterization of the Slow Phase of Decay of Substrate Radical

Figure 3.5 displays the $^{1}H/^{2}H$ IE values of the slow phase decay of substrate radical as a function of temperature, which shows that the $^{1}H/^{2}H$ IE values remain approximately constant from 190 to 207 K, with mean value and standard deviation (which is the standard deviation of the six mean $^{1}H/^{2}H$ IE values from 190 to 207 K) of 0.79 ± 0.11. The inverse IE on $k_{obs,s}$ implies that a normal primary kinetic IE from HT2 step does not contribute significantly to rate-determination of the slow phase of the substrate radical decay reaction. The origin of the inverse IE on $k_{obs,s}$ is not clear, but possible explanations based on the decay reaction and mechanism shown in Figure 1.3 are offered. The difference in the values of $k_{obs,s}$ and $k_{obs,f}$, and the different IE values on $k_{obs,s}$ and $k_{obs,f}$ suggest that different microscopic events are rate determining for the fast and slow phase decay. The narrow temperature range of approximately < 7 K for the transition that partitions the high temperature (T > 210 K) monoexponential decay population into the kinetically isolated fast phase and slow phase populations (T < 207 K) suggests that the fast phase and slow phase are distinguished by a change in the dynamical properties of the protein.[113] If the protein influence shifts the transition state for rearrangement to a later position on the N-migration coordinate, then the development of significant sp^2 hybridization at both C1 and C2 in an associative, cyclopropyl transition state,[136] or a dissociative allyloxy transition state,[137,138] may lead to an inverse α-secondary kinetic isotope effect.

The assignment of $k_{obs,s}$ to a specific step, or steps, is not well-supported, as for $k_{obs,f}$, and therefore, a detailed mechanistic interpretation of the $E_{a,s}$ and A_s values is not possible. The $E_{a,s}$ values are 3 to 4 kcal/mol higher than the $E_{a,f}$ values, which is

consistent with a shift in the position of the transition state away from the position for the fast phase, which is assumed to be the native process. The effect of the larger $E_{a,s}$ values on decreasing the rate constant is attenuated by an increase in A_s relative to A_f by a factor of approximately 10^2, which suggests more freedom in the transition state for the slow decay component compared to the fast decay component.

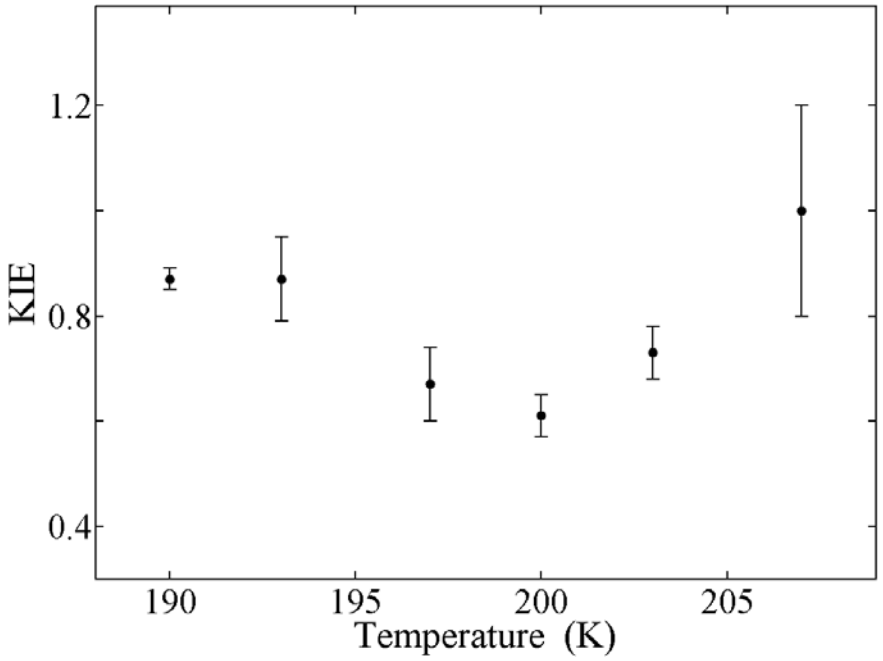

Figure 3.5: The $^1H/^2H$ IE values of the slow phase of the substrate radical decay as a function of temperature from 190 to 207 K. The data is presented in Table 3.1.

3.3 Conclusion

The $^1H/^2H$ substrate kinetic IE values of the fast phase decay remain approximately constant (1.35 ±0.08) from 190 to 207 K. The Arrhenius parameters for the fast phase of the ^1H- and ^2H-substrate radical decay reaction are same to within standard deviation, with A_f (2.5×10^{11} to 7.9×10^{11} s^{-1}) comparable with $k_B T/h = 4.2 \times 10^{12}$ s^{-1} at $T = 200$ K,

and E_a (13.5 to 13.9 kcal/mole) consistent with a*b initio* calculations (12 to 16 kcal/mol).[132,139] The rate-limiting step for the fast phase decay of the substrate radical is proposed to be the rearrangement step, and that $k_{obs,f}$ represents the observed first-order rate constant for the rearrangement reaction. The experiments also imply the radical rearrangement step is the rate limiting step of steady-state turnover of EAL on $^1H_4$-aminoethanol at room temperature, because the linear extrapolation of the low temperature Arrhenius plot for $k_{obs,f,H}$ to 298 K gives the value (6.2×10^1 s^{-1}) comparable to $k_{cat} = 5.2 \times 10^1$ s^{-1} for EAL turnover on $^1H_4$-aminoethanol.

The $^1H/^2H$ substrate IE values for the slow phase decay remain approximately constant (0.79±0.11) from 190 to 207 K. The Arrhenius parameters for the slow phase of the ^1H- and ^2H-substrate radical decay reaction are shown in Table 3.2, which are same to within one standard deviation. The origin of the inverse IE on $k_{obs,s}$ is not clear. We will further discuss the slow phase decay of substrate radical in Chapter V.

Chapter IV

Resolution of the Steady-state Hydrogen Isotope Effect Paradox in EAL

4.1 Background and Introduction

The minimal mechanism of coenzyme B_{12}-dependent EAL is shown in Figure 1.3 of Chapter I.[5,39] Low temperature relaxation of ^{1}H-aminoethanol-generated Co^{II}-substrate radical pair over the temperature range 190 to 223 K is discussed in Chapter II.[113] The decay kinetics of ^{1}H- and ^{2}H-substrate radical have been measured from 190 to 207 K to address the molecular mechanism of fast phase and slow phase decay of substrate radical [Zhu, C.; Warncke, K., *JACS*, Accepted].

In Chapter III, we concluded that the rearrangement step is rate-determining for the decay reaction of both the ^{1}H-substrate and ^{2}H-substrate Co^{II}-substrate radical pair states, over 190 to 207 K. The large observed room temperature ^{1}H/^{2}H IE (7.5)[34] on k_{cat} relative to the ^{1}H/^{2}H substrate kinetic IE (1.35) [Zhu, C.; Warncke, K., *JACS*, Accepted] at $T \leq$ 207 K suggests that $k_{obs,f,D}$ must deviate from the linear extrapolation at $T >$ 207 K. In order to address the discrepancy of the ^{1}H/^{2}H IE at low temperature and at room temperature, the measurement of the decay of $^2H_4$-aminoethanol-generated Co^{II}-substrate radical was extended to 223 K. A three-state, two-step model is proposed to address the temperature dependence of the ^{1}H/^{2}H IE. The model suggests that the large value of the ^{1}H/^{2}H IE at room temperature, relative to $T \leq$ 207 K, arises from HT2 as a partial rate limiting step for ^{2}H-substrate radical decay at $T >$ 207 K. The intrinsic ^{1}H/^{2}H IE of 25 on hydrogen transfer from C5' to the product radical, predicted from the ^{1}H/^{3}H IE (100)[5] by using classical theory,[140-142] is much larger than the ^{1}H/^{2}H IE (7.5)[34] on k_{cat} at room temperature. The discrepancy is addressed, and the results are well fitted by the three-state, two-step model. The model also suggests that the relaxation of the Co^{II}-substrate radical is associated with a large negative activation entropy change.

4.2 Resolution of $^{2}H/^{3}H$ Steady-state IE Paradox

4.2.1 Kinetics of $^{1}H_4$- and $^{2}H_4$-aminoethanol-generated Substrate Radical Decay from 190 to 223 K

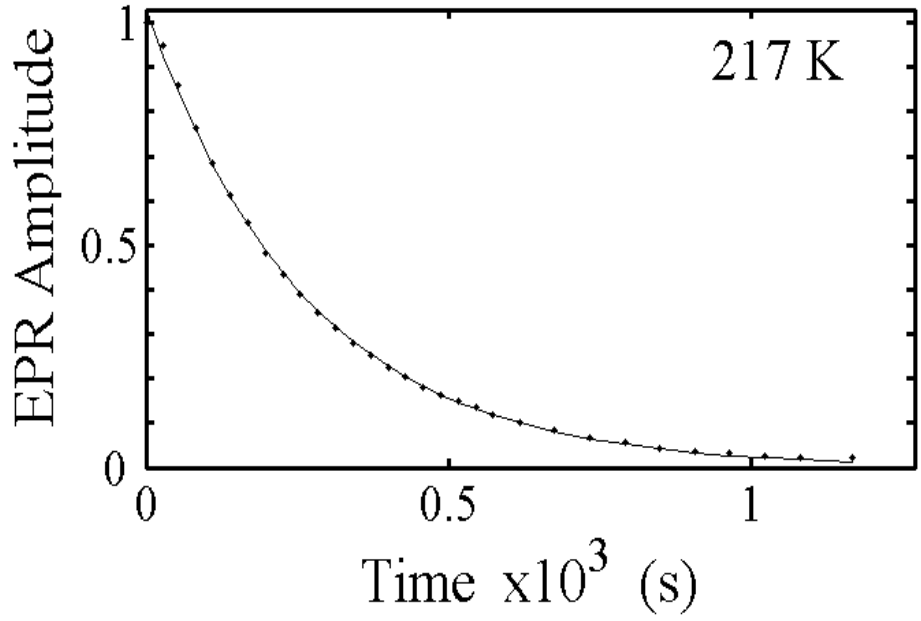

Figure 4.1: Representative decay of the $^{2}H_4$-substrate radical at 217 K, and overlaid monoexponential function. The EPR experimental conditions are as described in the legend to Figure 3.1. The overlaid solid curves correspond to simulations of the decay as monoexponential function (210 to 223 K) with best fitted parameters in Table 4.1.

Figure 4.1 shows a representative of 1,1,2,2-$^{2}H_4$-aminoethanol-generated substrate radical decay at 217 K, which is overlaid by the fit of a monoexponential function (Equation 2.1, N = 1). As discussed in Chapter II and III, the emergence of the slow phase of the substrate radical decay is proposed to be associated with a protein dynamic transition,[113] which will be addressed in Chapter V. Figure 4.2 shows the dependence of the normalized amplitudes of the fast phase and slow phase of the biexponential decay of the substrate radical, prepared with ^{1}H-substrate and ^{2}H-substrate, on temperature. The transition temperature region of the $^{2}H_4$-aminoethanol-generated substrate radical (207 to

210 K) is different from the transition temperature region of the $^{1}H_{4}$-aminoethanol-generated substrate radical (210 to 214 K). The decays of the ^{1}H and ^{2}H substrate radical at 210 K are biexponential and monoexponential, respectively, and the standard deviations of the fast phase and slow phase of the biexponential decay of the ^{1}H-substrate radical at 210 K is much larger compared to the those at T < 210 K. The temperature of 210 K corresponds to different decay regimes for ^{1}H-substrate radical (biexponential decay, characteristic of 190 to 207 K) and ^{2}H-substrate radical (monoexponential decay, characteristic of higher temperature). Therefore, the data point at 210 K will not be included in the following analysis.

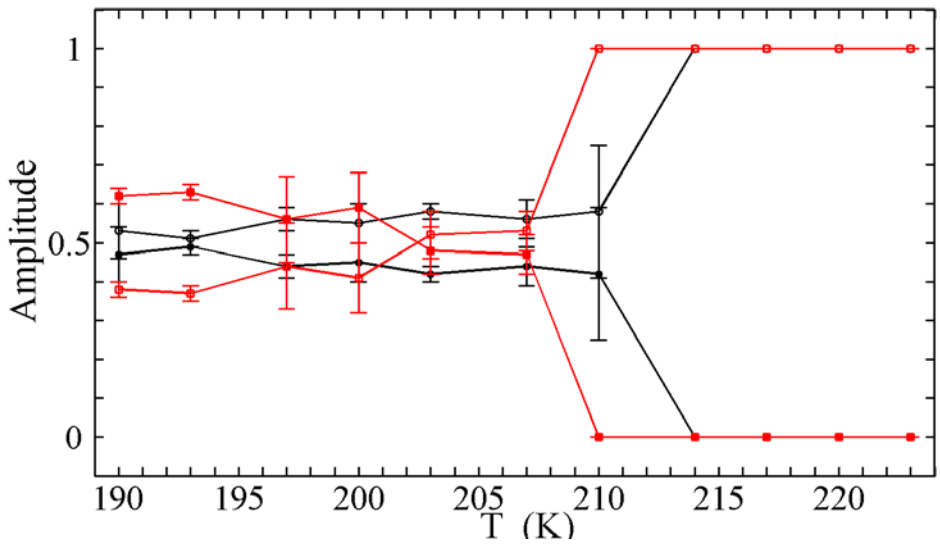

Figure 4.2: Amplitudes of the fast and slow decay phases of the biexponential decay of the ^{1}H-substrate ($A_{obs,f,H}$ and $A_{obs,s,H}$) and ^{2}H-substrate radical ($A_{obs,f,D}$ and $A_{obs,s,D}$), respectively, as a function of temperature. Data from Table 2.1 for the ^{1}H-substrate radical $A_{obs,f,H}$ (black open circles) and $A_{obs,s,H}$ (black solid circles), and Table 3.1 and 4.1 for the ^{2}H-substrate radical $A_{obs,f,D}$ (red open squares) and $A_{obs,s,D}$ (red solid squares) are shown. The curves are drawn to guide the eye.

Table 4.1 displays the first-order rate constants for ^{1}H- and ^{2}H-substrate radical decay reactions from 210 to 223 K, which corresponds to the temperature region of the monoexponential decay for the ^{2}H-substrate radical. The first-order rate constants for

decay of the ^{1}H- and ^{2}H-substrate radical in the biexponential decay region from 190 to 207 K are shown in Table 2.1 and Table 3.1, respectively.

Table 4.1: First-order rate constant and amplitude parameters for the fit of the bi- or monoexponential function to the decay kinetics of ^{1}H- and ^{2}H-substrate radical and ^{1}H/^{2}H hydrogen kinetic isotope effects at different temperatures, 210 to 223 K.

T (K)	$k_{obs,f}$ (s^{-1})	A_f [a]	$k_{obs,s}$ (s^{-1})	A_s [b]	R^2 [c]	*KIE*
^{1}H-substrate						
210	$3.2(\pm0.7) \times 10^{-3}$	0.58±0.17	$9.4(\pm3.0) \times 10^{-4}$	0.42±0.17	0.9993	--
214	$4.0(\pm0.4) \times 10^{-3}$	1.00±0.00	--	--	0.9981	1.74±0.19
217	$6.8(\pm0.4) \times 10^{-3}$	1.00±0.00	--	--	0.9969	1.84±0.12
220	$1.1(\pm0.1) \times 10^{-2}$	1.00±0.00	--	--	0.9993	2.00±0.19
223	$1.6(\pm0.1) \times 10^{-2}$	1.00±0.00	--	--	0.9991	2.10±0.19
^{2}H-substrate						
210	$2.3(\pm0.2) \times 10^{-3}$	1.00±0.00	--	--	0.9997	--
214	$2.3(\pm0.2) \times 10^{-3}$	1.00±0.00	--	--	0.9997	--
217	$3.7(\pm0.3) \times 10^{-3}$	1.00±0.00	--	--	0.9992	--
220	$5.5(\pm0.1) \times 10^{-3}$	1.00±0.00	--	--	0.9984	--
223	$7.5(\pm0.4) \times 10^{-3}$	1.00±0.00	--	--	0.9971	--

[a]The relative fitted amplitude for the fast phase, normalized to the sum, A_f+A_s.
[b]The relative fitted amplitude for the slow phase, normalized to the sum, A_f+A_s.
[c]R is Pearson's correlation coefficient.

4.2.2 Temperature Dependence of Rate Limiting Step

Figure 4.3 shows plots of the natural logarithms of the observed rate constants, $k_{obs,f}$ and $k_{obs,s}$, as a function of inverse absolute temperature for the relaxation of ^{1}H-substrate and ^{2}H-substrate radicals. The overlaid linear fits to the set of data for 190 to 223 K for the ^{1}H-substrate radical, and to the set of data for 190 to 207 K for the ^{2}H-substrate radical, are also shown in Figure 4.3. As discussed earlier, and presented in Table 2.2 and Table 3.2, the Arrhenius fitting parameters of the ^{1}H-substrate radical decay are the same

to within the standard error, for the temperatures ranges of 190 to 223 K (E_a = 13.4 ± 0.2 kcal/mol) and 190 to 207 K ($E_{a,f}$ = 13.9 ± 0.4 kcal/mol). It is, therefore, proposed that the rearrangement step is the rate limiting step for the ^{1}H-substrate radical decay from 190 to 223 K. However, the observed rate constants ($k_{obs,f,D}$, and $k_{obs,m,D}$) for the ^{2}H-substrate radical decay do not follow the same Arrhenius relationship from 190 to 223 K. Instead, the data for $T \geq 210$ K deviate significantly from the fit to the data for 190 to 207 K, as shown in Figure 4.3. This suggests that the rate limiting step for the ^{2}H-substrate radical decay changes as the temperature is increased from 190 to 223 K.

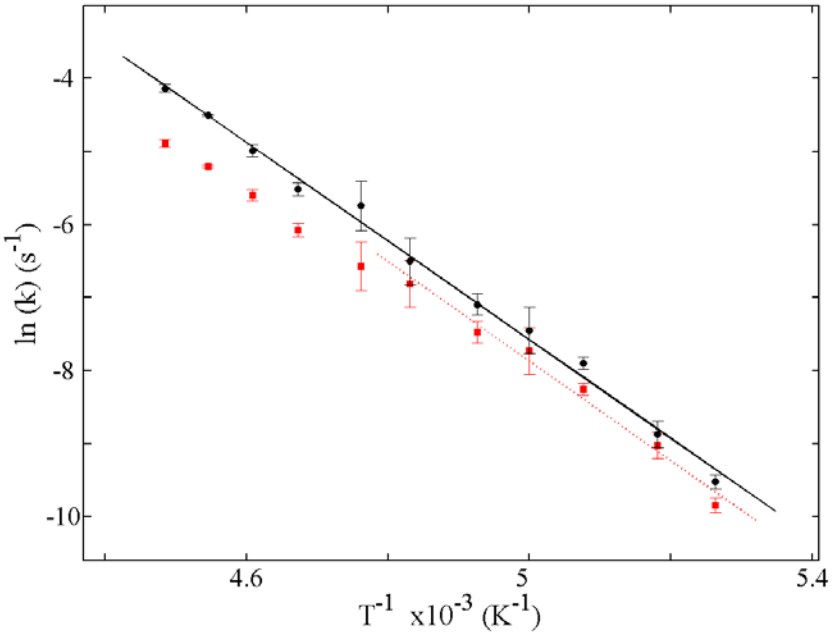

Figure 4.3: Arrhenius plots of the observed first-order rate constants for the decay of the natural abundance $^1H_4$-aminoethanol- and $^2H_4$-aminoethanol-generated substrate radicals from 190 to 223 K. Data from Table 2.1 for the ^{1}H-substrate radical $k_{obs,f}$ and $k_{obs,m}$ (black solid circles) and Table 3.1 and Table 4.1 for the ^{2}H-substrate radical $k_{obs,f}$ and $k_{obs,m}$ (red solid squares) are shown. The linear fits of the Arrhenius expression for the ^{1}H-substrate radical (black lines) from 190 to 223 K and for the ^{2}H-substrate radical from 190 to 207 K(red dash lines) are overlaid on the data. The A and E_a values derived from the fitting parameters are collected in Table 2.2 and Table 3.2.

Figure 4.4 shows the $^{1}H/^{2}H$ IE values for k_{obs} for the substrate radical decay as a function of temperature. Figure 4.4 shows that the $^{1}H/^{2}H$ IE values remain approximately constant (average, 1.35) for $T \leq 207$ K, and then increase as temperature increases above 210 K, reaching the value of 2.1 at 223 K. The increase of $^{1}H/^{2}H$ IE at $T \geq 214$ K suggests that at least one of the rate limiting steps for the ^{1}H- and ^{2}H-substrate radical decay changes as temperature increases above 210 K. The rearrangement step is proposed to be the only rate limiting step for the decay of ^{1}H-substrate radical from 190 K to room temperature [Zhu, C.; Warncke, K., *JACS*, Accepted]. A three-state, two-step model proposed below is used to address the temperature dependence of the $^{1}H/^{2}H$ IE, over the full temperature interval of 190 to 223 K and the emergence of a different rate-limiting step for the ^{2}H-substrate radical at higher temperature.

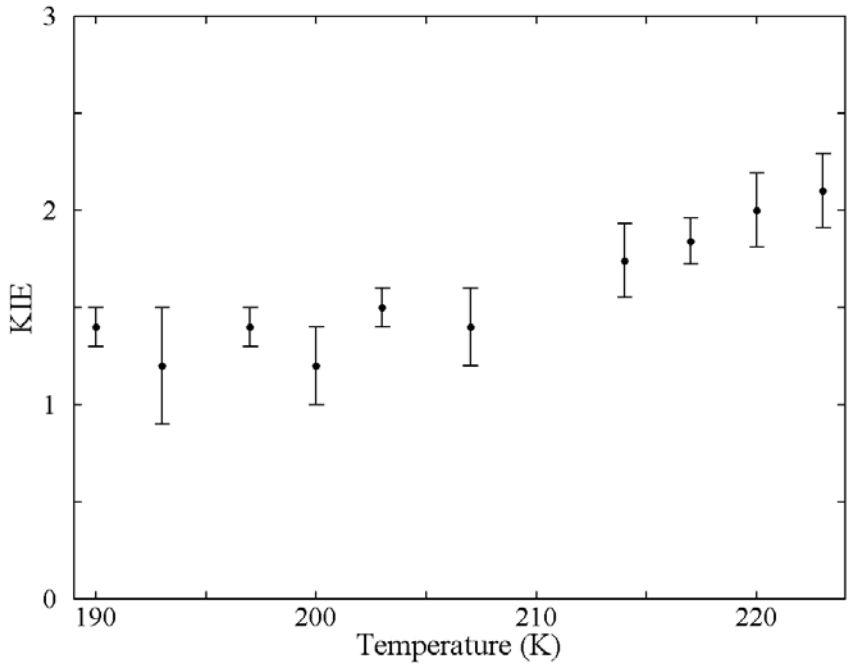

Figure 4.4: The $^{1}H/^{2}H$ IE values of the fast phase decay and monoexponential decay of substrate radical as a function of temperature from 190 to 223 K. The data is presented in Table 3.1 and Table 4.1.

4.2.3 Temperature and Isotope Dependent Three-state, Two-step Model

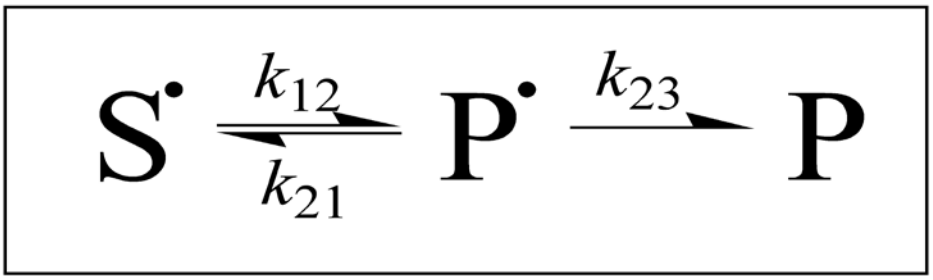

Scheme 4.1: Three-state, two-step model for the decay reaction of the cryotrapped substrate radical. The states are designated, as follows: S˙, substrate radical; P˙, product radical; PH, diamagnetic product state.

The above discussion suggests that decay of the substrate radical to the final diamagnetic product involves at least two distinguishable steps, which is consistent with the proposed minimal mechanism in Figure 1.3 (steps 3 and 4). We here propose a three-state, two-step model, which is shown in Scheme 4.1. This model is used to address, and account for, the following observations: (a), the decay kinetics of ^{1}H- and ^{2}H-substrate radicals, (b), the ^{1}H/^{2}H steady-state turnover IE of 7.4-7.5, or 7.8,[4,27,34] and (c), the ^{1}H/^{3}H IE of 100 on hydrogen transfer from the C5'-methyl group to the product radical.[5] In Scheme 4.1, S˙, P˙ and P, represent Co^{II}-substrate radical pair state, Co^{II}-product radical pair state and diamagnetic product state. The rate constants k_{12}, k_{21} and k_{23} are the rate constants for the rearrangement step, reverse of rearrangement step, and the forward step of HT2. The HT2 step represents the irreversible step in the substrate radical decay.

4.2.3.1 Derivation of Three-state, Two-step Model

From Scheme 4.1, the observed first-order rate constants k_{obs}, the microscopic rate constants, k_{12}, k_{21}, k_{23}, and the steady-state substrate radical concentration, [S˙], and product radical concentration, [P˙], have the following relationship:

$$[S^{\bullet}]k_{obs} = [P^{\bullet}]k_{23} \tag{4.1}$$

$$[S^{\bullet}]k_{12} = [P^{\bullet}](k_{21} + k_{23}) \tag{4.2}$$

The first rate constant, k_{obs}, is the observed kinetic rate constant of the fast phase decay ($T \leq 207$ K) or monoexponential decay ($T \geq 214$ K) of the substrate radical. Equations 4.1 and 4.2 are rearranged to obtain:

$$k_{obs} = \frac{[P^{\bullet}]}{[S^{\bullet}]}k_{23} = \frac{k_{12}k_{23}}{k_{21} + k_{23}} \tag{4.3}$$

The $^1H/^2H$ substrate radical kinetic isotope effect (IE) on k_{obs}, that is observed from 190 to 223 K, can be expressed as:

$$IE = \frac{k_{obs,H}}{k_{obs,D}} = \frac{k_{12,H}}{k_{12,D}}\frac{k_{23,H}}{k_{23,D}}\left[\frac{k_{21,D} + k_{23,D}}{k_{21,H} + k_{23,H}}\right] \tag{4.4}$$

The terms $\frac{k_{12,H}}{k_{12,D}}$ and $\frac{k_{23,H}}{k_{23,D}}$, represent the $^1H/^2H$ substrate IE for the rearrangement step and the intrinsic $^1H/^2H$ IE for HT2 step, respectively. The term $\frac{k_{21,D} + k_{23,D}}{k_{21,H} + k_{23,H}}$ arises from the $^1H/^2H$ substrate IE on the rate constants for forward or reverse egress from the product radical state in Scheme 4.1. In Chapter III, it is proposed that the rearrangement step is the only rate limiting step for ^1H-substrate radical decay from 190 K to room temperature, which is equivalent to the condition that $k_{21,H} << k_{23,H}$ from 190 K to room temperature. In the following derivation, the condition $k_{21,H} << k_{23,H}$ is assumed. Validity of the inequality will be evaluated, by estimating the ratio of $k_{21,H}$ to $k_{23,H}$, by using the intrinsic $^1H/^2H$ IE for the HT2 step. The intrinsic $^1H/^2H$ IE is estimated from the $^1H/^3H$ IE

value of 100,[5] following the completion of the kinetic derivation of the three-state, two-step model for our system. Under the condition, $k_{21,H} << k_{23,H}$, Equation 4.4 is reduced to:

$$IE \approx \frac{k_{12,H}}{k_{12,D}}\left[\frac{k_{21,D}+k_{23,D}}{k_{23,D}}\right] \tag{4.5}$$

Equation 4.5 indicates that the two terms, $\frac{k_{12,H}}{k_{12,D}}$, and $\frac{k_{21,D}+k_{23,D}}{k_{23,D}}$, are the main contributors to the observed $^1H/^2H$ IE. For the rearrangement step, the α-secondary kinetic IE for the change of hybridization of carbon from sp^3 to sp^2 is typically 1.1 to 1.2, and the theoretical maximum value has been calculated to be 1.4.[131] Thus, it is reasonable to assume that $\frac{k_{12,H}}{k_{12,D}}$ has a temperature-independent value of 1.3. This is consistent with a measured value of 1.35. Equation 4.5 therefore suggests that the temperature dependence of the observed $^1H/^2H$ IE is primarily caused by the term, $\frac{k_{21,D}+k_{23,D}}{k_{23,D}}$. We can conclude that $k_{21,D}$ is much smaller compared to $k_{23,D}$ at $T \leq 207$ K because of the constant $^1H/^2H$ IE of 1.35 from 190 to 207 K. Equation 4.5 also indicates that $k_{21,D}$ becomes comparable to $k_{23,D}$ at $T > 210$ K, because the $^1H/^2H$ IE increases from 1.7 to 2.1 over 214 to 223 K, up to a value of 7.5 at 293 K. Therefore, Equation 4.5 can be expressed as:

$$IE \approx \frac{k_{12,H}}{k_{12,D}} \qquad T \leq 207\ \text{K} \tag{4.6}$$

$$IE \approx \frac{k_{12,H}}{k_{12,D}}\frac{k_{21,D}+k_{23,D}}{k_{23,D}} \qquad T \geq 214\ \text{K} \tag{4.7}$$

For T > 210 K, the ratio of $k_{21,D}/k_{23,D}$, is temperature dependent, and must be estimated to obtain the $^1H/^2H$ IE as a function of temperature. Assuming that $k_{21,D}$ and $k_{23,D}$ follow individual Arrhenius relations over the temperature range addressed, the temperature dependence of $k_{21,D}$ and $k_{23,D}$ can be expressed as:

$$k_{21,D} = A_{21,D}e^{-E_{a21,D}/RT}$$
$$k_{23,D} = A_{23,D}e^{-E_{a23,D}/RT} \quad (4.8)$$

In Equation 4.8, $A_{21,D}$ and $E_{a21,D}$ represent the prefactor and activation energy that correspond to $k_{21,D}$, and $A_{23,D}$, and $E_{a23,D}$ represent the prefactor and activation energy that correspond to $k_{23,D}$.

To obtain the $^1H/^2H$ substrate IE on k_{obs}, as a function of temperature, at least two values of $\frac{k_{21,D}}{k_{23,D}}$ at two different temperatures must be estimated, because the two parameters $A_{21,D}$ / $A_{23,D}$ and $E_{a21,D}$- $E_{a23,D}$ have to be obtained. Temperatures of 293 and 207 K are chosen for the analysis. In order to calculate $k_{21,D}/k_{23,D}$ at 293 K, the ratio of $k_{obs,H}/k_{obs,D}$ must be determined. During the steady-state turnover of EAL on substrate, the concentration of product produced in a unit time can be expressed as:

$$\frac{d[\mathrm{P}]}{dt} = [\mathrm{S}^{\bullet}]k_{obs} \quad (4.9)$$

Here, $[\mathrm{S}^{\bullet}]$ is the concentration of substrate radical during the steady-state turnover of EAL, and k_{obs} is the observed rate constant from $\mathrm{S}^{\bullet}$ to final product. It is assumed here that the final product produced per unit of time during the steady-state turnover of EAL

can also be expressed by Equation 4.9. The relationship between the $^1H/^2H$ steady-state IE and $k_{obs,H}/k_{obs,D}$ can be obtained:

$$IE_{\text{turnover},T=293\,\text{K}} = \frac{d[\text{P}_\text{H}]/dt}{d[\text{P}_\text{D}]/dt} = \frac{[\text{S}_H^\bullet]}{[\text{S}_D^\bullet]}\left(\frac{k_{obs,H}}{k_{obs,D}}\right)_{T=293\text{ K}} \tag{4.10}$$

Here, $[\text{S}_H^\bullet]$ and $[\text{S}_D^\bullet]$ are the concentrations of ^{1}H- and ^{2}H-aminoethanol substrate radicals during the turnover of EAL at room temperature, respectively. We also denote the total concentration of EAL as $[\text{EAL}]$. It is reported that the value of $[\text{S}_H^\bullet]/[\text{EAL}]$ is 70±5% at 280 K.[50] The ratio of concentration of 1,1-$^2H_2$-aminoethanol generated substrate radical to the concentration of EAL during the steady-state turnover of EAL is same as $[\text{S}_H^\bullet]/[\text{EAL}]$ [G.H. Reed, private communication]. Therefore, it is reasonable to assume that $[\text{S}_H^\bullet]$ and $[\text{S}_D^\bullet]$ are equivalent given the same $[\text{EAL}]$, and that the steady-state concentration of substrate radical does not change from 280 to 293 K. We obtain:

$$\left(\frac{k_{obs,H}}{k_{obs,D}}\right)_{T=293K} \approx 7.5 \tag{4.11}$$

From Equations 4.7 and 4.11, and $\frac{k_{12,H}}{k_{12,D}} \approx 1.3$, $\frac{k_{21,D}}{k_{23,D}}$ is estimated as 4.8 at T = 293 K.

The $^1H/^2H$ substrate IE on $\frac{k_{obs,H}}{k_{obs,D}}$ is approximately constant (1.35±0.08) at $T \leq 207$ K, which suggests that $k_{21,D}$ is much smaller compared to $k_{23,D}$ at temperature $T \leq 207$ K. The $^1H/^2H$ substrate IE values start to increase at $T > 210$ K, implying $k_{21,D}$ and $k_{23,D}$ become more comparable. From these data, we assume values of $\frac{k_{21,D}}{k_{23,D}}$ in the range of

0.05 to 0.2, at T = 207 K, which correspond to the upper limit, before an IE is detectable. We then obtain:

$$\frac{\left(\frac{k_{21,D}}{k_{23,D}}\right)_{T=293K}}{\left(\frac{k_{21,D}}{k_{23,D}}\right)_{T=207K}} \approx [24-96] \tag{4.12}$$

Substituting Equation 4.8 into Equation 4.12, we obtain:

$$\frac{\frac{A_{21,D}e^{-E_{a21,D}/293R}}{A_{23,D}e^{-E_{a23,D}/293R}}}{\frac{A_{21,D}e^{-E_{a21,D}/207R}}{A_{23,D}e^{-E_{a23,D}/207R}}} = e^{-\left(\frac{E_{a21,D}-E_{a23,D}}{R}\right)\left(\frac{1}{293}-\frac{1}{207}\right)} \approx [24-96] \tag{4.13}$$

It is assumed that the $A_{ij,D}$ depends linearly on T (Arrhenius temperature dependence), and that the remaining contributions to the $A_{ij,D}$ are T-independent. From Equation (4.13), $E_{a21,D}$ -$E_{a23,D}$ can be estimated as 4.5-6.4 kcal/mol. Substituting $E_{a21,D}$ -$E_{a23,D}$ back into $\left[\frac{k_{21,D}}{k_{23,D}}\right]_{T=293\ K} = 4.8$, the ratio of $\frac{A_{21,D}}{A_{23,D}}$ is obtained as 1.0×10^4 to 2.8×10^5.

Before working on the simulation of $^1H/^2H$ IEs as a function of temperature by using our developing model, it is necessary to evaluate the assumption regarding the rate limiting step for the decay reaction of the ^1H-substrate radical from 190 K to room temperature. The assumption, that the rearrangement step is the only rate limiting step for the decay of ^1H-substrate radical from 190 K to room temperature, requires that $k_{21,H} << k_{23,H}$ holds at room temperature. The intrinsic $^1H/^2H$ IE is estimated as 25 for HT2 step, based on the $^1H/^3H$ IE value of 100.[5] It is assumed that $k_{21,H} \approx k_{21,D}$, which is a good

approximation because the IE on rearrangement step with forward direction is 1.3, which is relatively small, and it is likely that the IE on the reverse rearrangement step is also small. Together with $\left[\frac{k_{21,D}}{k_{23,D}}\right]_{T=293\ K} = 4.8$, the relationship between $k_{21,H}$ and $k_{23,H}$ is estimated as:

$$\left[\frac{k_{21,H}}{k_{23,H}}\right]_{T=293\ K} = \left[\frac{k_{21,D}}{25 \times k_{23,D}}\right]_{T=293\ K} = 0.19 \tag{4.14}$$

Equation 4.14 shows that our assumption, that $k_{21,H} << k_{23,H}$, is valid at room temperature to a good approximation, which means that the rearrangement step is the only rate limiting step for the decay of ^{1}H-substrate radical from 190 K to room temperature. It is always possible to substitute the ratio of $\frac{k_{21,H}}{k_{23,H}}$ at 293 K back into Equation 4.4 to interactively adjust the three-state, two-step model derivation. However, this substitution does not change the final result significantly. The values $E_{a21,D}$ -$E_{a23,D}$ and $\frac{A_{21,D}}{A_{23,D}}$ are increased by < 10%, and we do not show the adjustment here.

To further evaluate the proposed three-state, two-step model, the ^{1}H/^{2}H steady-state turnover IE at 277 K is measured and obtained as 5.5±0.4. This value is taken as an approximation of the ^{1}H/^{2}H substrate radical decay IE ($\left(\frac{k_{obs,H}}{k_{obs,D}}\right)_{T=276K} = 5.5$) for the same reason discussed above. A representative simulation of the ^{1}H/^{2}H IE versus temperature is shown in Figure 4.5.

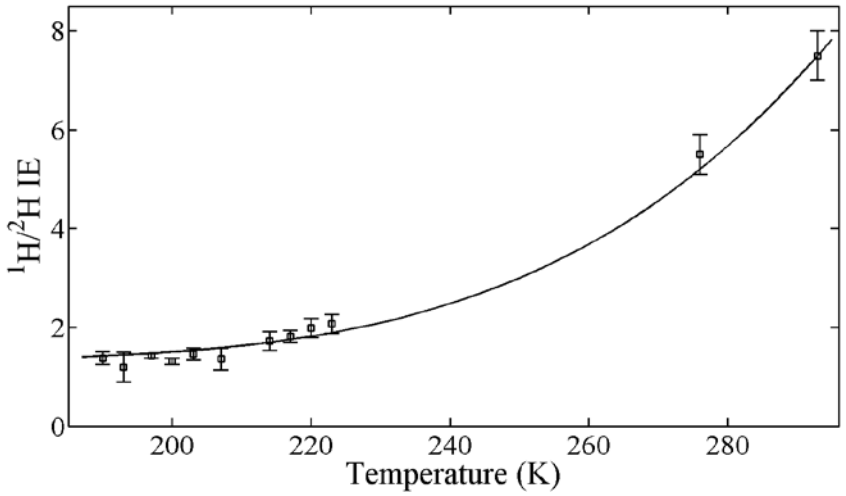

Figure 4.5: Simulation of ^{1}H/^{2}H IE values of the fast phase decay and monoexponential decay of substrate radical from the three-state, two-step model, as a function of temperature. Simulation parameters: $k_{12,H}/k_{12,D}$ = 1.3, and $k_{21,D}/k_{23,D,\ T=207\ K}$ = 0.2.

4.2.3.2 Relative Activation Entropy Values of the HT2 and Reverse Radical Rearrangement Steps

Based on the proposed three-state, two-step model discussed above, the observed temperature dependent ^{1}H/^{2}H substrate IE arises from the temperature dependent term, $\frac{k_{21,D}}{k_{23,D}}$. With the assumption that $k_{21,D}$ and $k_{23,D}$ follow the Arrhenius relation, the ratio of the prefactor ($A_{21,D}$) of $k_{21,D}$ to that ($A_{23,D}$) of $k_{23,D}$ is estimated as 1.0×10^4 to 2.8×10^5 and the difference between the activation energy ($E_{a,21,D}$) of $k_{21,D}$ and that ($E_{a,23,D}$) of $k_{23,D}$ is estimated as 4.5 to 6.4 kcal/mole from Equation 4.13. The large value of $A_{21,D}/A_{23,D}$ could not be addressed by the simple Arrhenius relation. Here, we introduce the transition state theory to account for the factor that is different between $A_{21,D}$ and $A_{23,D}$. The kinetic rate constant k can then be expressed by the Eyring equation, as follows:

$$k = \kappa \frac{k_B T}{h} e^{\frac{-\Delta G^{\ddagger}}{RT}} \tag{4.15}$$

In Equation 4.15, κ is the transmission coefficient, and $\Delta G^{\ddagger}$ is the activation free energy. The term, $\Delta G^{\ddagger}$ can also be expressed as:

$$\Delta G^{\ddagger} = \Delta H^{\ddagger} - T\Delta S^{\ddagger} \tag{4.16}$$

The Eyring equation can be rearranged into:

$$k = \kappa \frac{k_B T}{h} e^{\frac{\Delta S^{\ddagger}}{R}} e^{\frac{-\Delta H^{\ddagger}}{RT}} \tag{4.17}$$

Equation 4.17 suggests that the large ratio of $A_{21,D}/A_{23,D}$ arises from a difference in the large activation entropy change for the HT2 step relative to that of the reverse of the rearrangement step. The relation between $A_{21,D}$ and $A_{23,D}$ can be expressed as:

$$A_{23,D} = A_{21,D} e^{\Delta\Delta S^{\ddagger}/R} \tag{4.18}$$

Where $\Delta\Delta S^{\ddagger} = \Delta S^{\ddagger}_{23,D} - \Delta S^{\ddagger}_{21,D}$. From the Equation (4.18) and the estimated range of the ratio of $A_{21,D}/A_{23,D}$, $\Delta\Delta S^{\ddagger}$ is estimated in the range from -24.9 to -18.1 cal $K^{-1}mol^{-1}$.

As discussed in Chapter III, the rearrangement step involves relatively small activation entropy changes ($A_{12,H} \approx A_{12,D} \approx k_B T/h$). Therefore, if we assume that the reverse rearrangement reaction also has a small activation entropy, this suggests that the HT2 step is associated with a large negative activation entropy change of approximately 18 to 25 cal $K^{-1}mol^{-1}$.

From the derivation of the three-state, two-step model, the difference between the enthalpy of the reverse of the rearrangement step and that of the HT2 step is approximately 4.5 to 6.4 kcal/mol. Therefore, the product radical has a more favorable

enthalpic path to diamagnetic products, through HT2 step. However, the HT2 step involves a significant entropy decrease relative to the reverse of the rearrangement step (equivalent to 3.8 to 5.2 kcal/mol at 207 K or 5.4 to 7.4 kcal/mol at 293 K), which increases the activation free energy of the HT2 step as a function of temperature, relative to the reverse rearrangement step. Figures 4.6 and 4.7 show schematic representation of Gibbs free energy of the Co^{II}-substrate radical state, Co^{II}-product radical state, and the diamagnetic product state, at low temperature ($T \leq 207$ K) and at room temperature, respectively.

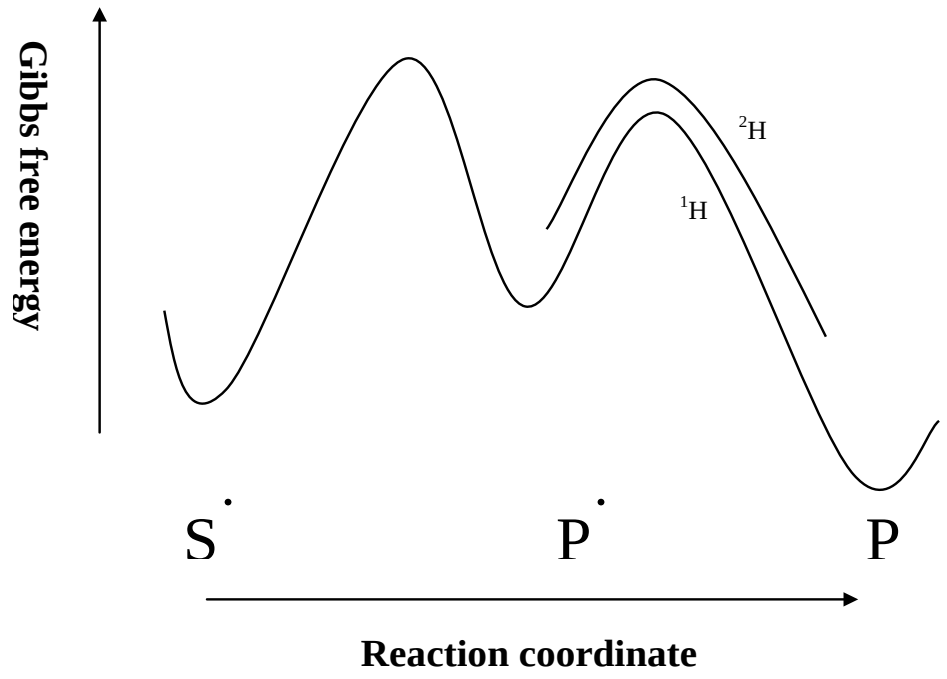

Figure 4.6: Schematic representation of the Gibbs free energy of Co^{II}-substrate radical state, Co^{II}-product radical state, and the diamagnetic product state, at low temperatures ($T \leq 207$ K). In the diagram, the difference of activation free energies for ^{1}H and ^{2}H-substrate is attributed to the transition state, in practice, it is usually a mixture of minimus states and transition state.

At temperature $T \leq 207$ K (Figure 4.6), the activation free energies of the HT2 step for ^{1}H-substrate radical ($\Delta G^{\ddagger}_{HT2,H}$), and ^{2}H-substrate radical ($\Delta G^{\ddagger}_{HT2,D}$), are both smaller than those of the reverse of the rearrangement step for ^{1}H-substrate radical ($\Delta G^{\ddagger}_{RRe,H}$) and ^{2}H-substrate radical ($\Delta G^{\ddagger}_{RRe,D}$). Thus, the rearrangement step is the rate limiting step for the decay of both ^{1}H- and ^{2}H-substrate radicals at $T \leq 207$ K, and only the modest ^{1}H/^{2}H substrate IE (1.35), which arises from rehybridization in the rearrangement step, is observed. As the temperature increases, the term $-T\Delta S^{\ddagger}$ becomes more significant, relative to the term $\Delta H^{\ddagger}$. At room temperature, Figure 4.7 shows that the Gibbs free energies of the HT2 step with deuterium or tritium transfer ($\Delta G^{\ddagger}_{HT2,D/T}$) are larger than those of the reverse of rearrangement step ($\Delta G^{\ddagger}_{RRe,D/T}$), and HT2 step is a partial or predominant rate limiting step. Therefore, the ^{2}H/^{3}H IE on HT2 step is fully manifested. However, the ^{1}H/^{2}H IE on HT2 step is not fully expressed in the measurement of the ^{1}H/^{2}H IE on the steady-state turnover of EAL on aminoethanol, because the rearrangement step is predominantly the only rate limiting step for the decay of the ^{1}H-substrate radical from 190 K to room temperature. These results and analysis resolve the decades-old conundrum of the hydrogen IE in EAL.

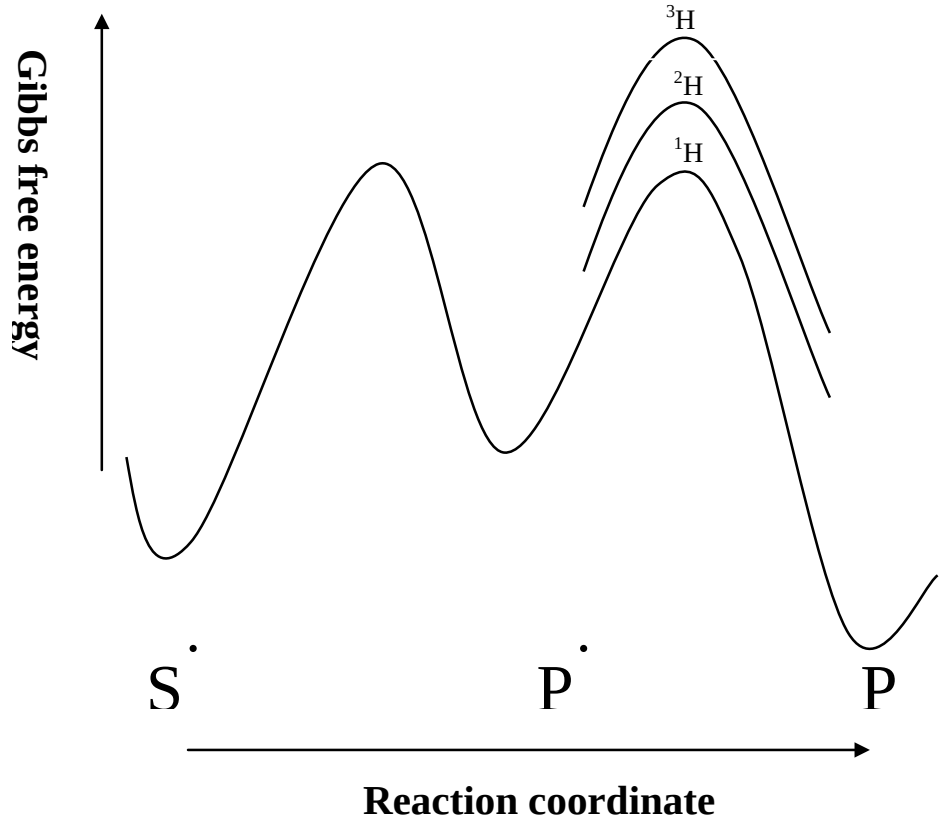

Figure 4.7: Schematic representation of the Gibbs free energy of Co^{II}-substrate radical state, Co^{II}-product radical state, and the diamagnetic product state, at room temperature (*T* = 293 K).

4.3 Conclusion

The decay kinetics of 1,1,2,2-$^1H_4$-aminoethanol and 1,1,2,2-$^2H_4$-aminoethanol generated Co^{II}-substrate radical pair have been measured by time-resolved, full-spectrum EPR spectroscopy from 190 to 223 K. The $^1H/^2H$ substrate IE is found to be temperature dependent. The IE 1.35 ±0.08 at $T \leq 207$ K, and increases to 2.1 ±0.1 at 223 K. Together with the previously reported $^1H/^2H$ IE (7.4-7.5,7.8)[34,43] of the steady-state turnover of

EAL on aminoethanol, a three-state, two-step model is proposed to address the temperature dependent $^{1}H/^{2}H$ IE.

From the proposed three-state, two-step model, the HT2 step involves a large negative activation entropy change (-24.9 to -18.1 $calK^{-1}mol^{-1}$), relative to the reverse of the rearrangement step. Since the term $-T\Delta S^{\ddagger}$ is temperature dependent, the activation free energy of the HT2 step is temperature dependent. At $T \leq 207$ K, the rate constant of the HT2 step for ^{2}H-substrate radical decay is much larger compared to that of the reverse of the rearrangement step, and rearrangement is predominantly the only rate limiting step for both ^{1}H- and ^{2}H-substrate radicals decay, leading to the modest observed $^{1}H/^{2}H$ IE (1.35), which arises from the rearrangement step, not HT2. As the temperature increases above 210 K, the rate constant of the HT2 step for ^{2}H-substrate radical decay is comparable to that of the reverse of the rearrangement step, whereas the rate constant of the HT2 step for ^{1}H-substrate radical decay is still much larger relative to that of the reverse of the rearrangement step. Both the HT2 step and the rearrangement step are the rate limiting step for the decay of ^{2}H-substrate radical above 210 K, but the rearrangement step is predominantly the only rate limit step for the decay of ^{1}H-substrate radical from 190 K to room temperature. This model successfully explains the kinetic IE paradox of the $^{1}H/^{2}H$ steady-state turnover IE (7.5) and $^{1}H/^{3}H$ IE (100) on transfer of hydrogen from C5'-methyl group to the product radical.

Chapter V

Decay Kinetics of the Co^{II}-substrate Radical Pair in the Transition Region

5.1 Background and Introduction

The characteristics of dynamical motion of proteins are different at low and high temperatures.[75,143] At low temperature (approximately, T < 180 K), harmonic modes of motion of the protein dominate.[144] The anharmonic motions, also called "protein-specific" motions, become more important as the temperature increases (T > 180 K in myoglobin) in hydrated proteins with h greater than ~0.2 (h: gram of water per gram of protein).[106,145] Protein functions appear to be dependent on the protein-specific motions, which arise from the transition among protein conformational substates.[106] Extensive research has been performed to detect protein specific motions, by various techniques, such as neutron scattering,[74] Mössbauer spectroscopy,[72] optical absorption spectroscopy,[146-148] and molecular dynamics simulation.[149-152] Protein specific motions, which are characterized by a sharp increase of the mean squared atomic displacement, $\langle r^2 \rangle$, have been observed in many proteins over a transition temperature range of approximately 180-230 K.[72,74,153] The presence of a dynamical transition has been recently questioned. It has been proposed that the transition is an artifact of the response time (bandwidth limitation) of the experimental methods.[83,84]

The protein dynamic transition has been correlated with measurable biochemical functions.[74,154-156] Protein specific motions seem to be a prerequisite for function.[106] However, exceptions have also been found.[157,158] For example, measurable enzyme activity of the glutamate dehydrogenase was detected down to 190 K, in 70% aqueous methanol, without significant deviation from Arrhenius behavior, well below the transition temperature observed at ~220 K.[157]

It has been shown that the cryotrapped Co^{II}-substrate radical pair intermediate in coenzyme B_{12}-dependent EAL [EC 4.3.1.7; cobalamin (vitamin B_{12})-dependent enzyme superfamily][127] from *Salmonella typhimurium*[3,5,128] relaxes to diamagnetic products during annealing over the temperature range of 190 to 223 K.[113] This suggests that the function of EAL has not been totally "frozen-out", at a temperature of at least T = 190 K. In fact, the linear Arrhenius temperature dependence of both $k_{obs,f}$ and $k_{obs,s}$ from 190 to 223 K and 190 to 207 K, respectively, suggest that the mechanism of the decay remains the same for temperatures of at least 190 K. The low temperature limit of 190 K is established by the temperature maintenance time of the temperature control equipment, and the long time scale gives a value for the effective τ at 190 K as low limit. From 190 to 207 K, the decay is biexponential with constant fast phase and slow phase amplitude, which correspond to two separate, non-interconverting populations of substrate radicals.[113] With increasing temperature over the range of $207 < T < 214$ K, the normalized amplitude of the fast phase increases to unity, while the amplitude of the slow phase decreases to zero. The narrow, < 7 K temperature range of the biexponential to monoexponential transition suggests an origin in a protein dynamical transition.[113] The evidence for this dynamical transition is based on a measurement of function, within the range of the time resolution of the transient measurement. Therefore, the evidence for a dynamical transition is not subject to the problem of bandwidth limitation, as are the different spectroscopic methods, which have led to the proposal that the dynamical behavior in the protein system is continuous. At $T \geq 214$ K, the decay is monoexponential, with Arrhenius parameters that match those for the fast phase decay component at 190 to 207 K. The first-order rate constant ($k_{obs,s}$) of the slow phase at 210 K is approximately

2.2-fold higher than the prediction from extrapolation of the low temperature (190 to 207 K) Arrhenius relation (4.2 x10^{-3} s^{-1}). This suggests a change in the mechanism of the slow phase to the mechanism of the fast phase of decay.[113] The molecular mechanism of the interconversion of the two populations remains unclear.

In order to address the mechanism of the transition, a detailed investigation, at 1 K temperature sampling intervals of the slow phase of substrate radical decay at 207 to 214 K has been performed, by using the two-temperature annealing technique introduced in Chapter II.

5.2 Two-temperature Annealing of the Co^{II}-substrate Radical Pair

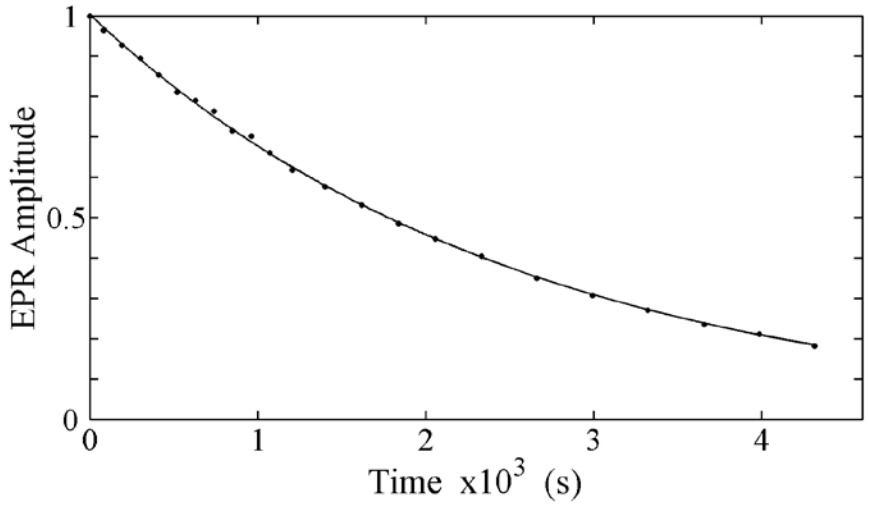

Figure 5.1: Decay of the substrate radical EPR amplitude at 208 K, following partial decay at *T* = 193 K. The sample was held at 193 K for 6 h, and the substrate radical amplitude decayed to 40% of the initial amplitude. The subsequent decay at *T*=208 K is shown, with overlaid monoexponential fit to the data (solid line). *Experimental Conditions:* microwave frequency, 9.3435 GHz; temperature, 208 K; microwave power, 20.25 mW; magnetic field modulation, 1.0 mT; modulation frequency, 100 kHz; scan rate: 3.89 mT/s; time constant, 2.56 ms. *Simulation parameters*: first-order rate constant, 4.3×10^{-4} s^{-1}; R^2=0.9998.

The rate constant of the fast phase population decay ($k_{obs,f}$) is approximately 5.2-fold higher than the rate constant for the slow phase population decay ($k_{obs,s}$) at T = 207 K, and the $k_{obs,f}/k_{obs,s}$ ratio increases as the temperature decreases, to a value of 14, at 190 K. The Co^{II}-substrate radical pair is therefore annealed at the low temperature of 193 K, to reduce the amplitude to 35 to 40% of the initial amplitude. The process prepares a nearly "pure" population of the slow phase component in the sample. The sample is then temperature-stepped to a higher temperature (207 to 214 K), to observe the "pure" decay of the slow phase component of the substrate radical at the higher temperature. The two-temperature experiment is performed because, at the higher temperature, where $k_{obs,f}$ and $k_{obs,s}$ become comparable, it is difficult to reliably deconvolute the two decay components by using the biexponential fit of data collected in the standard, "one-temperature", annealing experiment.

Table 5.1: First-order rate constant and amplitude parameters for the fit of the monoexponential function to the ^{1}H-substrate radical decay kinetics at different temperatures after incubation at 190 to 193 K for 6 to 9 hours. Approximately 40% of initial radical is left at the start of substrate radical decay at the elevated temperature.

T (K)	$k_{obs,2T}$ (s^{-1})	A	R^2 [a]
207	$3.55(\pm0.49) \times 10^{-4}$	1	0.9985
208	$4.88(\pm0.84) \times 10^{-4}$	1	0.9989
209	$7.38(\pm0.50) \times 10^{-4}$	1	0.9991
210	$1.12(\pm0.14) \times 10^{-3}$	1	0.9983
211	$1.59(\pm0.24) \times 10^{-3}$	1	0.9991
212	$2.07(\pm0.17) \times 10^{-3}$	1	0.9992
213	$2.54(\pm0.18) \times 10^{-3}$	1	0.9989
214	$3.80(\pm0.51) \times 10^{-3}$	1	0.9976

[a] R is Pearson's correlation coefficient.

Figure 5.1 shows a representative decay from the two-step annealing experiment (2*T*-experiment), which was performed at a combination of temperatures of 193 and 208 K. As shown in Figure 5.1, the decay of the sample at 208 K is well-fit by a monoexponential function with a rate constant of 4.3×10^{-4} s^{-1}. Similar 2*T*-experiments, at a low temperature of 193 K, and higher temperatures over the range, 207 to 214 K, have been performed at a temperature increment of 1 K. The decay kinetics of the slow phase of the substrate radical are well-fit by the monoexponential function in all cases. The average decay rate constants and standard deviations from at least three decay measurements at each temperature are presented in Table 5.1.

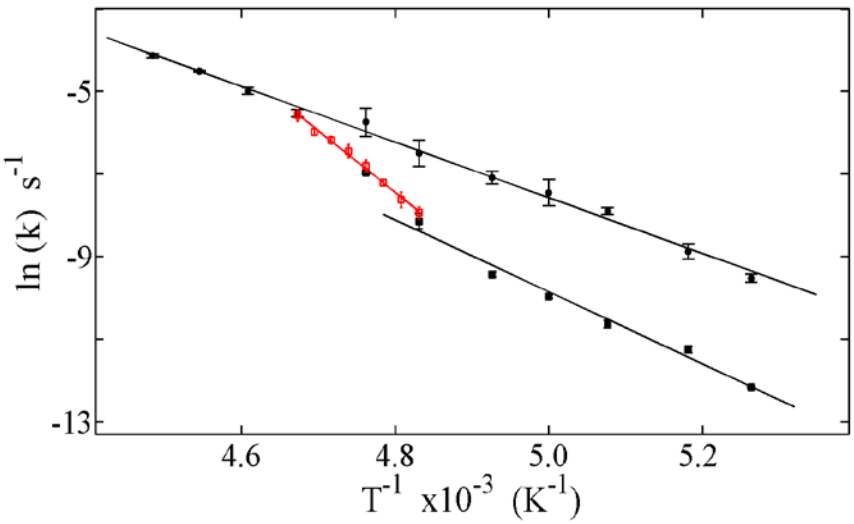

Figure 5.2: Arrhenius plots of the observed first-order rate constants for the decay of the Co^{II}-substrate radical pair, $k_{obs,m}$, $k_{obs,f}$ $k_{obs,s}$ and $k_{obs,2T}$. The combined $k_{obs,m}$ and $k_{obs,f}$ values (black solid circles) are fitted by the upper line. The $k_{obs,s}$ values corresponding to $190 \leq T \leq 207$ K (black solid squares) are fitted by the lower black line. The $k_{obs,s}$ value for 210 K (black open square) is not included in the fit. The $k_{obs,2T}$ values corresponding to $207 \leq T \leq 214$ K (red open squares) are fitted by the red line. The data are from Table 2.1 and Table 5.1.

Figure 5.2 shows plots of the natural logarithms of the observed rate constants for the 2*T* experiments $k_{obs,2T}$ as a function of inverse absolute temperature. The parameters

($A_{app,2T}$ = $10^{27.9\pm1.0}$ s^{-1}, E_a = 29.7 ±0.5 kcal/mol) derived from a linear fit to the Arrhenius plot of the first-order rate constants from the 2*T* experiment for substrate radical decay from 207 to 214 K differ significantly from those ($A_{app,s}$ = $10^{13.8\pm1.0}$ s^{-1}, E_a = 17.3 ± 0.6 kcal/mol) of the slow phase component of the substrate radical decay from 190 to 207 K. The significant change of Arrhenius fitting parameters indicates discontinuity between the transition region Arrhenius dependence and the fast phase and slow phase Arrhenius dependences. This suggests the presence of a dynamical transition, which is not likely to arise from the pure chemical reaction. The value of $k_{obs,2T}$ is the same as that of $k_{obs,m}$ at 214 K, which implies that the slow phase population of the substrate radical converts into the fast phase population at $T \geq 214$ K.

5.3 Three-temperature Annealing of the Co^{II}-substrate Radical Pair

To address whether the partitioning into fast and slow populations observed at low temperature arises from sample preparation at room *T*, or is a property of the sample at low temperature, a three-temperature (3*T*) experiment was designed and performed. In the 3*T* experiment, the substrate radical sample is annealed first at 193 K, until ~40% signal remains. The sample is then annealed at 220 to 224 K for ~30 to 60 s. Finally, the sample is annealed at a temperature in the range of 190-207 K, and the time course of decay is measured by full-spectrum EPR. At the beginning of the decay measurement at 190 to 207 K in the 3*T* experiment, approximately 20 to 25% of the original radical amplitude remains. The amount of the cryotrapped ^{2}H-aminoethanol-generated substrate radical sample is 3-4-fold higher than that of the cryotrapped ^{1}H-aminoethanol-generated substrate radical sample. Therefore, the ^{2}H-substrate radical sample is employed in the 3*T*

experiments, in order to obtain higher SNR. Figure 5.3 shows a representative decay for the 3*T* experiment, which was performed for a temperature sequence of 193, 223 and 203 K. The decay is well fitted by a biexponential function, with normalized fast phase and slow phase amplitudes of 0.58 and 0.42, respectively. The fitted first-order rate constants of the fast and slow phases are $k_{obs,f} = 5.1 \times 10^{-4}$ s^{-1} and $k_{obs,s} = 9.0 \times 10^{-5}$ s^{-1}, which are consistent with the average rate constants ($k_{obs,f} = 5.7 \pm 0.8 \times 10^{-4}$ s^{-1} and $k_{obs,s} = 1.1 \pm 0.1 \times 10^{-4}$ s^{-1}) of ^{2}H-substrate radical decay at 203 K, which are shown in Table 3.1. This suggests that partitioning into fast and slow populations is a property of the EAL protein system at low temperature.

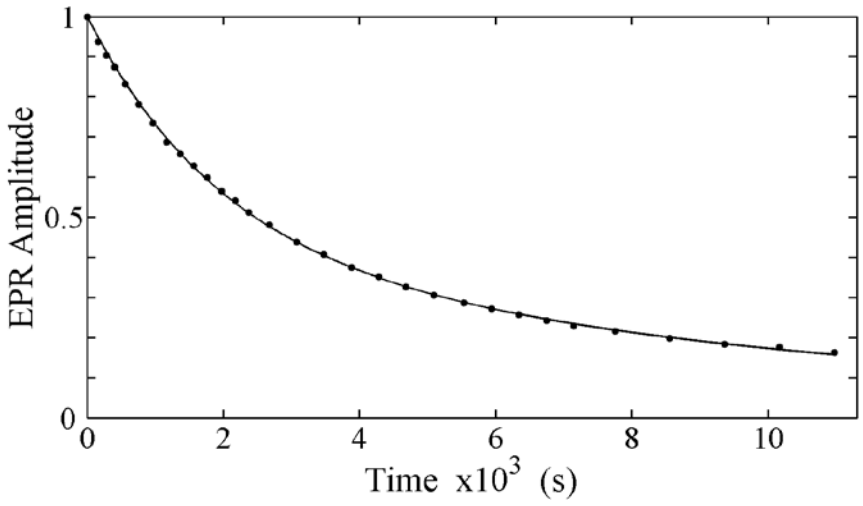

Figure 5.3: Decay of the substrate radical EPR amplitude at 203 K, following partial decay at *T* = 193 and 223 K. The sample was held at 193 K for 13 h and 223 K for 50 s, and the substrate radical amplitude decayed to 23% of the initial amplitude. The subsequent decay at *T* = 203 K is shown, with overlaid biexponential fit to the data (solid line). *Experimental Conditions:* microwave frequency, 9.3416 GHz; temperature, 203 K; microwave power, 20.25 mW; magnetic field modulation, 1.0 mT; modulation frequency, 100 kHz; scan rate: 3.89 mT/s; time constant, 2.56 ms. *Simulation parameters*: A_f=0.58, $k_{obs,f}$=5.1×10^{-4} s^{-1}; A_s=0.42, $k_{obs,s}$=9.0×10^{-5} s^{-1}; R^2=0.9999.

5.4 Conclusion

The kinetic decay of the Co^{II}-substrate radical pair exhibits two-phases at $T \leq 207$ K, representing two separate, non-interconverting populations of substrate radical, with first-order rate constants ($k_{obs,f}$ and $k_{obs,s}$) that differ by ~5-fold at 207 K and ~14-fold at 190 K. A transition in the kinetics of substrate radical decay arises within the temperature interval, 207-214 K, and the substrate radical decay displays a monoexponential function at $T \geq 214$ K, with first-order rate constants $k_{obs,m}$. In the narrow, < 7 K transition temperature range, 2*T* experiments have been performed to address the temperature dependent decay kinetics of the slow phase population of the substrate radical.

The rate constants ($k_{obs,2T}$) of slow phase population decay show a sharper dependence on *T*, at 207 to 214 K, relative to the temperature dependence of the rate constants ($k_{obs,s}$) of the slow phase of substrate radical decay at 190 to 207 K. The $k_{obs,2T}$ value is the same as the rate constant ($k_{obs,m}$) of the monoexponential substrate radical decay at 214 K, suggesting the slow phase population converts into fast phase population at $T \geq 214$ K. The narrow, < 7 K temperature range of the observed kinetic transition is consistent with a protein dynamical transition. The 3*T* experiments imply that partitioning into fast and slow populations is a property of the substrate radical sample at low temperature, rather than from a physical difference between protein states that is present in the sample at room temperature. The transition of the kinetics of substrate radical decay is proposed to arise from a dynamical transition of protein. There are probably two subpopulations of EAL, and the interconverstion among the two subpopulations of EAL is slow relative to the substrate radical decay at $T < 207$ K. As the temperature increases above 210 K, the interconversion among different subpopulations of EAL experiences a

sudden increase in rate, and the decay of substrate radical exhibits monoexponential function. This rate constant corresponds to $k_{obs,f}$. This qualitative explanation will be tested by simulating the data with a detailed kinetic mechanism in future work.

Chapter VI

Trapping of the Co^{II}-product Radical Pair Intermediate and Kinetic Characterization of Recombination Reaction Steps

6.1 Background and Introduction

The minimal catalytic mechanism for EAL[34,128] shown in Figure 1.3 suggests that at least three different paramagnetic intermediate species are formed, which are Co^{II}-substrate radical pair, Co^{II}-product radical pair and Co^{II}-5'-deoxyadenosyl radical pair.[41-44,159] However, only the Co^{II}-substrate radical pair has been observed, by EPR spectroscopy, in the natural system, when the EAL reaction is performed with the two known substrates, aminoethanol and 2-aminopropanol. Transient kinetics measurements, with EPR spectroscopic detection, have now been used to study two stages of the reaction cycle of EAL. The reaction of the ternary complex of holo-EAL and aminopropanol has been addressed by rapid-mix freeze-quench (RMFQ) methods,[41,50] and by temperature-step in a low temperature DMSO/water cryosolvent system.[125] The rise of the Co^{II}-substrate radical pair is detected. The second stage of reaction that has been studied is the decay of the Co^{II}-substrate radical pair, either by the decay of the intermediate in steady-state conditions, after substrate depletion,[29,47] or by the annealing induced decay of the intermediate in frozen solution, as reported in this dissertation.[113] In the low temperature systems, individual steps have been isolated for kinetic study: In the DMSO/water cryosolvent system, the Co-C bond cleavage step is rate determining (M. Wang and K. Warncke, manuscript in preparation), and in the frozen solution system, the radical rearrangement step is rate determining. The stage of reaction of the product radical to form the Co^{II}-5'-deoxyadenosyl radical pair, followed by recombination to reform the intact cofactor and final product, has been enigmatic. In order to continue the effort to kinetically isolate individual reaction steps and detect intermediate states, the reverse of the final two canonical steps in the reaction cycle will be studied by RMFQ.

RMFQ methods have been previously employed to trap the reaction intermediates of EAL after mixing with aminoethanol/aminopropanol, from 10 ms to completion of the reaction. Only the Co^{II}-substrate radical pair is detected by EPR spectroscopy.[50] This suggests that Co-C bond cleavage and HT1 step are "kinetically coupled", or that the Co^{II}-5'-deoxyadenosyl radical pair state is high in free energy, compared to the ternary complex and Co^{II}-substrate radical pair states. Evidence for a trapped Co^{II}-product radical pair intermediate was not obtained. This is consistent with our results for decay of the Co^{II}-substrate radical pair in the frozen solution systems, and with the relatively high energy calculated (5-9 kcal/mol) for the Co^{II}-product radical pair,[122,123,139] relative to the Co^{II}-substrate radical pair.

The complete decay of the aminoethanol-generated Co^{II}-substrate radical pair EPR amplitude suggests that at least one step in the recombination process is irreversible. This is consistent with the experiment showing that mixing of excess acetaldehyde and ammonium to holoenzyme do not yield detectable substrate radical signals.[113] However, it is found that every step of the steady-state turnover of EAL on (*S*)-2-aminopropanol is reversible.[4,5] Based on the insights gained from the low temperature kinetic studies, it is predicted that the Co^{II}-product radical pair can be trapped, if the reverse of the reaction of EAL and (*S*)-2-aminopropanol is studied. The basic idea of reverse reaction is as follows: If the mixing of propionaldehyde (propanal) and ammonium with the holoenzyme yields the Co^{II}-substrate radical pair, it is possible that the Co^{II}-product radical pair can be trapped by RMFQ methods, before the equilibrium is reached.

To evaluate the feasibility that the Co^{II}-product radical pair can be trapped in the reverse reaction of propanal, ammonium and holoenzyme, two prerequisites must be

satisfied. First, a significant amount of Co^{II}-substrate radical pair must be accumulated during the steady-state reaction of propanal, ammonium and holoenzyme, so that the signal can be detected by EPR spectroscopy. The experiment to assess the first prerequisite is shown in the next section. Second, the time constant of the reaction step from product radical to substrate radical should be ≥ 5 to 10 ms, which is the dead time for RMFQ equipment. The rate constant of the rearrangement step from substrate radical to product radical, is approximately equal to the turnover of EAL on (*S*)-2-aminopropanol, 0.12 to 0.27 s^{-1} (time constant 3.7 to 8.3 s) at room temperature.[28,29] The RMFQ experiment could be performed at 4 °C, where the time constant of the rearrangement step is assumed to be approximately 50 s. The dead time for RMFQ is 5 ms, which suggests that the Co^{II}-product radical pair may be trapped, if the rate constant of the reverse reaction of rearrangement step is ~10^4-fold or less, compared to that of rearrangement step. The upper limit of rate constant ratio of ~10^4-fold corresponds to a 5 kcal/mol higher free energy for the product radical state relative to the substrate radical state, which is close to the calculated 5 to 9 kcal/mol.[123,132]

6.2 Experimental Procedures

Enzyme was purified from the *E.coli* overexpression strain incorporating the cloned *S. typhimurium* EAL coding sequence[30] essentially as described[114], with the exception that the enzyme was dialyzed against buffer containing 100 mM HEPES (pH 7.5), 10 mM potassium chloride, 5 mM dithiothreitol, and 10% glycerol[115]. Enzyme activity[116] was determined as described by using the coupled assay with alcohol dehydrogenase/NADH.

The specific activity of the purified enzyme with aminoethanol as substrate was 20 to 30 mol/min/mg.

Material and general methods

Adenosylcobalamin (Sigma Chemcial Co.), propionaldehyde and ammonium chloride (Aldrich Chemical Co.) were purchased from commercial sources. Stocks of 1 M propionaldehyde and ammonium chloride in 10 mM potassium phosphate (KP_i) were prepared with pH adjusted to 7.5. The reactions were performed in air-saturated buffer containing 10 mM potassium phosphate (pH 7.5), or in anaerobic buffer. The anaerobic samples were prepared in glove box. All manipulations were carried out on ice under dim red safe-lighting. The final concentration of enzyme was 9 mg/ml, which is equivalent to the concentration of 100 μM active sites. Adenosylcobalamin was added to 200 μM (2-fold excess over active sites). The final concentration of propionaldehyde and ammonium chloride were 20 to 40 mM, and 20 mM, respectively.

The samples for reverse reaction of propionaldehyde, ammonium and holoenzyme were prepared by using a procedure for cryotrapping. Briefly, following manual mixing of the enzyme-adenosylcobalamin solution with propionaldehyde and ammonium chloride stock, the sample was loaded into a 4 mm o.d. EPR tube, and the tube was plunged into liquid nitrogen-chilled isopentane (T = 150 K).

Preparation of samples by RMFQ

The preparation of RMFQ samples was performed as previously described,[160] by using an Update Instruments Model 100 unit with a home-built quenching bath. EAL and AdoCbl were premixed at 0.1 mM (active sites) and 0.2 mM, respectively, to form the holoenzyme in 10 mM KPi. The holoenzyme was mixed with 20 mM ammonium and 45

mM propionaldehyde in a 2:1 (v/v) ratio using the rapid mixing apparatus. The reactions were performed at 4 °C and were freeze-quenched by injecting into cold isopentane (-130 °C) at various times (14 ms to 30 s) after mixing. The quenched samples were stored in liquid nitrogen, prior to EPR spectroscopy.

X-band CW-EPR spectroscopy at 6 K

EPR spectroscopy at 6 K was performed by using a Bruker ELEXSYS E500 spectrometer, with ER 4123SHQE X-band resonator, an Oxford Instruments ESR-900 continuous-flow liquid helium cryostat and Oxford 3120 temperature controller.

6.3 Results

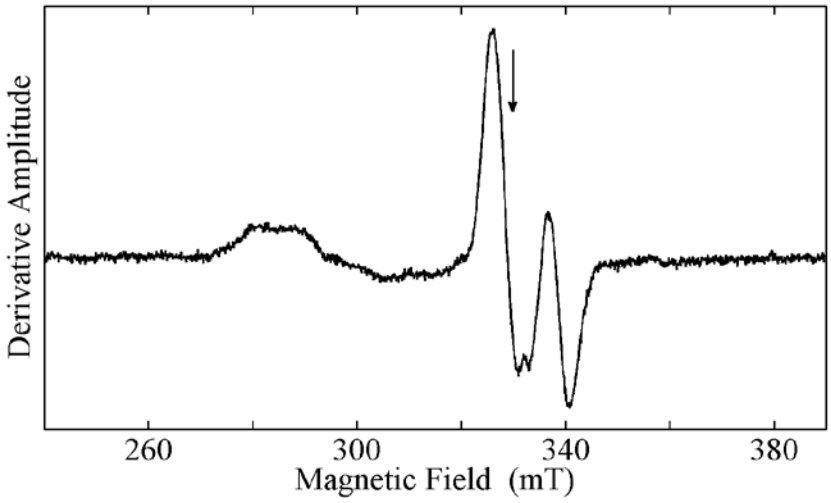

FIGURE 6.1: X-band continuous-wave EPR spectrum of the Co^{II}-substrate radical pair intermediate generated by mixing propionaldehyde, ammonium and holoenzyme under aerobic conditions, and cryotrapped by liquid nitrogen-chilled isopentane. The free electron resonance position at g = 2.0 is shown by the arrow. *Experimental Conditions:* microwave frequency, 9.3446 GHz; temperature, 120 K; microwave power, 20.25 mW; magnetic field modulation, 1.0 mT; modulation frequency, 100 kHz; scan rate: 6.52 mT/s; time constant, 2.56 ms; average of 3 scans.

Figure 6.1 shows a representative X-band CW-EPR spectrum, measured at 120 K, of the sample prepared by manually mixing propionaldehyde, ammonium and holoenzyme, and cryotrapped in liquid nitrogen-chilled isopentane at ~130 °C. The manual mixing time is 15 to 20 s, and samples with longer incubation time up to 5 minutes yield the same EPR spectra as that in Figure 6.1. The EPR line shape is characteristic of the (*S*)-2-aminopropanol-generated Co^{II}-substrate radical pair intermediate.[40,161,162] The $g_{\perp}$ value of isolated cob(II)alamin is approximately 2.26, which is consistent with prominent Co^{II} intensity found in the region around 285 mT.[119,120,163] The line shape of the substrate radical ranges from approximately 325 to 345 mT. The unresolved doublet splitting and inhomogeneous line broadening are caused by the interaction with the unpaired electron spin on Co^{II}.[42,120,162] All the features of the radical pair spectrum can be accounted by EPR simulations, which are the same as those for Co^{II}-substrate radical pair. This provides the evidence that the (*S*)-2-aminopropanol-like Co^{II}-substrate radical pair intermediate accumulates during the steady-state reaction of propionaldehyde, ammonium and holoenzyme. The SNR of the EPR spectrum in Figure 6.1 is ~35, and the amplitude of the EPR signal implies approximately 10% of the active sites contains the Co^{II}-substrate radical pair.

Figure 6.2 shows representative EPR spectra recorded at 6 K, during the reaction time course of propionaldehyde, ammonium and holoenzyme by RMFQ, with mixing times of 14 ms, 92 ms, 424 ms and 45 s, respectively. No Co^{II}-radical pair is observed, over the reaction time ranges from 14 ms to 45 s. The results are inconsistent with the observed accumulation of Co^{II}-substrate in the hand prepared sample by mixing propionaldehyde, ammonium and holoenzyme.

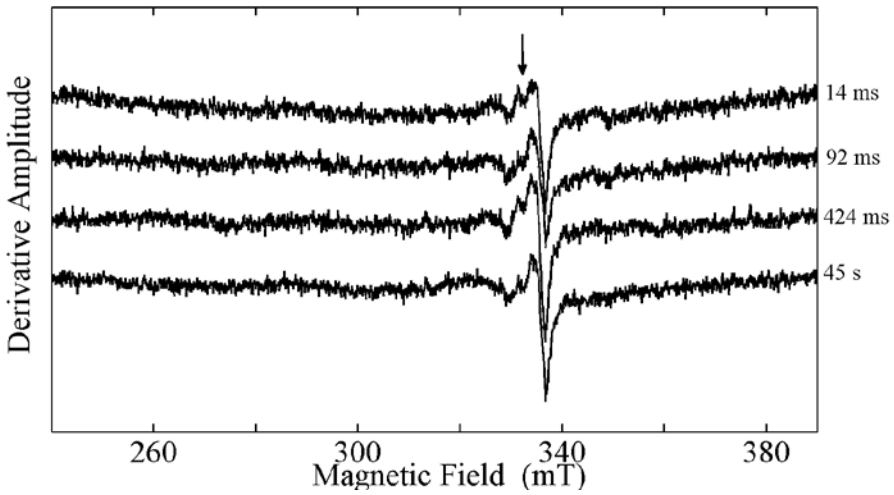

Figure 6.2: Time course of the EPR spectra at 6 K of the reaction of propionaldehyde, ammonium and holoenzyme by RMFQ under anaerobic conditions, with mixing time of 14 ms, 92 ms, 424 ms and 45 s, respectively. The free electron resonance position at g = 2.0 is shown by the arrow. *Experimental Conditions:* microwave frequency, 9.4451 GHz; temperature, 6 K; microwave power, 20.25 mW; magnetic field modulation, 1.0 mT; modulation frequency, 100 kHz; scan rate, 0.45 mT/s; time constant, 40.96 ms.

The inconsistency of EPR spectra of the reaction sample prepared by hand mixing and by RMFQ suggests that the reaction of propionaldehyde, ammonium and holoenzyme is oxygen dependent. The saturated oxygen concentration in water is approximately 0.28 mM at 4°C and atmospheric pressure, which is two orders of magnitude smaller relative to the final concentration of propionaldehyde or ammonium (20-40 mM). The sample prepared by hand is exposed to air during the operation, which allows more oxygen to be dissolved in the reaction solution if oxygen is consumed. However, sample prepared by RMFQ is isolated from air, and oxygen in air could not access the reaction solution during the sample preparation.

The proposal of oxygen dependent reaction of propionaldehyde, ammonium and holoenzyme, may be related to the anaerobic bacteria that contain EAL, and is supported by the following two experiments: First, sample prepared by RMFQ equipment, and exposed to air for 45 s before freeze quenched by liquid nitrogen-chilled isopentane, shows the appearance of Co^{II}-substrate radical pair, which is shown in Figure 6.3. Second, anaerobic sample preparation by using hand mixing of the reaction of propionaldehyde, ammonium and holoenzyme does not show the accumulation of Co^{II}-substrate radical pair above EPR detectable level (unpublished data).

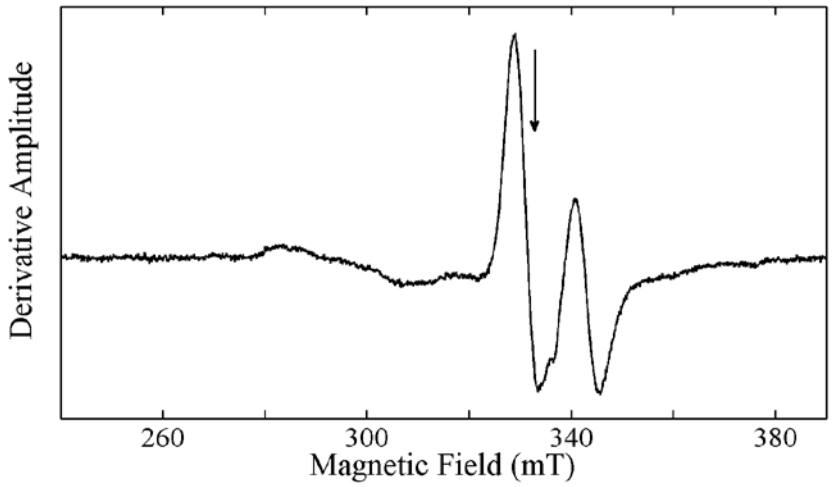

Figure 6.3: EPR spectrum at 6 K of the reaction of propionaldehyde, ammonium and holoenzyme by RMFQ under aerobic conditions, with mixing time of 92 ms, and followed by exposure to air for 45 s. The free electron resonance position at *g*=2.0 is shown by the arrow. *Experimental Conditions:* microwave frequency, 9.4451 GHz; temperature, 6 K; microwave power, 20.25 mW; magnetic field modulation, 1.0 mT; modulation frequency, 100 kHz; scan rate, 0.45 mT/s; time constant, 40.96 ms.

6.4 Conclusion

Previous experiments and simulations show that it is improbable to trap the Co^{II}-product radical pair or Co^{II}-5'-deoxyadenosyl radical pair from the forward reaction of

EAL and aminoethanol or aminopropanol, because of their high free energies relative to that of the Co^{II}-substrate radical pair state.[123,125,132,139] We propose a reverse reaction experiment, by using the RMFQ method, to trap the Co^{II}-product radical pair.

Sample prepared by hand-mixing propionaldehyde, ammonium and holoenzyme shows accumulation of Co^{II}-substrate radical pair in the steady-state reaction. However, the time course of the reaction of propionaldehyde, ammonium and holoenzyme by using the RMFQ method does not show EPR detectable accumulation of Co^{II}-substrate radical pair, for mixing times from 14 ms to 45 s. This result, and manual mixing control experiments, performed with anaerobic samples, suggest that the appearance of the Co^{II}-substrate radical pair from the reaction of propionaldehyde, ammonium and holoenzyme is oxygen-dependent. The molecular origin of this effect is not known, at present.

Bibliography:

(1) Buckel, W.; Golding, B. T. *Chem Soc Rev* **1996**, *25*, 329.

(2) Banerjee, R. *Chemistry and Biochemistry of B12*; Wiley: New York, 1999.

(3) Brown, K. *Chem. Rev.* **2005**, *105*, 2075.

(4) Babior, B. M. In *B12, Volume 2*; Dolphin, D., Ed.; Wiley: New York, 1982; Vol. 2, p 263.

(5) Bandarian, V.; Reed, G. H. In *Chemistry and Biochemistry of B12*; Banerjee, R., Ed.; John Wiley and Sons: New York, 1999, p 811.

(6) Carty, T. J.; Babior, B. M.; Abeles, R. H. *J. Biol. Chem.* **1971**, *246*, 6313.

(7) Barker, H. A.; Iodice, A. A.; Rooze, V.; Suzuki, F. *J Biol Chem* **1964**, *239*, 3260.

(8) Marsh, E. N. G.; Ballou, D. P. *Biochemistry* **1998**, *37*, 11864.

(9) Pierik, A. J.; Ciceri, D.; Broker, G.; Edwards, C. H.; McFarlane, W.; Winter, J.; Buckel, W.; Golding, B. T. *Journal of the American Chemical Society* **2002**, *124*, 14039.

(10) Pierik, A. J.; Ciceri, D.; Lopez, R. F.; Kroll, F.; Broeker, G.; Beatrix, B.; Buckel, W.; Golding, B. T. *Biochemistry* **2005**, *44*, 10541.

(11) Moore, B. S.; Eisenberg, R.; Weber, C.; Bridges, A.; Nanz, D.; Robinson, J. A. *Journal of the American Chemical Society* **1995**, *117*, 11285.

(12) Marsh, E. N. G. *Bioessays* **1995**, *17*, 431.

(13) Chirpich, T. P.; Zappia, V.; Costilow, R. N.; Barker, H. A. *J Biol Chem* **1970**, *245*, 1778.

(14) Wolthers, K. R.; Rigby, S. E. J.; Scrutton, N. S. *J Biol Chem* **2008**, *283*, 34615.

(15) Babior, B. M.; Li, T. K. *Biochemistry* **1969**, *8*, 154.

(16) Manitto, P.; Speranza, G.; Fontana, G.; Galli, A. *Helvetica Chimica Acta* **1998**, *81*, 2005.

(17) Klopotow.T; Wiater, A. *Arch Biochem Biophys* **1965**, *112*, 562.

(18) Ghambeer, R. K. *Indian Journal of Biochemistry* **1967**, *4*, 36.

(19) Kratky, C.; Faerber, G.; Gruber, K.; Wilson, K.; Dauter, Z.; Nolting, H.-F.; Konrat, R.; Kraeutler, B. *Journal of the American Chemical Society* **1995**, *117*, 4654.

(20) Hay, B. P.; Finke, R. G. *Polyhedron* **1988**, *7*, 1469.

(21) Hay, B. P.; Finke, R. G. *Journal of the American Chemical Society* **1987**, *109*, 8012.

(22) *B12*; Dolphin, D., Ed.; Wiley: New York, 1982; Vol. 1.

(23) Kratky, K.; Krautler, B. In *Chemistry and Biochemistry of B12*; Banerjee, R., Ed.; John Wiley and Sons: New York, 1999, p 9.

(24) Pratt, J. M. *Inorganic Chemistry of Vitamin B12*; Academic Press INC.: New York, 1972.

(25) Bradbeer, C. *J. Biol. Chem.* **1965**, *240*, 4669.

(26) Bradbeer, C. *J Biol Chem* **1965**, *240*, 4669.

(27) Sun, L.; Groover, O. A.; Canfield, J. M.; Warncke, K. *Biochemistry* **2008**, *47*, 5523.

(28) Poyner, R. R.; Anderson, M. A.; Bandarian, V.; Cleland, W. W.; Reed, G. H. *Journal of the American Chemical Society* **2006**, *128*, 7120.

(29) Bandarian, V.; Reed, G. H. *Biochemistry* **2000**, *39*, 12069.

(30) Faust, L. P.; Connor, J. A.; Roof, D. M.; Hoch, J. A.; Babior, B. M. *J. Biol. Chem.* **1990**, *265*, 12462.

(31) Faust, L. R.; Connor, J. A.; Roof, D. M.; Hoch, J. A.; Babior, B. M. *J Biol Chem* **1990**, *265*, 12462.

(32) Faust, L. R. P.; Connor, J. A.; Roof, D. M.; Hoch, J. A.; Babior, B. M. *J Biol Chem* **1990**, *265*, 12462.

(33) Hollaway, M. R.; Johnson, A. W.; Lappert, M. F.; Wallis, O. C. *Eur. J. Biochem.* **1980**, *111*, 177.

(34) Bandarian, V. R., G.H. In *Chemistry and Biochemistry of B12*; Banerjee, R., Ed.; Wiley: New York, 1999, p 811.

(35) Bandarian, V.; Reed, G. H. *Biochemistry* **1999**, *38*, 12394.

(36) Bandarian, V.; Poyner, R. R.; Reed, G. H. *Biochemistry* **1999**, *38*, 12403.

(37) Sun, L.; Warncke, K. *Proteins: Structure, Function, and Bioinformatics* **2006**, *64*, 308.

(38) Genomics, J. C. F. S. **2007**.

(39) Toraya, T. *Chem Rev* **2003**, *103*, 2095.

(40) Babior, B. M.; Moss, T. H.; Orme-Johnson, W. H.; Beinert, H. *J. Biol. Chem.* **1974**, *249*, 4537.

(41) Bandarian, V.; Reed, G. H. *Biochemistry* **2002**, *41*, 8580.

(42) Canfield, J. M.; Warncke, K. *J. Phys. Chem. B* **2002**, *106*, 8831.

(43) Weisblat, D. A.; Babior, B. M. *J. Biol. Chem.* **1971**, *246*, 6064.

(44) Carty, T. J.; Babior, B. M.; Abeles, R. H. *J. Biol. Chem.* **1974**, *249*, 1683.

(45) Licht, S. S.; Lawrence, C. C.; Stubbe, J. *J. Am. Chem. Soc.* **1999**, *121*, 7463.

(46) Hollaway, M. R.; White, H. A.; Joblin, K. N.; Johnson, A. W.; Lappert, M. F.; Wallis, O. C. *Eur. J. Biochem.* **1978**, *82*, 143.

(47) Wallis, O. C.; Bray, R. C.; Gutteridge, S.; Hollaway, M. R. *Eur. J. Biochem.* **1982**, *125*, 299.

(48) Poyner, R. R.; Anderson, M. A.; Bandarian, V.; Clelland, W. W.; Reed, G. H. *J. Am. Chem. Soc.* **2006**, *128*, 7120.

(49) Babior, B. M. *J. Biol. Chem.* **1969**, *244*, 449.

(50) Bender, G.; Poyner, R. R.; Reed, G. H. *Biochemistry* **2008**, *47*, 11360.

(51) Ke, S. C.; Torrent, M.; Museav, D. G.; Morokuma, K.; Warncke, K. *Biochemistry* **1999**, *38*, 12681.

(52) Atherton, N. M. *Principles of Electron Spin Resonance*; Ellis Horwood-Prentice Hall: New York, 1993.

(53) Bender, C. J. B., L.J. *Computational and instrumental methods in EPR*; Springer: New Youk, NY, 2006.

(54) Wertz, J. E.; Bolton, J. R. *Electron Spin Resonance*; Chapman and Hall: New York, 1986.

(55) Altshuler, S. A. K., B. M. *Electron Paramagnetic Resonance*; Academic Press: New York, 1964.

(56) Scott, R. A. *Applications of physical methods to inorganic and bioinorganic chemistry*; Wiley: Hoboken, NJ, 2007.

(57) Warncke, K.; Schmidt, J. C.; Ke, S. C. *Journal of the American Chemical Society* **1999**, *121*, 10522.

(58) Ke, S.-C. *Biochim. Biophys. Acta* **2003**, *1620*, 267.

(59) Canfield, J. M.; Warncke, K. *J Phys Chem B* **2005**, *109*, 3053.

(60) Jeschke, G.; Schweiger, A. *Principles of Pulse Electron Paramagnetic Resonance*; Oxford University Press: New York, 2001.

(61) Mims, W. B. *Phys. REv. B* **1972**, *5*, 2409.

(62) Bloch, F.; Hansen, W. W.; Packard, M. *Physical Review* **1946**, *69*, 680.

(63) Bloch, F.; Hansen, W. W.; Packard, M. *Physical Review* **1946**, *69*, 127.

(64) Hahn, E. L. *Physical Review* **1950**, *80*, 580.

(65) Tan, S. L.; Kopczynski, M. G.; Bachovchin, W. W.; Orme-Johnson, W. H.; Babior, B. M. *J. Biol. Chem.* **1986**, *261*, 3483.

(66) Ke, S.-C.; Warncke, K. *J. Am. Chem. Soc.* **1999**, *121*, 9922.

(67) Warncke, K.; Utada, A. S. *Journal of the American Chemical Society* **2001**, *123*, 8564.

(68) Warncke, K. *Biochemistry* **2005**, *44*, 3184.

(69) Ke, S. C.; Warncke, K. *Journal of the American Chemical Society* **1999**, *121*, 9922.

(70) Canfield, J. M.; Warncke, K. *J. Phys. Chem. B* **2005**, *109*, 3053.

(71) Ringe, D.; Petsko, G. A. *Biophysical Chemistry* **2003**, *105*, 667.

(72) Parak, F.; Knapp, E. W.; Chang, I.; Nienhaus, G. U. *Hyperfine Interact* **1992**, *70*, 1125.

(73) Parak, F.; Frolov, E. N.; Mossbauer, R. L.; Goldanskii, V. I. *J Mol Biol* **1981**, *145*, 825.

(74) Doster, W.; Cusack, S.; Petry, W. *Nature* **1989**, *337*, 754.

(75) Hartmann, H.; Parak, F.; Steigemann, W.; Petsko, G. A.; Ponzi, D. R.; Frauenfelder, H. *Proceedings of the National Academy of Sciences of the United States of America-Biological Sciences* **1982**, *79*, 4967.

(76) Loncharich, R. J.; Brooks, B. R. *J Mol Biol* **1990**, *215*, 439.

(77) Doster, W.; Bachleitner, A.; Dunau, R.; Hiebl, M.; Luscher, E. *Biophys J* **1986**, *50*, 213.

(78) Demmel, F.; Doster, W.; Petry, W.; Schulte, A. *European Biophysics Journal with Biophysics Letters* **1997**, *26*, 327.

(79) Mattos, C. *Trends in Biochemical Sciences* **2002**, *27*, 203.

(80) Teeter, M. M.; Yamano, A.; Stec, B.; Mohanty, U. *P Natl Acad Sci USA* **2001**, *98*, 11242.

(81) Vitkup, D.; Ringe, D.; Petsko, G. A.; Karplus, M. *Nature Structural Biology* **2000**, *7*, 34.

(82) Lee, A. L.; Wand, A. J. *Nature* **2001**, *411*, 501.

(83) Sokolov, A. P.; Roh, J. H.; Mamontov, E.; García Sakai, V. *Chem Phys* **2008**, *345*, 212.

(84) Khodadadi, S.; Pawlus, S.; Roh, J. H.; Sakai, V. G.; Mamontov, E.; Sokolov, A. P. *J Chem Phys* **2008**, *128*.

(85) Khodadadi, S.; Pawlus, S.; Sokolov, A. P. *J Phys Chem B* **2008**, *112*, 14273.

(86) Blumenfeld, L. A.; Davydov, R. M.; Magonov, S. N.; Vilu, R. O. *FEBS Lett.* **1974**, *45*, 256.

(87) Blumenfeld, L. A.; Davydov, R. M.; Magonov, S. N.; Vilu, R. O. *FEBS Lett.* **1974**, *49*, 246.

(88) Blumenfeld, L. A.; Burbaev, D. S.; Davydov, R. M.; Kubrina, L. N.; Vanin, A. F.; Vilu, R. O. *Biochim. Biophys. Acta* **1975**, *379*, 512.

(89) Symons, M. C. R.; Petersen, R. L. *P Roy Soc Lond B Bio* **1978**, *201*, 285.

(90) Symons, M. C. R.; Petersen, R. L. *Biochim. Biophys. Acta* **1978**, *537*, 70.

(91) Gasyna, Z. *FEBS Lett.* **1979**, *106*, 213.

(92) Davydov, R.; Kofman, V.; Fujii, H.; Yoshida, T.; Ikedo-Saito, M.; Hoffman, B. *J. Am. Chem. Soc.* **2002**, *124*, 1798.

(93) Davydov, R.; Matsui, T.; Fujii, H.; Ikeda-Saito, M.; Hoffman, B. M. *J. Am. Chem. Soc.* **2003**, *125*, 16208.

(94) Davydov, R.; Kofman, V.; Nocek, J. M.; Noble, R. W.; Hui, H.; Hoffman, B. M. *Biochemistry* **2004**, *43*, 6330.

(95) Davydov, R.; Perera, R.; Jin, S.; Yang, T.-C.; Bryson, T. A.; Sono, M.; Dawson, J. H.; Hoffman, B. M. *J. Am. Chem. Soc.* **2005**, *127*, 1403.

(96) Ericson, A.; Hedman, B.; Hodgson, K. O.; Green, J.; Dalton, H.; Bentsen, J. G.; Beer, R. H.; Lippard, S. J. *J. Am. Chem. Soc.* **1988**, *110*, 2330.

(97) De Witt, J. G.; Bentsen, J. G.; Rosenzweig, A. C.; Hedman, B.; Green, J.; Pilkington, S.; Papaefthymiou, G. C.; Dalton, H.; Hodgson, K. O.; Lippard, S. J. *J. Am. Chem. Soc.* **1991**, *113*, 9219.

(98) Davydov, R.; Kuprin, S.; Gräslund, A.; Ehrenberg, A. *J. Am. Chem. Soc.* **1994**, *116*, 11120.

(99) Valentine, A. M.; Tavares, P.; Pereira, A. S.; Davydov, R.; Krebs, C.; Hoffman, B. M.; Edmondson, D. E.; Huynh, B. H.; Lippard, S. J. *J. Am. Chem. Soc.* **1998**, *120*, 2190.

(100) Gibson, Q. H. *J. Physiol.* **1956**, *134*, 112.

(101) Austin, R. H.; Beeson, K. W.; Eisenstein, L.; Frauenfelder, H.; Gunsalus, I. C. *Biochemistry* **1975**, *14*, 5355.

(102) Frauenfelder, H.; Fenimore, P. W.; McMahon, B. H. *Biophysical Chemistry* **2002**, *98*, 35.

(103) Fenimore, P. W.; Frauenfelder, H.; McMahon, B. H.; Parak, F. G. *P Natl Acad Sci USA* **2002**, *99*, 16047.

(104) Fenimore, P. W.; Frauenfelder, H.; McMahon, B. H.; Young, R. D. *P Natl Acad Sci USA* **2004**, *101*, 14408.

(105) Dantsker, D.; Samuni, U.; Friedman, J. M.; Agmon, N. *Biochim. Biophys. Acta* **2005**, *1749*, 234.

(106) Frauenfelder, H.; Parak, F.; Young, R. D. *Ann. Rev. Biophys. Biophys. Chem.* **1988**, *17*, 451.

(107) Tetreau, C.; Tourbez, M.; Gorren, A.; Mayer, B.; Lavalette, D. *Biochemistry* **1999**, *38*, 7210.

(108) Tetreau, C.; Mouawad, L.; Murail, S.; Duchambon, P.; Blouquit, Y.; Lavalette, D. *Biophys J* **2005**, *88*, 1250.

(109) Lavalette, D.; Tetreau, C. *Eur. J. Biochem.* **1988**, *177*, 97.

(110) Ehrenstein, D.; Nienhaus, G. U. *Proc. Natl. Acad. Sci.* **1992**, *89*, 9681.

(111) Lukoyanov, D.; Barney, B. M.; Dean, D. R.; Seefeldt, L. C.; Hoffman, B. M. *Proc. Natl. Acad. Sci.* **2007**, *104*, 1451.

(112) Warncke, K.; Schmidt, J. C.; Ke, S. C. *J. Am. Chem. Soc.* **2008**, *130*, 6055.

(113) Zhu, C.; Warncke, K. *Biophys J* **2008**, *95*, 5890.

(114) Faust, L. P.; Babior, B. M. *Arch. Biochem. Biophys.* **1992**, *294*, 50.

(115) Harkins, T. T.; Grissom, C. B. *Journal of the American Chemical Society* **1995**, *117*, 566.

(116) Kaplan, B. H.; Stadtman, E. R. *J. Biol. Chem.* **1968**, *243*, 1787.

(117) Warncke, K.; Schmidt, J. C.; Ke, S.-C. *J. Am. Chem. Soc.* **1999**, *121*, 10522.

(118) Moore, J. W.; Pearson, R. G. *Kinetics and Mechanism*; Wiley and Sons: New York, 1981.

(119) Pilbrow, J. R. In *B12*; Dolphin, D., Ed.; Wiley: New York, 1982; Vol. 1, p 431.

(120) Boas, J. F.; Hicks, P. R.; Pilbrow, J. R.; Smith, T. D. *J Chem Soc Farad T 2* **1978**, *74*, 417.

(121) Mansoorabadi, S. O.; Magnusson, O. T.; Poyner, R. R.; Frey, P. A.; Reed, G. H. *Biochmistry* **Web 110906**, *ASAP*.

(122) Wetmore, S. D.; Smith, D. M.; Bennet, J. T.; Radom, L. *J. Am. Chem. Soc.* **2002**, *124*, 14054.

(123) Sandala, G. M.; Smith, D. M.; Radom, L. *J. Am. Chem. Soc.* **2005**, *127*, 8856.
(124) Semialjac, M.; Schwarz, H. *J. Org. Chem.* **2003**, *68*, 6967.
(125) Wang, M.; Warncke, K. *J. Am. Chem. Soc.* **2008**, *130*, 4846.
(126) Angell, C. A. *Science* **1995**, *267*, 1924.
(127) Hubbard, T. J. P.; Ailey, B.; Brenner, S. E.; Murzin, A. G.; Chothia, C. *Nucleic Acids Res.* **1999**, *27*, 254.
(128) Toraya, T. *Chem. Rev.* **2003**, *103*, 2095.
(129) Cleland, W. W. *J Biol Chem* **2003**, *278*, 51975.
(130) Cook, P. E. *Enzyme mechanisms from isotope effects*; CRC Press: Boca Ration, 1991.
(131) Anslyn, E. V. D., D.A. *Modern Physical Organic Chemsitry*; University Science Books, 2006.
(132) Wetmore, S. D.; Smith, D. M.; Bennett, J. T.; Radom, L. *J. Am. Chem. Soc.* **2002**, *124*, 14054.
(133) Semialjac, M.; Schwartz, H. *J. Org. Chem.* **2003**, *68*, 6967.
(134) Smith, D. M.; Golding, B. T.; Radom, L. *J. Am. Chem. Soc.* **2001**, *123*, 1664.
(135) Sun, L.; Warncke, K. *Proteins-Structure Function and Bioinformatics* **2006**, *64*, 308.
(136) Golding, B. T. In *B12*; Dolphin, D., Ed.; Wiley: New York, 1982; Vol. 1 Chapter 15.
(137) Foster, T.; West, P. R. *Can. J. Chem.* **1974**, *52*, 3589.
(138) Foster, T.; West, P. R. *Can. J. Chem.* **1974**, *52*, 4009.
(139) Semialjac, M.; Schwartz, H. *J. Am. Chem. Soc.* **2002**, *124*, 8974.
(140) Kreevoy, M. M. *Isotopes in organic chemistry*, 1976; Vol. 2.
(141) Bigeleisen, J.; Mayer, M. G. *The Journal of Chemical Physics* **1947**, *15*, 261.
(142) Bigeleisen, J. *The Journal of Chemical Physics* **1949**, *17*, 675.
(143) Cordone, L.; Ferrand, M.; Vitrano, E.; Zaccai, G. *Biophys J* **1999**, *76*, 1043.
(144) Melchers, B.; Knapp, E. W.; Parak, F.; Cordone, L.; Cupane, A.; Leone, M. *Biophys J* **1996**, *70*, 2092.
(145) Parak, F.; Frauenfelder, H. *Physica A* **1993**, *201*, 332.
(146) Dipace, A.; Cupane, A.; Leone, M.; Vitrano, E.; Cordone, L. *Biophys J* **1992**, *63*, 475.
(147) Leone, M.; Cupane, A.; Militello, V.; Cordone, L. *Eur Biophys J* **1994**, *23*, 349.
(148) Cupane, A.; Leone, M.; Vitrano, E.; Cordone, L. *Eur Biophys J* **1995**, *23*, 385.
(149) Steinbach, P. J.; Brooks, B. R. *Biophys J* **1997**, *72*, Mp468.
(150) Steinbach, P. J.; Brooks, B. R. *Chem Phys Lett* **1994**, *226*, 447.
(151) Steinbach, P. J.; Brooks, B. R. *P Natl Acad Sci USA* **1993**, *90*, 9135.
(152) Steinbach, P. J.; Hodoscek, M.; Brooks, B. R. *Biophys J* **1993**, *64*, A183.
(153) Rasmussen, B. F.; Stock, A. M.; Ringe, D.; Petsko, G. A. *Nature* **1992**, *357*, 423.
(154) Parak, F.; Knapp, E. W. *P Natl Acad Sci USA* **1984**, *81*, 7088.
(155) Ferrand, M.; Dianoux, A. J.; Petry, W.; Zaccai, G. *P Natl Acad Sci USA* **1993**, *90*, 9668.
(156) Ostermann, A.; Waschipky, R.; Parak, F. G.; Nienhaus, G. U. *Nature* **2000**, *404*, 205.
(157) Daniel, R. M.; Smith, J. C.; Ferrand, M.; Hery, S.; Dunn, R.; Finney, J. L. *Biophys J* **1998**, *75*, 2504.
(158) Dunn, R. V.; Reat, V.; Finney, J.; Ferrand, M.; Smith, J. C.; Daniel, R. M. *Biochemical Journal* **2000**, *346*, 355.

(159) Babior, B. M.; Moss, T. H.; Ormejohn.Wh; Beinert, H. *J Biol Chem* **1974**, *249*, 4537.

(160) Hurshman, A. R.; Krebs, C.; Edmondson, D. E.; Marletta, M. A. *Biochemistry* **2003**, *42*, 13287.

(161) Bandarian, V.; Poyner, R. R.; Reed, G. H. *Biochemistry* **1999**, *38*, 12403.

(162) Bandarian, V.; Reed, G. H. *Biochemistry* **2002**, *41*, 8580.

(163) Carr, S. G.; Smith, T. D.; Pilbrow, J. R. *J. Chem. Soc. Faraday II* **1974**, 497.

Appendix

Manuals and Protocols

Appendix A: Instruction for Oxford Cryostat System with Bruker E560 Console

Preparation of the Helium Tank

1. The Helium Tank (60 L or 100 L) should be steadily stored near the location (within 3 feet) where it will be during experiment for at least 12 hours before starting the experiment.
2. The safety vent valve should be open.

Preparation of the Bruker ESR900 Cryostat

1. Place the Helium purge gas inlet adaptor on top of the chimneystack and plug in the outlet adaptor on the entry arm. Turn on the GF3 mechanic pump, the pressure shown on VC41 should drop below -800 millibar in seconds. Then turn off the pump, the pressure should remain below -800 millibar for minutes. If the pressure rises, check for leaks.
2. Use the Helium gas to flush the system for 5 minutes.
3. Turn on the GF3 mechanic pump to vacuum the cryostat for 20 minutes.
4. Repeat step (2) and (3) for another 2 cycles.
5. Open the Helium purge gas.

Preparation of the transfer line

1. If the transfer line has not been used for weeks, complete the following steps:
    a. Put the transfer line on diffusion pump for overnight in the machine shop. The final pressure is ~$3.2*10^{-6}$ torr.
    b. Use the nitrogen gas with the plastic stem adaptor to flush the transfer line for minutes;

c. Double check the transfer line nozzle tip. Make sure it is straight.

2. Connect the transfer line needle valve cable to the ITC503.
3. Turn on the ITC503. Wait until the gas control light stops flashing.
4. Manually dial the gas flow rate to 99.99% and wait until the transfer line motor stops.
5. Gently disconnect the transfer line.

Inserting the transfer line stem in the liquid Helium tank

Warning! To avoid possible damage to the transfer line (both the front nozzle tip and the needle valve motor are very fragile), two persons are required to finish this part. Make sure the transfer line stem is not bended during the whole process.

1. Open the helium gas vent valve to lower the tank pressure to one atmosphere. Open the top insertion valve and loose the top brass nut.
2. Use the ladder to SLOWLY insert the stem into the liquid Helium tank. Watch out for the obstacles on the roof to protect the motor. The gas vent valve should remain wide open during the insertion process.
3. Quickly tighten the top brass nut and close the gas vent valve. The safety vent valve should remain OPEN.
4. Use a small flask of ethanol to perform the bubble test by immersing the front nozzle tip into the liquid. If no bubbles, check if the flow rate is still 99.99% by connecting the transfer line cable to ITC503. If the gas flow rate is incorrect, you have to remove the transfer line, warm up to room temperature.

Inserting the transfer line to the ESR900 cryostat

1. Slowly move the Helium tank with the transfer line to make the cryostat entry arm

and the transfer line nozzle close enough for a convenient insertion.

2. Make sure the helium gas purge in ESR900 is still on. Take off the purge gas outlet adaptor and quickly insert the transfer line nozzle into the cryostat until it stops. But do not tighten the nut on the transfer line.
3. Connect the pump line and the needle valve line to the transfer line.
4. Quickly take off the inlet helium gas purge adaptor and substitute it with the black seal hat. Close the He gas cylinder gauge.
5. Turn on the GF3 pump. The initial gas flow rate should be almost 0 and the cryostat pressure should be lowered again to below -800 millibar.
6. After 5 to 10 minutes, the gas flow rate will rise quickly to the top limit. At this time point, quickly tighten the nut all the way to the bottom. The gas flow rate will immediately drop and the temperature will go up slightly first and then start to fall. If the temperature could not fall below 273 K within 10 minutes after you finish the above steps, you have to restart from the very beginning.
7. Slowly lift the transfer line stem 1 inch from the tank bottom and retighten the brass nut. Use a Teflon tape to monitor the stem position.

Connecting to the computer console

1. Start the E560 system, open the Xepr software on the computer and connect to the spectrometer.
2. Select Acquisition -> Spectrometer configuration menu. Click the Misc. Tab. Under the TEMPRATURE CONTROLLER, select Type from a pulling down menu to be ITC 503, select Heater Sensor from another pulling down menu to be SENSOR 1. On the bottom of the window, click Apply and then click Close

button.

3. Under the main graphic panel, click the Temperature Controller icon. In the following window under the Temperature tab, first select Use VTU, then adjust the following parameters to be: Temperature -> 6 K (or your desired temperature), Tolerance -> 0.2 K, Setting Time -> 5 s. Switch to the ITC5 Tab, in the multiple choices of ITC5 OPERATION MODES, select the HEATER Control to be Auto and the Gas Flow Control to be Manual. Then select Unlock PID SETTING. Set the Gas Flow to be 99% initially. Input 100 in the HEATER Power Limit (%). Under the PID Parameters, set Proportion to be 50 K, the Integral Time to be 0.2 min and the Derivative Time to be 0.2 min.
4. Wait until the temperature falls below 80 K, then set the Gas Flow to be ~20% if desired temperature is 6 K. (Power off the pump and insert your sample at this time if needed. Repower on the GF3 pump)
5. Wait until desired temperature is reached. Make fine adjustment of the Gas Flow rate (by step of 0.5 at most) until a stabilized temperature ($\leq$ 0.2 K) is achieved.
6. Start scanning spectrum. Do not touch the liquid Helium tank during the experiment.

Changing Samples:

1. Set the microwave bridge in Tune mode.
2. Thoroughly clean the EPR tube for the next scan by multiple (at least 3 times) wiping of the tube wall.
3. Power off the GF3 pump and wait until the pressure meter on VC41 to reach 0 millibar.

4. Quickly take out the sample with the top seal adaptor and put on the black hat seal.
5. Take of the seal adaptor from the old sample and put it on the sample for next scan.
6. Quickly take off the black hat seal and switch in the new sample.
7. Slowly lowering down the sample to find the bottom dip inside the cryostat. Once the bottom position is found, tighten the EPR tube seal adaptor.
8. Power on the GF3 pump and wait until the temperature stabilizes. Make fine adjustment (less than 0.5) of the Gas Flow rate if necessary.

Turning off equipment:

Warning: To avoid possible damage to the transfer line (both the front nozzle tip and the needle valve motor are fragile), two persons are required to finish this part. Also make sure the transfer line stem is straight during the whole process.

1. Turn off the GF3 pump.
2. Quickly take out your sample and put on the black hat seal.
3. Power down the spectrometer and ITC503.
4. Use an electric heater to heat up the joining section between the white plastic pump line and the transfer line. Then disconnect the pump line.
5. Gently disconnect the needle valve line.
6. Loose the transfer line nut completely and pull out the transfer line from the cryostat entry arm.
7. Connect the inlet and outlet adaptor to the ESR900 cryostat to perform a 30 minutes He gas purge.
8. Use the ladder to pull out the transfer line from the liquid Helium tank.

Appendix B: Instruction for Pulse EPR Console

Janis Cryostat Evacuation and Cool-Down Procedure:

The procedure should be performed one day before the experiment. The liquid Helium transfer line may require evacuation if it has not been evacuated for 1 month.

Valve near top of EPR header:

Top, blue handle: port to the sample chamber

Bottom, yellow handle: port to the liquid Helium reservoir

Pump-down the sample chamber and liquid Helium reservoir:

1. Check sample rod entry port, coupler control port, and needle valve are closed.
2. Check rubber stoppers in liquid Helium reservoir vent ports on top of cryostat are tight.
3. Close the sample chamber and liquid Helium reservoir valves.
4. Attach red rubber vacuum hose to sample chamber port.
5. Turn on master valve of Helium gas cylinder, and flow with pressure to modest level. Attach the tygon tubing from Helium gas cylinder to liquid Helium reservoir port.
6. Turn on vacuum gauge, note the vacuum of approximately 200 mTorr (1 Torr = 133.322 Pa). Open blue valve and sample chamber under vacuum.
7. Open the needle valve 4 turns. Pump down the sample chamber and liquid Helium reservoir to 200-300 mTorr.

Back-fill with Helium gas and prepare cryostat for liquid N_2 fill:

1. Close sample chamber, then open liquid Helium reservoir. Let Helium gas fill sample and Helium reservoirs for 30-60 sec.

2. Close liquid Helium reservoir, then open sample chamber.
3. Pump-down the sample and liquid Helium reservoir to 200-300 mTorr.
4. Repeat step 1-3 for 3 times. Close the needle at the last time of Helium gas fill.
5. Place a copper line elbow over liquid N_2 port on top of cryostat, and fill liquid N_2.

Janus Cryostat Helium Fill Procedure

The procedure is performed just before the experiment. The entire procedure, from initiation until the sample area temperature is stable at 6 K, will take 0.5-1 hour.

1. Attach the hose that terminates in the flow gauge to the liquid Helium reservoir port nozzle. Attach the plain hose to the sample chamber port nozzle.
2. Refill the liquid N_2 reservoir; Turn liquid Helium level meter and temperature reader on Tower 2.
3. Turn on Helium gas, and create mild flow.
4. Inert liquid Helium T adapter into liquid Helium tank, and tighten the knurled adapter screw.
5. Place the Helium gas hose onto the T adapter nozzle, and close the Helium gas valve on T adapter.
6. Open top valve and close release valve on liquid Helium tank.
7. Make the transfer line adapter knurled screw mildly tight on top of T adapter. (Check the rubber stopper of liquid Helium reservoir is somehow loose.)
8. Grasp the liquid Helium transfer line, and slowly insert the transfer line into the liquid Helium tank. Insert the transfer line to the bottom of tank, and then pull it up a few centimeters. (*Keep the pressure reading on gauge at 0.75 psi (2 psi offset) during Helium filling.*)

9. Remove the rubber stopper from the left-hand liquid Helium reservoir port, and insert the transfer line. Prop the transfer line with Kimwipe box if necessary.
10. Remove the rubber stopper from the right-hand liquid Helium reservoir port, and then place a copper pipe elbow over the port. (*The liquid Helium monitor read "10.6 in" at "cold empty" level. Full reservoir will read "24.0 in", which corresponds to 10 liters liquid Helium.*)
11. Use rubber stopper to block the liquid Helium reservoir ports firmly after filling the Liquid Helium. Simultaneously, open yellow liquid Helium reservoir handle, adjust the ball to 5.
12. Open needle valve counter-clockwise for 3-3.5 turns and blue valve simultaneously. (Turn on the instruments and software.) As valve T goes ~6 K, close needle valve 1 turn. If valve T continues to drop ~4.3K, close needle valve about 1 turn. Roughly 1-1.5 turns are left open finally.

Instrument Turn-on procedure

1. Tower1: microwave source, HFS, and DSO.
2. Tower2: switches on power supply unit (2 on right, 1 upper left).
3. Tabletop: SR445 amplifier.
4. Magnet: tap water, heat exchanger, magnet power supply.
5. *Last item:* TWT amplifier (Tower 1), warming up for 30 minutes.

Software Initialization

1. Open Matlab71, and execute MainGUI.
2. Turn on channels o f HFS.
3. Magnetic field, 0 → mod, and 3105 → CF (9 GHz), or 3964 → CF (11GHz).

4. Microwave source → “local” → “RF on”.
5. TWT, press “operate”.
6. Gain → 0 -10 dB, and attenuation → ~ 9-11.2 dB.
7. Tuning (sample position, coupler, microwave source and magnetic field), and run.

Shut-down procedure

1. Gain → 40 dB, and attenuation → Max. TWT→standby. Wait 20 minutes.
2. Close sample chamber blue handle, then take out sample with clockwise rotating when observing from up. Then open blue handle again. Refill liquid N_2.
3. Microwave source → local → RF off.
4. Put samples back and water soaker around rubber stopper.
5. Turn off TWT and SR445 on tabletop.
6. Tower2: switches on power supply unit, Lakeshore 330, T-controller.
7. Tower1: DSO, HFS, and microwave source.
8. Magnetic field, 2000 → CF, 1000 → CF, Reset. Power supply → DC off. Turn off heater exchanger, and water.
9. Close needle valve, and sample reservoir blue handle.

Appendix C: Protocol of Cell Growth

Checking suppliers

1. Pre-made 2xYT culture with 75 μg/ml ampicillin
2. Pre-made LB agar plate with 100 μg/ml ampicillin
3. 350 g 2xYT powder
4. 1.1 g ampicillin
5. 3.1 g IPTG

Preparation of inoculums

1. Day 1: Grow *E. coli* cells overnight in a culture tube of 4ml 2xYT culture with 75 μg/ml ampicillin. (*use sterile techniques in the following steps*)
    a. Transfer 4 ml 2xYT into a culture tube.
    b. Inoculate 2xYT from a glycerol stock in the -80 °C freezer. Use a sterilized pipette tip to touch the surface of the glycerol stock and put it in the culture tube. Do it quickly so that the glycerol stock doesn't melt.
    c. Flame the tube and its cap before putting in to the incubator.
    d. Set the incubator to 37 °C, 225 rpm.
    e. Make sure the cap of the culture tube is at the second position, i.e. not fully closed.
2. Day 2: Put the culture tube in 4 °C fridge in the morning. Streak *E. coli* cells on an agar plate in the late afternoon, and incubate at 37 ℃ overnight. Make sure the incubator shaking is off.

Preparation of fermenter

1. Day 3: Check for colonies of inoculums, wrap the plate with para-film and move it to 4 ℃ fridge.

2. Assembly of fermenter:
    a. Assemble the sampler attachment; make sure to put on clamps on the two small tubing.
    b. Put on the 6 screws for the head plate. Hand tight them and make sure the head plate and the vessel are in perfect contact.
    c. Put on the condenser if it is not on. Check the o-ring, and apply more grease if necessary.
    d. Attaching the harvest tubing to the harvest port. Fill the vessel with distilled water, wait for 10 minutes, and let it drain.
    e. Put on a clamp on the harvest tubing and make sure it is close fully. Refill the vessel with 9.5 liter distilled water.
    f. Weigh 295 g (31 g/L x 9.5 L) 2xYT powder. Pour it in through the inoculation port (the big port) carefully using a funnel.
    g. Put on the agitator, and connect it to the main controller. Set agitation to 200 to help the 2xYT powder dissolve. Remove the agitator after the powder is fully dissolved.
    h. Put on filters on the condenser and air intake port.
    i. Put on short tubes on the foam trap port and the air-intake filter. Clamp them tightly.
    j. Wrap all filters with aluminum foil. Make sure the condenser port is NOT covered.
    k. Put the O_2 probe into the head plate.

l. Put in the pH probe after calibrating the pH probe with 7.0 and 4.0 standards. If the pH probe has an unreasonably high reading, check its connection, and restart the console if necessary. *Important: use extra care when putting in the pH probe.*

m. Recheck all the clamps.

n. Recheck all the screws and ports on the head plate and make sure they are tight.

o. Remove the white plastic tubing connector from the harvest tubing to prevent melting during autoclaving.

p. Put on protection caps on the central shaft and pH probe. (Black and red caps, respectively)

3. Prepare 2 flasks of 500 ml 2xYT broth with aluminum foil caps.
4. Autoclaving and fermenter set up:
    a. Autoclave the fermenter and 2 flasks for 25-minutes in the liquid cycle.
    b. Check for spills, and damages on the tubing after autoclaving.
    c. Connect the cooling water to the condenser and the internal cooling coil of the vessel. Connect their corresponding drains. Turn on the main water valve.
    d. Put in temperature probe. The temperature should be reading high now. Set temperature to 37 °C in the main controller, and control to “Auto”. The internal cooling water should be running automatically.
    e. Put on the agitator and set it to 200 rpm to help with cooling.

f. Prepare 11 ml 0.1 g/ml ampicillin solution. After the liquids cools down to less than 40 °C, add 9.5 ml to the fermenter vessel, and 0.375 ml to each of the 500 ml flasks. *Important: use sterile techniques.*

g. Put on heat blanket.

h. Turn off agitator. Connect the O_2 and pH cables. Remove all the foils.

Cell growth

1. Late in Day 3: inoculate one colony and two colonies to the two flasks, respectively. Put them in the incubator at 37 °C and 255 rpm. Let the cell grow for about 8 hours.
2. In Day 4:
    a. Measure and record OD_{600} of the 2 flasks' culture, and choose the one has OD closer to 0.6 for inoculation.
    b. Put on the air tubing. Turn on the main air valve slowly.
    c. Calibrate O_2 probe. First disconnect O_2 probe temporarily, set the zero. Then reconnect the cable, set the air flow to more than 5 liter/minutes, and agitation back to 200 rpm.
    d. Prepare a sterile funnel by washing with ethanol. Clean all the ethanol with Kim-wipe. Inoculate the 500-ml culture through the inoculation port.
    e. Set dO_2 to 30% in the main controller, its control to "auto" and cascade to "agit". Now in the main controller display, the agitation control should change from "auto" to "dO_2".
    f. Watch it often while growing. Make sure the pH is within 6.7 and 7.2 range. If not, adjust with HCl or 10% NaOH accordingly.

g. Let it grow until OD_{600} reaches 0.8, induce with 3.1 g IPTG through the inoculation port carefully.

h. Let it grow for another 4 hours after induction.

Cell harvesting

1. Measure and record OD before harvesting.
2. Turn off air and water.
3. In the main controller, set everything to “off”.
4. Prepare 5 2-liter flasks on ice. Pour the culture broth in the flasks through the harvest tubing. Cover them with para-film. Remove and clean the pH probe and put it in 3 M KCl.
5. Change the rotor for RC5B centrifuge, and rotor code to 10.
6. Centrifuge culture broth in batches in 250 ml bottles. Centrifuge at 3800 rpm for 15 minutes or 5000 rpm for 10 minutes. Dispose the supernatant. Dissolve the cell pellet with pH 7.5 40 mM KPi, and transfer to a flask on ice.
7. Centrifuge the cell pellet with KPi in the flask. Weigh and record the new pallet. Dissolve with minimum pH 7.5 40mM KPi and transfer to a labeled 50 ml centrifuge tube. Flash freeze with liquid N_2 and put it in the -80 °C freezer.
8. Refill fermenter vessel with water and soap. Leave it overnight.
9. Make sure to clean to rotor, the centrifuge and everything else. Use ethanol to kill ampicillin-resistant bacteria.

Fermenter cleaning

1. Detach agitator.
2. Remove the temperature probe.

3. Remove the 6 screws on the head plate.
4. Detach the heat blanket.
5. Detach and wash tubing and filters.
6. Detach and wash the sampler assembly.
7. Detach O_2 probe.
8. Detach the condenser.
9. Drain all the water through the harvest port.
10. Pull the head plate off. Clean the head plate carefully so that you don't bend anything.
11. Check ports and o-rings on the head plate. Apply more grease if necessary.
12. Carefully clean the vessel.
13. Put the vessel back. Apply more grease on the rim if necessary.
14. Put the head plate back.

Appendix D: Protocol of EAL Isolation and Purification

Checking suppliers

1. 0.4 M KPi (pH 7.5)
2. 0.2 M PMSF in n-butanol
3. KCl
4. Urea
5. DTT
6. Glycerol
7. HEPES
8. KOH pellets
9. Streptomycin sulfate
10. Ammonium sulfate

Preparation of dialysis buffers

1. Day 1: Prepare 2 liters of Buffer A by adding 50 ml 0.4 M KPi, 1.5 g KCl, 1.5 g DTT, 1.2 g urea and 200 ml glycerol, and then adjust pH to 7.5 using ~40-60 KOH pellets.
2. Prepare 2x2 liters of Buffer T by adding 47.6 g HEPES, 1.5 g KCl, 1.5 g DTT, 1.2 g urea and 200 ml glycerol, and then adjust pH to 7.5 using ~40-60 KOH pellets.
3. Store Buffer A and Buffer T in fridge at 4 °C, and add stir bar and stir.

Cell breaking and EAL isolation

1. Day 2: Take frozen cells in tube with ~50 ml from -80 °C, and thaw cells in nanopure water. *(All operations are performed on ice.)*

2. Add 0.4 ml of 0.1 M PMSF to 150 ml of 40 mM KPi, dissolve frozen cells in PMSF/KPi buffer and homogenize the cell solution.
3. Break cell solution by French Press at 1000 psi, and centrifuge the cell solution at 10000 rpm for 20 minutes.
4. Pour supernatant in a beaker, add stir bar and stir; discard the pellet.
5. Pre-mix 2.6 g streptomycin sulfate in 26 ml water, and add 26 ml of 10% streptomycin sulfate in EAL cell solution drop by drop; Stir 10 minutes on ice.
6. Centrifuge the cell solution at 10000 rpm for 20 minutes.
7. Pour supernatant into grad cylinder and record volume; discard the pellet.
8. Place supernatant in beaker, add stir bar and stir medium speed. (DO NOT over agitate.)
9. Slowly add ammonium sulfate into cell supernatant (0.164 g per ml measured above); stir 30 minutes on ice; centrifuge the supernatant at 5000 rpm for 20 minutes.
10. Add spatula tip of Na2EDTA in 500 ml water, cut ~12-14" piece of dialysis tubing (12-14,000 MWCO), place dialysis tubing in solution, boil the solution, and rinse it with distilled water. (*Make sure dialysis tubing is NOT leaking.*)
11. Discard cell supernatant; resuspend cell pellet in Buffer A to 60 ml.
12. Place protein suspension in dialysis tubing.

Dialysis, concentration and storage

1. Late in Day 2 (Dialysis):

a. Dialyze protein suspension in 2 liters Buffer A for approximately 8 hours at 4 °C in fridge. (*The translucent pale yellow-orange suspension becomes transparent and yellowish*.)
b. Dialyze protein suspension in Buffer T #1 for another 8 hours. (*The transparent yellowish solution becomes turbid and yellow-orangish*.)
c. Early in Day 3: Dialyze protein suspension in Buffer T #2 for approximately 6 hours. (*The solution remains turbid and yellow-orangish*.)

2. Day 3 (Concentration and storage):
   a. Remove dialysis bag from Buffer T #2, and dry bag with Kimwipe.
   b. Make sure there is ~ ≥1 inch bedding of dry "Aquicide III" in the 4 liter plastic beaker.
   c. Place the dialysis bag on the bedding, and cover the bag with additional Aquicide.
   d. Remove the dialysis bag from Aquicide after 45 minutes; remove the caked-on, wet aquicide with distilled water; dry the bag with Kimwipe.
   e. Repeat step 2 to 5 until desired volume achieved. (~25 ml)
   f. Transfer protein suspension to a disposable 50 ml conical centrifuge; Break up the aggregates by drawing solution rapidly into 10 ml pipette and pushing out. (*Do not create bubbles by blowing air into the protein solution*.)
   g. Label with "EAL concentrate", cell growth #, initials and date.
   h. Store the protein preps in -80 °C; remove a small aliquot of the uniformly dispersed solution for protein concentration assay.

Appendix E: List of Coded Programs

Xepr2mat.m: Read EPR spectrum from Xepr program into .mat file that can be further analyzed in Matlab.

PolyFit_AmpPick.m: Correct the baseline of EPR spectrum, and then find the amplitudes of substrate radical signal as different decay times.

BiExpFit.m: Fit the decay kinetics of the substrate radical by biexponential function.

MonoExpFit.m: Fit the decay kinetics of the substrate radical by monoexponential function.

PowerFit.m: Fit the decay kinetics of the substrate radical by power law function.

ArrheniusFit.m: Fit the rate constants of the substrate radical decay using the Arrhenius relation.

SimKIEs.m: Fit the $^{1}H/^{2}H$ substrate radical decay IE as a function of temperature, using the proposed three-state, two-step model.

All the programs are available on the physics network server at:

\\Luma\gr_warncke\czhu\Programs